HIGH RESOLUTION STUDY OF MICRO-METER PARTICLE DETACHMENT AND RESUSPENSION ON DIFFERENT SURFACES

A Dissertation

by

ASMAA SADEK KASSAB

Submitted to the Office of Graduate Studies of
Texas A&M University
in partial fulfillment of the requirements for the degree of

DOCTOR OF PHILOSOPHY

Approved by:

Co-Chair of Committee,	Yassin A. Hassan
	Victor M. Ugaz
Committee Members,	Kalyan Annamalai
	William H. Marlow
Head of Department,	Jerald A. Caton

December 2012

Major Subject: Mechanical Engineering

ABSTRACT

In an effort to understand the resuspension phenomena, interactions of spherical micro-meter particles (glass beads (GB) and Stainless steel (SS)) were investigated experimentally on different surfaces (glass, ceramic, hardwood, metal and chemical agent resistant coated metal (CARC)). Particles were deposited on the lower surface of a 10 cm square wind tunnel by gravitational settling. Air flows were imposed from an open entrance at average velocities up to 16 m/s. Individual particle trajectories obtained by high-speed imaging reveal three different types of motion: rolling/bouncing, immediate liftoff and complex motion. Surface roughness significantly affects the particle initial motion prior to liftoff. The majority of particle trajectories from the glass substrate were parallel to the surface with complex motion, covering 25% of the total distance traveled in rolling/bouncing motion before liftoff. Hardwood substrates took the longest time for initial particle movement ($t > 1$ s) causing a more rapid liftoff. The ceramic substrate showed the most rolling/bouncing motion, for 80% of the particles. Additionally, single layer detachment showed that the detachment percentage initially follow an exponentially increasing trend for a period of ~ 1 s, followed by a plateau phase for a period of 5 s. Changing velocity, substrate and particle size significantly affects GB particle detachment. Furthermore, detachment from the metal substrate was consistently higher than the CARC substrates. However, particle density is not a significant difference in the bigger particle size studied. Initial 3-D particle tracking showed that particles seem to travel in a constant angle to the left rather than going

straight in the flow direction. A detachment mode model showed that the detachment by direct liftoff required a much higher speed than rolling motion with a minimum of 14 m/s for both GB70 and SS70 on glass and metal surface, and the velocity increased to 21 m/s for the smaller particle. Incorporating the different types of particle motion prior to liftoff into resuspension models, and how their relative contributions change with different particle and substrate materials, can potentially yield improved predictive capabilities.

DEDICATION

Dedicated to my father.

ACKNOWLEDGEMENTS

I would like to thank my committee co-chairs, Dr. Hassan, and Dr. Ugaz, my committee members, Dr. Annamalai, and Dr. Marlow, for their guidance and support throughout the course of this research.

Thanks also go to my friends and colleagues in both Dr. Hassan and Dr. Ugaz groups and the department faculty and staff for making my time at Texas A&M University a great experience. I also want to extend my gratitude to Dr. King, for her continuous help and support throughout my journey in the Aerosol Laboratory, her calm and organized environment encourage me to give it all.

Thanks to my father, mother, sisters and parents in-law for their encouragement and to my beloved husband for his patience and support.

Finally, I would like to tell my son, that you are number one for me. Son, I only did it so you could be proud of your mother.

TABLE OF CONTENTS

Page

LIST OF FIGURES

FIGURE Page

FIGURE Page

FIGURE Page

LIST OF TABLES

1. INTRODUCTION

Resuspension refers to particles detachment from a surface and their transport away from that surface. In other words, particles that are settled on the surface and then are entrained in the fluid streams can be called resuspended particles (Hinds, 1999). Early work was concerned with erosion and soil transport. Since the advent of nuclear technologies, interest has also been focused on health aspects due to the resuspension of deposited material from nuclear weapon tests or possible future accidental releases from the nuclear industry. According to Lassey (1980), the inhalation of resuspended particles in the first few weeks after a contamination event might be at least as important as the direct inhalation of the contaminating cloud. The significance of the rapid change of particle resuspension with time may be important in considering precautions that may be necessary due to the occurrence of a change in environmental conditions. It may be anticipated that initial resuspension will be high and sheltering or protection from harmful contaminant materials may be especially important during the first few minutes after the onset of such conditions. Therefore, knowledge of resuspension processes is required if the full effects of a contamination event are to be assessed (Nicholson 1993).

Particle resuspension occurs in both indoor and outdoor environments. For indoor resuspension the time scale of interest is relatively short. In contrast, outdoor resuspension may need to be followed for time scales of several years (Kim, et al. 2010). The resuspension process usually contains two regimes. The first regime (short-term resuspension) lasts for a brief period of time (e.g., about 1 min). During this period, the

most easily resuspended particles (i.e., with less adhesion force) are removed either in groups or individually. The second regime (long-term resuspension) has much lower resuspension rate(s) (Ibrahim 2004). In many of the currently reported experiments, almost half the material removed during the entire duration of those experiments was lost from the surface within the first 10 s (Nicholson 1993). However, most of the existing data on resuspension were obtained months to years after initial deposition. These long term data sets are poor surrogates for short-term emergency response scenarios (Loosmore 2003, Kim et al. 2010).

Before particles become airborne, resuspension may involve rolling or sliding (Jordan 1954 and Hinds 1999). However, microvideographic observations of individual microparticle detachment conducted by Ibrahim (2004) and Ibrahim et al. (2003 and 2004a) showed that detachment of glass substrates occurs primarily as rolling motion along the surface and not as a lift off, until today no further effort has been conducted in quantifying such behavior experimentally especially in the first few seconds of particle detachment from the surface. Therefore, the aim of this study is to enhance the current knowledge about the fundamental dynamics of micro-particles in motion on surfaces, specifically in the short term resuspension, which occurs during the first few seconds of the particle detachments (Krauter and Biermann 2007). In addition, we seek to conduct a full study of particle resuspension from spherical microparticles under different environmental relevant conditions such as time, flow rate, particle size, particle type surface roughness and relative humidity.

2. LITERATURE REVIEW

2.1 Introduction

Determining source mechanisms for particles is difficult because the removal of particles from a surface involves a complex interaction of forces including fluid drag and lift, adhesion of particles to the surface, and the impact from particles in the flow striking particles on the surfaces Figure 2.1. The forces that promote or resist resuspension are

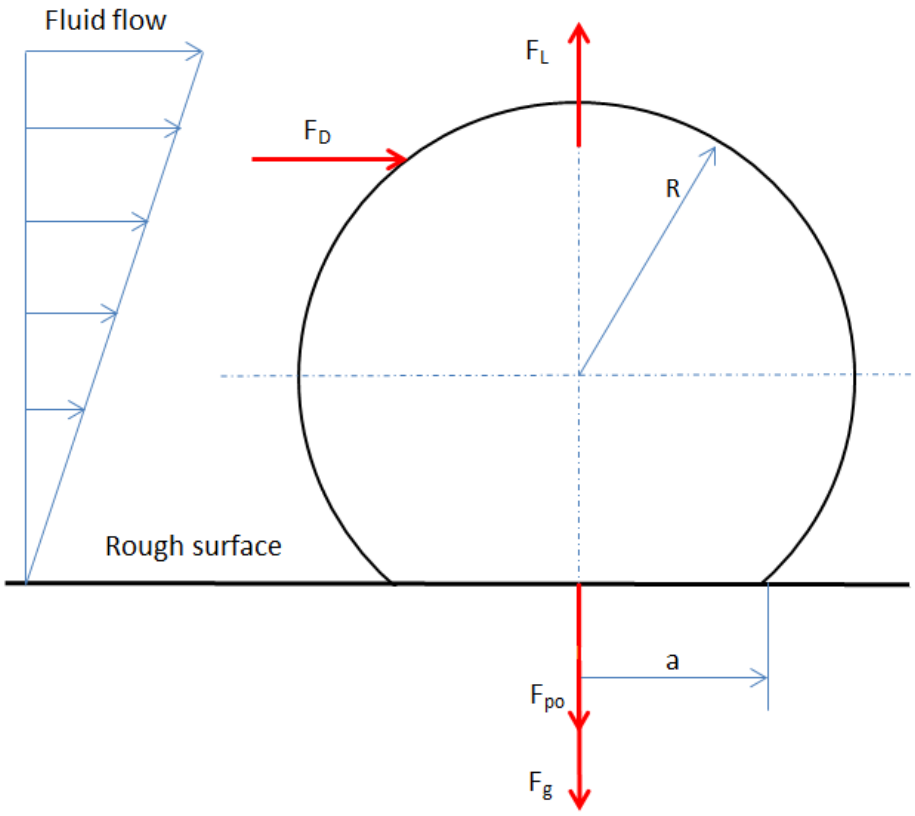

Figure 2.1 Forces acting on particles.

dependent on properties of the mean flow, surface roughness, and physical characteristics of the particle. It is not surprising, then, that resuspension of particles has been observed to vary over many orders of magnitude (Braaten et al. 1990).

In this section, the boundary layer condition and different forces acting on particles will be introduced, the resuspension phenomena will be discussed from the experimental and modeling point of view and finally problem statement and objectives will be clearly identified.

2.2 Boundary Layer

A boundary layer is a relatively thin layer of fluid close to a solid boundary in which the fluid velocity changes rather rapidly with distance from the boundary. Due to the effect of viscosity, the fluid in contact with a solid surface must move at the same velocity as the surface (the 'no-slip' condition). If the wall is stationary, the fluid velocity must fall to zero at the wall. Therefore, there will be a velocity transition between the near wall region and the boundary. At large Reynolds numbers this transition takes place in a thin layer near to the wall, Prandtl and Tietjens (1934) named this layer the boundary layer. The thickness of a boundary layer (the height from the solid surface where 99% of free stream speed) varies with streamwise position on the boundary. The boundary layer may be laminar or turbulent which depends on the Reynolds number but viscous forces dominate very near the wall even in the turbulent case (Figure 2.2).

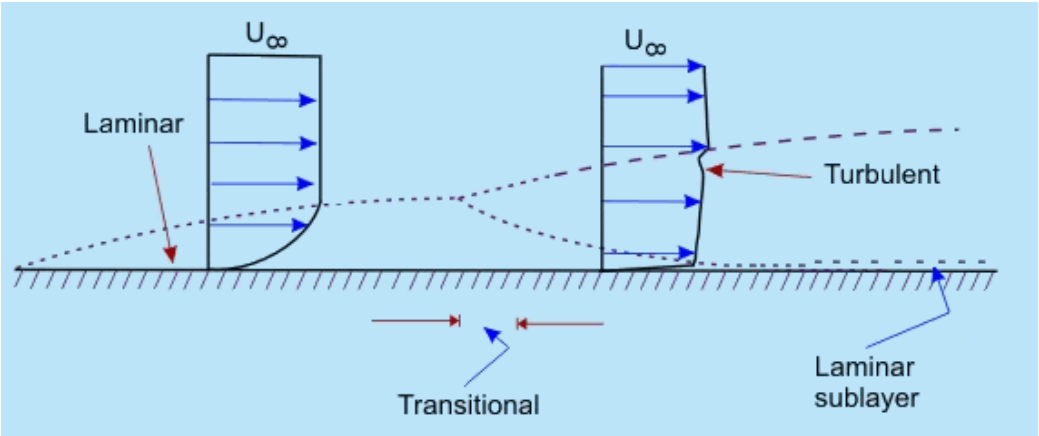

Figure 2.2. Laminar-turbulent transition.

In this study, particles resuspension is only considered in turbulent boundary layer. In a turbulent boundary layer, turbulent eddies rather than molecular viscosity are responsible for the exchange of mass, momentum and energy (except for the very thin viscous layer adjacent to the surface), and thus take place on a much bigger scale than for the laminar boundary layer (Boor, 2010 and Cleaver and Yates 1973).

The microparticles used in this study resided fully in the viscous sublayer, which is defined by wall-unit height $y^+ < 5$. The wall unit y equals yu*/ν in which y is the physical height above the wall and ν is the dynamic viscosity of the flowing medium and u* is the friction velocity (Ibrahim et al. 2008).

In general three regions in the flow are usually considered (Kay and Nedderman 1974):

Region 1: is the laminar sublayer which is a very thin layer close to the wall where turbulence is suppressed and viscous forces dominate, Equation 2.1.

$$U^+ = Y^+, \left(0 < Y^+ \le 5\right) \tag{2.1}$$

Region 2: is the buffer zone where turbulence is generated and viscous and turbulence stresses are of same order of magnitude, Equation 2.2.

$$U^+ = 5\ln Y^+ - 3.05, \left(5 < Y^+ \le 30\right) \tag{2.2}$$

Region 3: is the outer layer where turbulence dominates, Equation 2.3.

$$U^+ = 2.5\ln Y^+ + 5.5, (30 < Y^+) \tag{2.3}$$

where, $U^+ = \frac{U}{u*}$, $Y^+ = \frac{yu^*}{\nu}$, U is the average air velocity recorded using the hot film anemometry (HFA) and u^* is the friction velocity calculated from Equation (2.4).

$$u^* = U\sqrt{\frac{C_f}{2}} \tag{2.4}$$

where, C_f is the friction coefficient, $C_f = \frac{f}{4}$, f is Moody (or Darcy) friction factor that is commonly obtained from Moody diagram (Moody and Princeton, 1944). In addition to depending on Reynolds number, the friction factor is a function of the tube surface conditions. It is minimal for smooth surfaces and increases with increasing surface roughness (Incropera and DeWitt 2002). However, the friction velocity calculations using the Miller (1996) equation as a suggested iteration for Moody diagram, $f = 0.25\left[\log\left(\frac{\varepsilon/D}{3.7} + \frac{5.74}{\mathrm{Re}^{0.9}}\right)\right]^{-2}$, showed that in our surface roughness range the friction velocity change due to roughness effect was in the 10^{-4} order (which can be assumed insignificant) and the results agreed till 10^{-3} with that obtained from the Blasius

correlations $f = \frac{0.316}{\mathrm{Re}^{0.25}}, \mathrm{Re} \le 10^5$. Hence, for simplicity the Blasius form was used to obtain the friction factor in this study. *Re*, the Reynolds number, was calculated based on the hydraulic diameter, D taken to be the hydraulic diameter, and ε is taken as the mean roughness, Ra. It should be noted that the Blasius correlation is valid for turbulent flow in smooth pipes using the hydraulic diameter, in the Reynolds calculations according to Fox et al. (2004), provided that the turbulent entry length to reach the fully developed turbulence flow, $\left(x/d_h \right)_{entry} = 0.623\,\mathrm{Re}^{0.25}$ (Kays et al. 2005) and the Turbulent boundary layer thickness $\delta = 0.37\left(\frac{\nu}{U}\right)^{1/5} x^{4/5}$ (Prandtl and Tietjens 1934).

2.3 Forces Acting on a Particle

When a particle is moving in a flow, different forces are generated from either the fluid properties such as viscosity or the properties of the particle itself. In this section, the aerodynamic forces will be described in detail.

2.3.1 Drag Force and Faxen Force

The Stokes drag for a sphere in a uniform steady incompressible flow in the absence of any wall is given by Equation (2.5).

$$F_d = 3\pi\mu_f dV \tag{2.5}$$

where *V* is the uniform flow velocity and μ_f is the fluid viscosity.

In 1968, O'Neill suggested that the presence of the wall increases the drag by a factor f_o=1.7 as given by Equation (2.6)

$$F_d = 3\pi f_0 \mu_f dV \tag{2.6}$$

The Stokes drag force is based on a uniform free stream velocity; for non-uniform flow field an additional force was derived by Happel and Brenner (1973) which is called the Faxen force (Equation 2.7)

$$F_F = \pi \mu_f R^2 \nabla^2 V \tag{2.7}$$

where R is the particle spherical radius.

2.3.2 Gravitational Forces

The gravitational force for a spherical particle with radius *R* and material density ρ_p can be calculated from Equation (2.8)

$$F_g = \frac{4}{3}\pi R^3 \rho_p g \tag{2.8}$$

2.3.3 Lift Force and Magnus Forces

Lift force is the force generated due to particle inertia and shear rate, which causes the particle to travel normally to the flow direction (perpendicular to the direction of the drag) and was extensively discussed in literature. Several authors have estimated the lift forces on spheres by obtaining approximate solutions to the equations of motion of a fluid around a sphere and obtained different formulas as shown in the following set as will be discussed in details in this section.

O'Neill (1968) derived a solution for the forces acting on a sphere upon a surface by assuming that only viscous effects contributed to the forces experienced by the particle, effects due to the inertia of the fluid being neglected. In this case, there was no force normal to the direction of flow. Saffman (1965) derived an expression for the force acting upon the sphere in a direction normal to the fluid flow. However, this solution is only valid for a particle in the body of a fluid and would not be expected to hold for a sphere on or near to a surface. Leighton and Acrivos (1985) extended O'Neill's analysis to include first-order effects of inertia in a similar manner to Saffman. However, their solution is only strictly valid when the shear Reynolds number is much less than one, and is therefore of limited applicability, Equation (2.9)

$$F_L^+ = 9.22 R^{+4}, R^+ \ll 1 \tag{2.9}$$

Hall (1988), measured the mean lift force on a sphere several millimeters in diameter and obtained Equation (2.10)

$$F_L^+ = (20.90 \pm 1.57) R^{+(2.31 \pm 0.02)}, 1.8 < R^+ < 70 \tag{2.10}$$

Mollinger and Nieuwstadt (1996), measure the mean and fluctuating lift force, Equation (2.11)

$$F_L^+ = (56.9 \pm 1.1) R^{+(1.87 \pm 0.04)}, 0.3 < R^+ < 2 \tag{2.11}$$

where F_L^+ is defined as $F_L \Big/ \rho_f \nu^2$, F_L is the mean aerodynamic lift forces, ρ_f is the fluid density, $R^+ = Ru^* / \nu$.

The Magnus force is caused by particle rotation. Due to the velocity difference between the two sides of the particle, there is a pressure difference across the particle

surface. In 1961, Rubinow and Keller derived an analytical expression for the Magnus lift force on a spinning sphere Equation (2.12).

$$F_M = \frac{1}{8}\pi\rho_f D^3 \left[\left(\frac{1}{2}\nabla \times u - w_p \right) \times (u - v) \right] \tag{2.12}$$

2.3.4 Normal Pull-off Forces

The normal pull-off force is the force applied in the normal direction required to overcome the adhesion force. Adhesive forces include intermolecular forces such as van der Waals interactions, various chemical (Krupp 1967). Surface roughness also plays an important role in adhesion. The adhesion of small particles on rough surfaces is mainly determined by the geometrical features of the surface particle system (Katainen et al. 2006).

In 1896 Hertz investigated the contact between two smooth elastic bodies and demonstrated that the contact radius (distance between the centers of the mass of two bodies) between two spheres is a function of the sphere radii and the force acting on them, Equation (2.13)

$$R_c^2 = \frac{3}{4}\pi (k_1 + k_2) \frac{R_1 R_2}{R_1 + R_2} F_{pf} \tag{2.13}$$

where R_c is the contact radius, R_1 and R_2 are sphere radii, F_{pf} is the interaction force (Press forces) between spheres and, k_1 and k_2 are elastic constants for each sphere Equation (2.14).

$$k_i = \frac{1 - \nu_i^2}{E_i} \tag{2.14}$$

where, ν_i is Poisson ratio and E_i is the Young modulus of elasticity.

Johnson et al. (1971) modified Hertz contact equation to develop the JKR adhesion model by taking into account the surface energy effects within the contact region and by allowing for deformation of the particle and the substrate surface Equation (2.15). The JKR model considered one of the most commonly used adhesion models beside the DMT (Deryagin et al. 1975) Model.

$$\frac{a^3 K}{R} = P + 3\pi\gamma R + \sqrt{6\pi\gamma RP + (3\pi\gamma R)^2} \tag{2.15}$$

where a is the contact radius made by microsphere when it resides on the surface, γ is the surface energy of adhesion, P is the applied load and K is the effective material stiffness, Equation (2.16).

$$K = \frac{4}{3(k_1 + k_2)} \tag{2.16}$$

The JKR theory predicts that separation would occur upon application of a negative load as shown in Equation (2.17) with a radius, a_s Equation (2.18).

$$F_{po_s} = 1.5\pi\gamma R \tag{2.17}$$

$$a_s = \frac{a_{eq}}{4^{1/3}} \tag{2.18}$$

where, at equilibrium, P=0 and a_{eq} is given by Equation (2.19)

$$a_{eq} = \left(\frac{6\pi\gamma R^2}{K} \right)^{1/3} \tag{2.19}$$

By contrary, the DMT model assumes that adhesion acts outside Hertz contact region and the normal pull-off force can be estimated by the following set of equations, as earlier shown by Ibrahim (2004).

$$\frac{a^3 K}{R} = P + 2\pi\gamma R \tag{2.20}$$

$$F_{pos} = 2\pi\gamma R \tag{2.21}$$

$$a_{eq} = \left(\frac{2\pi\gamma R^2}{K} \right)^{1/3} \tag{2.22}$$

In both models the Van der Waals adhesion forces was considered under a normal load for a perfectly smooth micro-particle and substrate. Several attempts have been made to reconcile the two approaches. Tabor (1977) theorized that the JKR model applied to soft systems (low elastic moduli, high surface energies), while the DMT model applied to hard systems (high elastic moduli, low surface energies).

It is clear that the pull-off forces estimated from the DMT model (Equation 2.21) is 4/3 times the JKR force given by Equation 2.17. Accordingly, Tabor (1977), investigated such difference by introducing Tabor's parameter, μ_T (Equation 2.23).

$$\mu_T = \left(\frac{R\gamma^2}{E^2 \varepsilon^3} \right)^{1/3} \tag{2.23}$$

The Tabor's parameter is a non-dimensional parameter that considers the adhesion surface energy (γ), microsphere radius (R), equilibrium spacing, ε, and material elastic modulus (E) given by Equation (2.24).

$$\frac{1}{E} = \frac{1-\nu_{r1}^2}{E_1} + \frac{1-\nu_{r2}^2}{E_2} \tag{2.24}$$

where, E_1, E_2 are the Young modulus for the microparticle and the surface and ν_{r1}, ν_{r2} are the Poisson's ratio modulus for the microparticle and the surface.

According to Tabor (1977), the DMT model is valid for $\mu_T < 0.1$ and the JKR model is valid for $\mu_T > 5$.

2.3.5 Surface Roughness Effect

Increasing surface roughness significantly reduces the pull-off forces (Cheng et al. 2002). In Cheng (2002) study they produced a map that can be used to find the reduced pull-off forces due to the surface roughness effect for different Tabor parameter values (Figure 2.3). The non-dimensional mean pull-off force, C is the ratio between the rough and the smooth pull-off forces, Equation (2.25) and σ_S can be obtained from $\sigma_S = \frac{\sigma_s}{\varepsilon}$ where $\varepsilon \approx 4$Å and $\sigma_s = R_a$ (mean surface roughness).

$$C = \frac{F_{po}}{F_{po_S}} \tag{2.25}$$

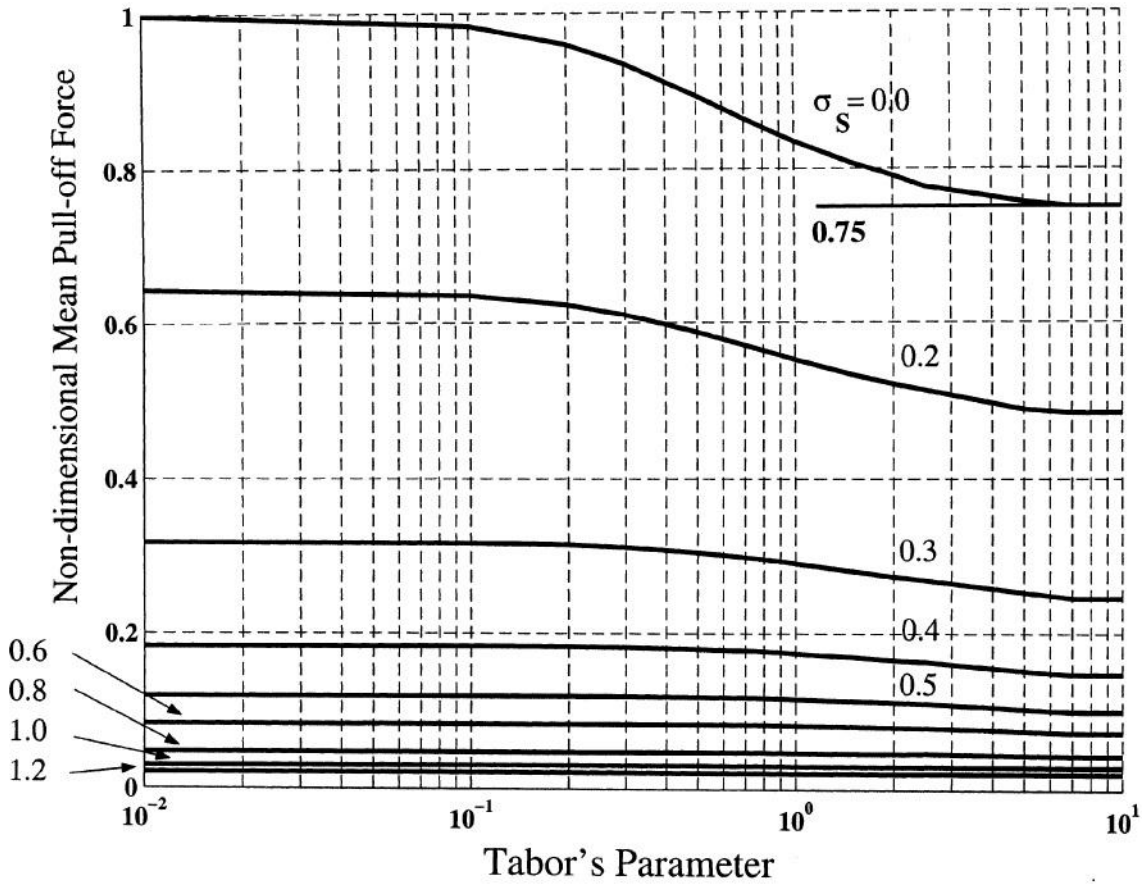

Figure 2.3 The mean Pull-off force as a function of Tabor's parameter and surface roughness (Cheng et al. 2002).

2.4 Experiments

The term *resuspension* refers to a phenomenon in which particles, initially on a surface, join the passing fluid stream. In the literature, previous resuspension investigations proposed different ways to quantify the resuspension phenomena. The commonly used techniques are based on the calculation of percentage lost (Jordan, 1954

and, Corn and Stein 1966), removal efficiency (Corn and Stein 1965), resuspension rate (Nicholson 1993, Wu et al. 1992, and Qian and Ferro 2008), resuspension fraction (Ardy and Mayinger 1998), detachment fraction (Ibrahim et al. 2003; 2004b; 2006), percentage detached (Goldasteh et al. 2010), or effectiveness (entrainment efficiency) (Grzybowski and Gradoń 2007). All of these methods require counting of the number or mass of seeded particles on the sample by either a filter that collects the resuspended particles (Grzybowski and Gradoń 2007), microscope (Corn and Stein 1965 and Wu et al. 1992) or camera recording (Ibrahim et al. 2003 and Goldasteh et al. 2010). Another approach to characterize resuspension involves measuring the threshold velocity or saltation velocity. Threshold velocity is usually defined as the velocity required to resuspend a single particle (Braaten 1994) or the velocity to resuspend 50% of the particles (Ibrahim et al. 2003; Ibrahim 2004). However, the saltation velocities are limited to the minimum fluid velocities required to carry solids at a specified rate without allowing them to settle in a horizontal pipe (Zenz 1964). Another term to quantify the resuspension is the relative resuspension fraction, defined as the ratio of particles removed under the given flow conditions to the total particles available for removal by the passing flow (Mukai et al. 2009).

Regardless of the experimental techniques that were used to quantify the resuspension throughout the years, the main target was to increase the accuracy of the previous experiments to enhance the current knowledge about the resuspension phenomena. In our experiment we will use a high speed camera (up to 4000 frame/s) to enable high-speed high-resolution tracking of individual particle trajectories near

surfaces within the period of 0 to 5 s. The analysis will be based on the terms detachment percentage defined as the number of particles detached from the surface at a certain time compares to the number of particles initially deposited on the surface and the resuspension rate, defined as the fraction of deposited particles resuspension per unit time (Slinn 1978). The assumption of no particle deposition onto the surface during the experimental measurements will be considered throughout the full investigation (Wu et al. 1992). The first term, detachment percentage as discussed earlier is mainly used in the previous experimental investigations, however the second term, resuspension rate is commonly used in the imperial modeling (Kim et al. 2010) due to the difficulties associated in its evaluation in field conditions. However few works discussed how to obtain it experimentally (Wu et al. 1992 and Nicholson 1993).

Aerosol particles attach firmly to any surfaces they contact which distinguish them from gas molecules and from millimeter-sized particles (Hinds 1999). While the transport of molecular species in gas phase flows is relatively well understood because they generally follow the bulk flow, transport behavior in particulate laden flows is considerably more complex and is strongly affected by different environmental conditions such as time, flow rate, particle size, particle type, surface roughness and relative humidity.

In turbulent airstream, there is a thin layer of laminar flow at the surface called the boundary layer or laminar sublayer. Particles smaller than this layer are partially protected from reentrainment by being submerged in the boundary layer. Reentrainment of these particles occurs as a result of occasional bursts of turbulent eddies penetrating

through the boundary layer to detach particles. Such reentrainment is time dependent because the probability that a particle will encounter a turbulent burst with sufficient energy to cause detachment increases with time (Corn and Stein 1965; Grzybowski and Gradoń 2007). These results also suggest that the fluctuation of the air velocity associated with the unsteady state flow conditions helps either the penetration of eddies of turbulence into the boundary layer from the main stream, or the turbulence created in the laminar sublayer by particle interaction with the air stream that will increase particle resuspension. The resuspension rate was observed to fall rapidly with increasing time for both grass and concrete surfaces (i.e. that resuspension rate declines with time as most of the resuspendable particles are removed) (Nicholson 1993). Corn and Stein (1966) exposed a glass substrate (microscope slide) with atmospheric dustfall particles to a high velocity air stream with a well-defined velocity profile. It required bulk air velocities as large as 150 m/s to remove 50% of adhering atmospheric dust particles of 11.5 μm. However, it was even more difficult to remove glass beads than the fly ash particles of the same size.

The important factor in the handling of dust is the fact that the particles will adhere to each other and to solid surfaces. Jordan (1954) raised the importance of changing the surface roughness for particle resuspension. The surface roughness could change the lift force up to factor of six. Roughness can reduce the lift force if the particle is deposited between roughness elements and can increase it if the particle is on the top of a single roughness element (Hall 1988). The deposition of surrogate biological weapon agents was significantly different in the three duct materials evaluated (Krauter

and Biermann 2007). Spore transport efficiency ranged from 9 to 13% in steel and fiberglass ducts; transport efficiency was far less (0.1 to 4%) in plastic duct. Dominant factors affecting the deposition velocity included the static charge attraction between spores and the plastic duct, the macro roughness of folds in the plastic film, or the joint-seam and corrugated connectors in galvanized steel. Qian and Ferro (2008) concluded that hard floor could be a better choice than carpet for reducing particle resuspension. Lohaus et al. (2008) found that velocities of more than 5 m/s were required to resuspend 50% of 3.2 μm particles from linoleum and wood surfaces. In general, high turbulence and high velocity conditions minimized the differences between materials (Mukai et al. 2009). Goldasteh et al. (2010) showed that resuspension from wood flooring was easier than from linoleum flooring and they suggested that the difference in the adhesion force (surface energy) and the nature of the micro roughness is the main reason for such behavior. Experiments have shown that adhesion forces increased with increasing relative humidity (Hinds 1999). A common formulation of the resuspension process of deposed particles is based on a balance of all forces applied to a particle. The main reference value is the minimum flow velocity, where aerodynamic lift plus viscous drag and adhesion sticking the particle to the boundary surface counterbalance each other. When humidity leads to additional adhesion / cohesion by capillary forces and surface tension, this reference velocity reaches a maximum (Ardey and Mayinger 1998). Generally, the resuspension rate should be reduced at high relative humidity, according to Cohen (1977) and Ibrahim et al. (2003), due to the adsorption of water vapor at the particle-surface interface and its effects on adhesion. Corn and Stein (1965) found

almost no change in adhesion forces when the relative humidity was below 30%, however, detected a rapid increase at higher values. Grzybowski and Gradoń (2007) reported that increasing the relative humidity from 15% to 80% increase the efficiency from 26% to 58% respectively. However, this particular study was based on powder samples (multilayer of dust) conditioned for over 10 hours compared to a single layer of microparticles in the Ibrahim study. While individual particles with sizes less than 10 μm are not likely to be removed by common forces, a thick layer of such particles may be easily dislodged in large (0.1-10mm) chucks (Hinds 1999). Very likely, increasing the relative humidity causes the particles to adhere tightly to each other, forming large agglomerates that can be easily blown or shaken from the surface. On the other hand, no significant effect was found for relative humidity in the 30–50% range on particle resuspension of 0.1–10 μm test particles, (Qian and Ferro 2008). This disagreement in the literature evoked our interest to further investigate the effect of the relative humidity on particle resuspension.

On the other hand, resuspension may involve rolling or sliding (Jordan 1954, Masironi and Fish 1964, and Hinds 1999). Ibrahim et al. (2003) indicated that the microspheres undergo pure rolling along the surface before possible entrainment and this sweeping motion plays a role in the detachment process. However, the effect of particle surface interaction remained unknown since only microscopic glass surfaces were used during his entire investigation. Similarly, the particle trajectory immediately before liftoff was not investigated.

2.5 Problem Statement and Objectives

Despite extensive resuspension studies, there is still a significant lack of information regarding the path of particles very close to the surface (Harris and Davidson 2008). Such information is needed to provide insight in the micro-mechanism of particle removal (Zhang and Ahmadi 2000). This work presents an experimental investigation of the conditions under which a transient fluid flow causes spherical glass microparticles, 10-100 μm in size range, to detach from different surfaces. The general approach is to observe individual microparticle motion during short term resuspension, and to focus on the basic detachment mechanisms of the resuspended particles to fully understand and quantify their behavior immediately before liftoff. In our experiments we use a significantly higher frame rate (up to 4000 frame/s) to precisely capture the trajectories of individual particles immediately before liftoff from different surfaces. These new observations can help provide a better understanding of particle surface interactions prior to liftoff under different environmentally relevant conditions.

3. MATERIALS AND EXPERIMENTAL METHODS

3.1 Materials

3.1.1 Particles

Different micro-particles were used to test the resuspension phenomena with different densities, size and shapes. The different particles where, glass beads, GB, (Polysciences, Inc., Warrington, PA), spherical in shape with specific gravity of 2.48-2.52 g/cm^3 with different size ranges (Poisson ration: 0.28, Young Modulus: 80.1 GPa), (Figure 3.1), stainless steel microspheres, SS, (Duke Scientific; diameter: 64-76 μm), (Figure 3.2), with a much higher density of 8000 kg/m^3 (Poisson ration: 0.28, Young Modulus: 215 GPa) and finally, *Bacillus thuringiensis* var. *kurstaki (Btk)* a clusters of about 5-7 μm, (Figure 3.3).

A Multisizer™ 3 Coulter Counter (Beckmann Coulter, Inc., Fullerton, CA) was used to verify the particle size distribution and obtain the mean diameter corresponding to each particle size range for the glass beads particles (Figure 3.4). The mean diameters are 26.41 μm for the 10-30 μm particles range, 36.24 μm for the 30-50 μm particles range, and 45.31 μm for the 50-100 μm particles range.

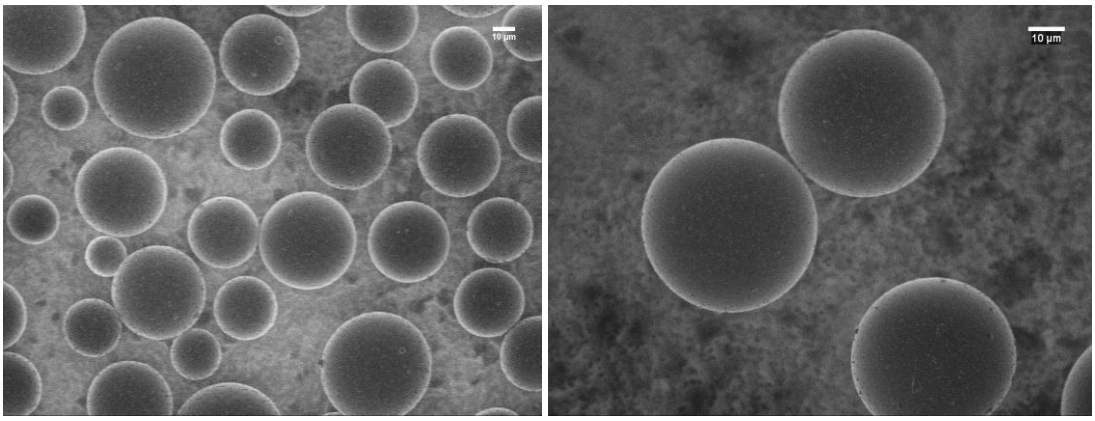

a **b**

Figure 3.1 Field emission scanning electron microscope (FE-SEM) images of the spherical microparticles used in the experiment, a) (10-30) µm glass beads, and b) (30-50) µm glass beads.

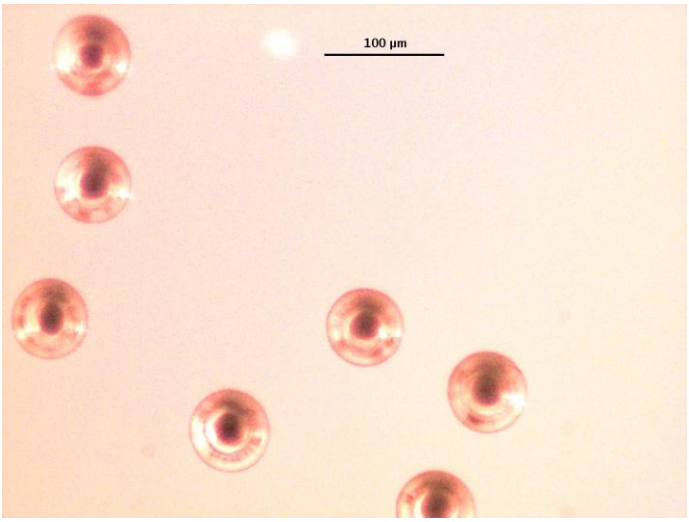

Figure 3.2 Stainless steel microparticles (64-76 µm) taken with an optical microscope (Ibrahim, 2004).

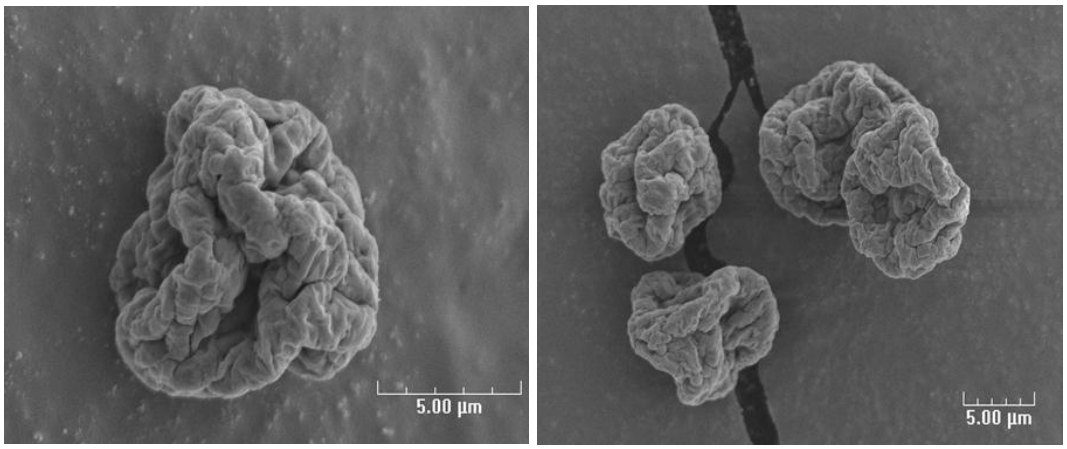

Figure 3.3 Scanning electron microscope (SEM) images for the *bacillus thuringiensis* var. *kurstaki* (Btk) clusters generated by the ink jet aerosol generator (IJAG).

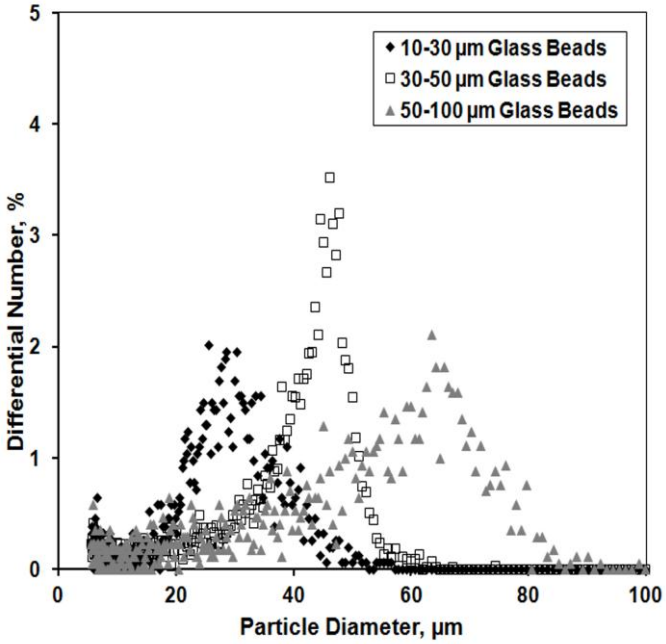

Figure 3.4 Particle size distribution of the glass beads particles using a multisizer™ 3 coulter counter.

On the other hand, *Bacillus thuringiensis* var. *kurstaki (Btk)* is a member of the genus Bacillus and like the other members of the taxon has the ability to form endospores that are resistant to inactivation by heat, desiccation and organic solvents. The spore formation of the organism varies from terminal to subterminal in sporangia that are not swollen, therefore, *B. thuringiensis* resembles other Bacillus species in morphology and shape (Stahly et al. 1991). The organism is Gram-positive and facultative anaerobe. The shape of the cells of the organism is rod. The width of the rod varies 3-5 μm in size when grown in standard liquid media. The most distinguishing feature of *B. thuringiensis* from closely related bacillus species (e.g. *B. cereus, B. anthracis*) is the presence of a parasporal crystal body that is near to the spore, outside the exosporangium during the endospore formation, which is shown in Figure 3.5 (Andrews et al. 1985; Andrews et al. 1987; Bulla et al. 1985).

Due to the current camera resolution, a maximum of 0.9 μm/pixel. A single *Bacillus thuringiensis* var. *kurstaki (Btk)* was hardly detected by the MTLAB code; hence bigger clusters of about 6.41 μm aerodynamic diameter will be considered during our entire investigation, Figure 3.6.

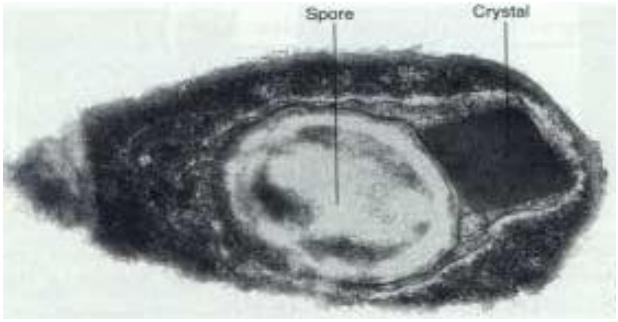

Figure 3.5 Formation of the toxic parasporal crystal in *B. thuringiensis* (Madigan et al., 2000).

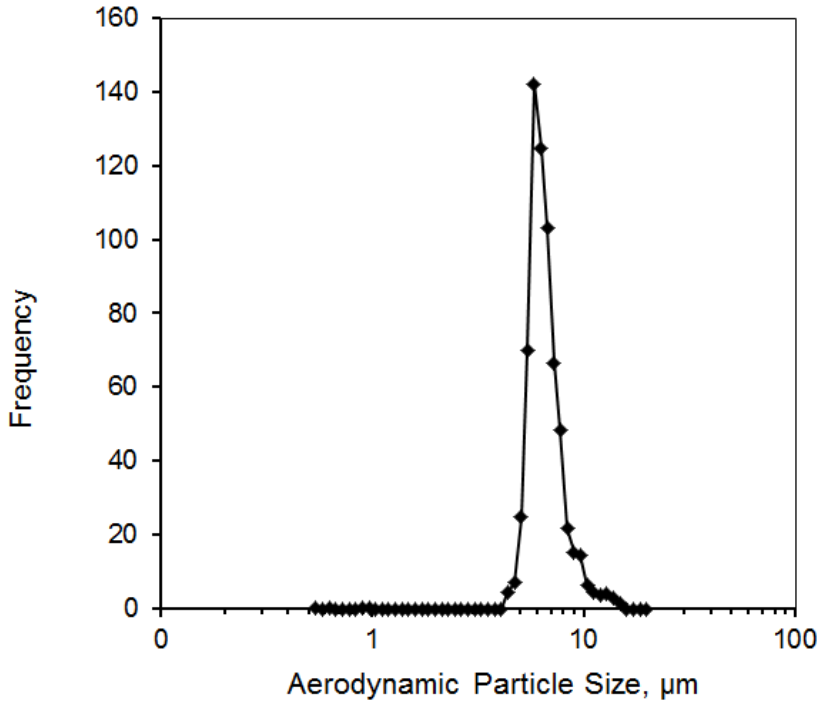

Figure 3.6 Particle size distribution for the Btk by the aerodynamic particle sizer.

3.1.2 Substrates

3.1.2.1 Common Flooring

The substrates used in these experiments were hardwood, ceramic and glass slides (Fisherbrand 0.16 to 0.19 mm thick; Size: 22 mm).

Atomic force microscopy (AFM) (Veeco, Plainview, NY) was used to scan the glass surfaces and determine their roughness-height distributions as done earlier by Ibrahim et al. (2003), (Figure 3.7). For the other substrates, the surface characteristics of the samples were analyzed using a Dektak 3 Stylus Profilometer (Veeco, Plainview, NY) based on the method of Boor et al. (2011).

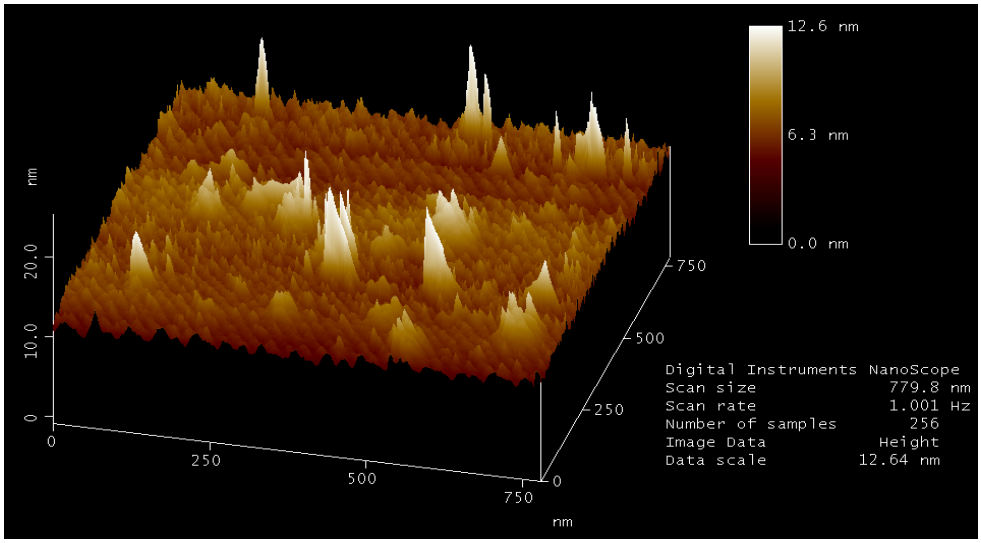

Figure 3.7 3-D Roughness-height distributions of the glass surfaces measured using an atomic force microscope (AFM).

In this study the surface roughness parameter was taken as the mean roughness (Ra), defined as the arithmetic average deviation from the center plane. Results based on 3 different replicates show Ra values of $(0.536 \pm 0.054) \times 10^{-3}$ µm, 0.038 ± 0.020 µm, and 0.072 ± 0.002 µm for glass, ceramic and hardwood substrates respectively.

3.1.2.2 Paint Coating Effect on Metal Substrate

The substrates used in these experiments were Chemical Agent Resistant Coated metal (CARC) or non-coated metal used in military tanks. Stylus Profilometer was used to scan both surfaces and determine their roughness-height distributions. In this study the surface roughness parameter was taken as the mean roughness (Ra), defined as the arithmetic average deviation from the center plane. Results based on 5 different replicates show Ra values of 0.09 ± 0.04 µm, and 1.2 ± 0.5 µm for non-coated metal, and CARC coated metal substrates respectively.

3.2 Experimental Methodology

In this section, the different experimental setups used to produce the experiments will be discussed in details. First the main setup (Resuspension setup) that was used to resuspend the different particles will be discussed in details. Next the Bacterial spore clusters generation will be discussed as the deposition setup. In addition to the relative humidity and velocity measurements different setups arrangements will also be detailed in this section.

3.2.1 Resuspension Setup

A schematic of the Resuspension experimental setup used in this study is shown in Figure 3.8. The setup consists of a 10 cm x 10 cm (4" x4") square duct that is 180 cm long (6 feet). The square duct was divided into 3 sections: an entrance section of 91 cm (3 feet) length made from aluminum material, a 30 cm (1 foot) length of PC-300™ Polycarbonate that will be later referred to as the test section, and a final 61 cm (2 feet) length of the same material as the entrance section. Both particle flow visualization and flow-field velocity measurements were conducted in the test section. The test section incorporates a clear antistatic polycarbonate material to eliminate any static charges surrounding deposited particles and enable a clear view of particle motion. Four adjustable speed blowers (Thermo Anderson, Smyrna Georgia, USA) were connected to the setup using a flexible connection to minimize vibration caused by the blower and setup. A 2.5 cm thick layer of insulation material was added to the bottom of the setup to enable flush mounting the different substrates. The substrates were inserted at the bottom of the test section at a distance of 80 cm upstream from the blowers. The substrates were cleaned with ethanol to neutralize the surface, minimize contamination and reduce electrostatic charges (Boor et al. 2011).

High speed cameras (Photron, Fastcam Ultima APX Imager) and/or (Phantom, Vision Research) were used to monitor the particles detached from the surface with respect to time. The camera locations were different depending on the type of measurement obtained. To attain a global idea about particle detachment and resuspension rate, the camera was located in the top (x-y plane) to detect the change of particle numbers with

respect to time which is a widely used technique in literature (Ibrahim et al. 2003). In this case the particles were initially deposited as a single layer on the top of different substrates by gravitational settling. Additionally, to get a more details idea about the effect of particle surface interaction on particle initial motion prior to liftoff, the camera was located in the side (x-z plane). In this case, individual particles were tracked to specify the type of motion.

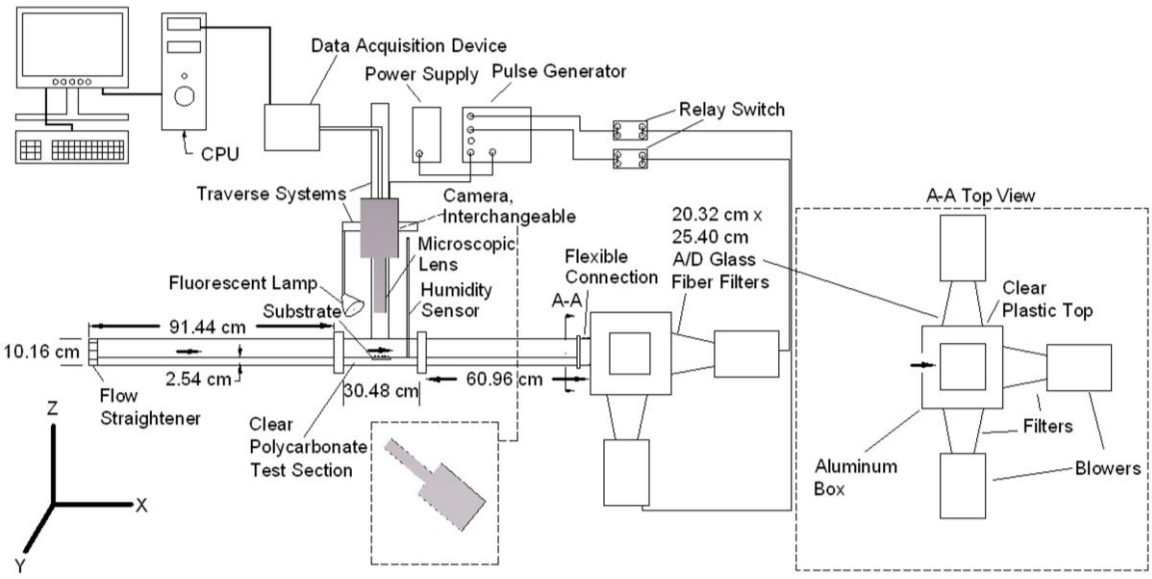

Figure 3.8 Test setup used in the resuspension studies.

the particle path trajectory obtained prior to particle liftoff. Although the particle motion prior liftoff was identified numerically in literature as rolling/ sliding (Hinds 1999 and Ibrahim et al 2003), it was never been verified experimentally (Harris and Davidson,

2008, and Zhang and Ahmadi 2000). In addition, initial 3-D measurements were also conducted by taking measurements for individual particles from both top and side cameras simultaneously (x-y-z plane). A telecentric lens (1-4.5x magnification and/or 10x magnification (Moritex U.S.A., Inc. San Jose, CA)) was mounted on the cameras to clearly capture individual particle motion, using a halogen light source. A calibration frame was taken before each experiment to determine the field of view for both camera locations (side and top view). The camera displacement was adjusted using a BiSlide traverse system (VELMEX, Inc., Bloomfield, NY). Image acquisition was synchronized with the blowers to automatically trigger the camera while starting the air flow with a specially designed electric circuit. The circuit contains 2 relay switches (TE Connectivity Solid State Relays, TX, USA), a regulated power supply (Model PAD, Kikusui Electronics Corporation, Japan) and a pulse generator (Quantum Composers, Bozeman, MT). The triggering was mainly added to capture the time dependence of particle detachment with the minimum error possible. In this case the error can be a maximum of 1/frame rate. The camera output is connected to a computer for image analysis. Particle detection and centroid estimations for the videos and frames taken by the high speed camera were calculated based on a MATLAB code developed by Estrada-Pérez (2009).

The air was drawn to resuspend the particles from an open entrance using 4 adjustable speed blowers. A flow straightener was located at the entrance of the duct to eliminate swirl and to produce highly repeatable flow profile. Each blower was connected to A/D glass fiber filters (8x10", Pall Corporation, Michigan) and a variable

autotransformer (STACO Energy Product Co., Dayton, OH. USA). A freshly calibrated air velocity meter (VelociCalc, TSI, Inc. Shoreview, MN) was located in the test section downstream the substrate to simultaneously monitor the speed and the environmental conditions (air flow relative humidity and temperature). All experiments were initially conducted at room temperature and relative humidity of 24.1 ºC ± 0.9 ºC with 0.03 ºC/ºC uncertainty and 38.5% ± 3.0 % with 0.2% RH/ºC uncertainty respectively.

3.2.2 Deposition Setup

To create single layer deposition of aerosolized single clusters *Bacillus thuringiensis* var. *kurstaki* (Btk), tests with the Ink Jet Aerosol Generator, IJAG were conducted. The exhaust flow tube of the IJAG, which is 15 mm diameter, was placed in close proximity to the center of glass substrate to capture the generated particle. To generate the bacterial stock suspension, 25 mg of the Btk powder was suspended in 5 mL of MQ water and centrifuged using Centrifuge 5804 (Eppendorf, Hamburg, Germany) at 4000 rpm for 7 minutes in order to remove traces of the culture medium. The supernatant was aspired and the pellet was resuspended in 500 mL of 5% PBST (Phosphate Buffer Saline with 0.1% Triton X-100, pH 7.4).

An Ink Jet Aerosol Generator, IJAG (Bottiger et al. 1998, Bottiger and Deluca 1999) Figure 3.9, was used to create near-monodisperse clusters of Btk through atomization of a stock suspension that was prepared using powdered Btk spores. The IJAG has provisions for drying and electrically neutralizing the aerosol, and has an output aerosol flow rate of 1 L/min. It produces near-monodisperse droplets that are

approximately 50 μm diameter at a selectable rate that is typically 50/s. Mean size of the clusters was controlled through selection of Btk concentration in the hydrosol. Aerosol output from the IJAG was sampled with an Aerodynamic particle sizer, APS, (Model 3321, TSI Inc, Shoreview, MN) before and after each near-monodisperse particle test, using the arrangement shown in Figure 3.9, where the 1 L/min output flow rate of the IJAG was drawn into the APS, which has a sampling flow rate of 1 L/min. Particle size distribution analyzed by the APS shows a peak values at 6.5 μm Figure 3.6.

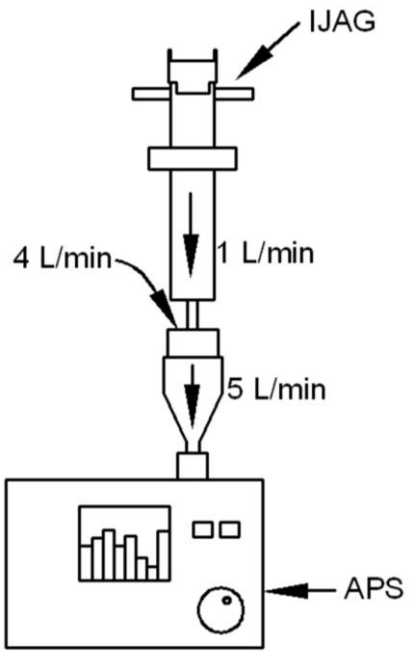

Figure 3.9 Schematic for the ink jet aerosol generator (IJAG) used to generate the *Bacillus thuringiensis* var. *kurstaki* (Btk) clusters.

3.2.3 Relative Humidity Setup

The setup shown in Figure 3.10 was constructed to increase the substrates relative humidity for the relative humidity study that was mainly investigated using the glass substrates. The relative humidity was adjusted by aerosolized water droplets using a six-jet Collison nebulizer (Model CN60, BGI Incorporated, Waltham, MA) with a 30 mL of the MQ water. Filtered air pressure for the nebulizer was set at 138 kPa (20 psig). The nebulizer was connected to a 3 inch PVC pipe diameter of 38 inch long to insure a sufficient drying path. The pipe was then mounted vertically with one end connected to the nebulizer with HEPA filter supplied air and the other end is connected to the center top of a 12"x 12" x 12" chamber. The particles were initially deposited on the glass substrates (18x18 square No.1½ Corning® cover glasses are made from No. 0211 zinc titania glass and are 0.16 to 0.19mm thick) by gravitational settling then inserted on the bottom of 12" x 12" x 12" chamber. A mixing element was also mounted in the top of the chamber to insure a uniform mixing during aeroslization. The seeding time period was adjusted to provide sufficient concentration to reach the desire relative humidity, typically 90% in this case. The relative humidity was monitored at all-time using the VelociCalc air velocity Meters (TSI, Inc. Shoreview, MN).

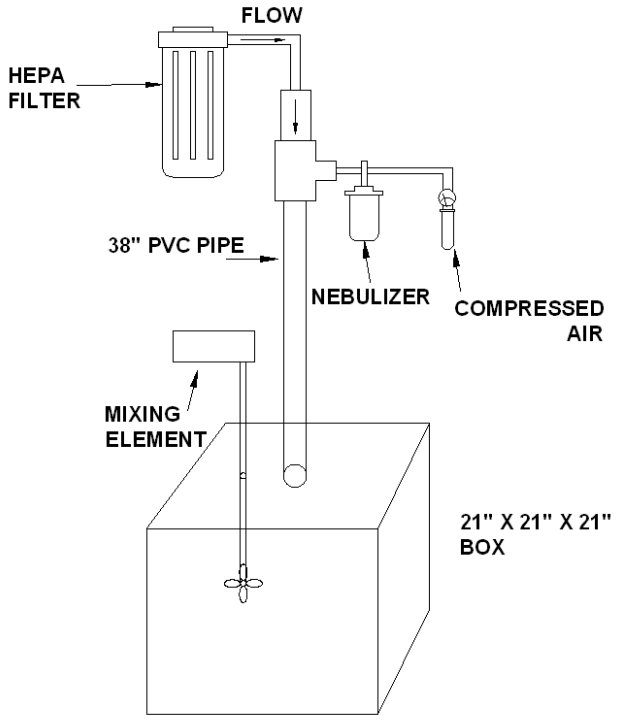

Figure 3.10 Relative humidity experimental setup.

3.2.4 Air Velocity Setup

A single probe TSI IFA 300 constant temperature hot film anemometer (HFA) was used to verify the velocity profile (Figure 3.11). The HFA calibration procedure was based on a flow with known and uniform velocity field (Figure 3.12). A calibration curve was developed based on King's Law with a mean square error of 0.997×10^{-3}. A relation between measured voltage and velocity was developed based on King's law shown below in Equation 3.1. For the calibration performed in this experiment the

constants were found to be; A=1.58; B=0.844, 1/n=0.5 with a mean square error of 0.000997.

$$E^2 = A + BU^n \tag{3.1}$$

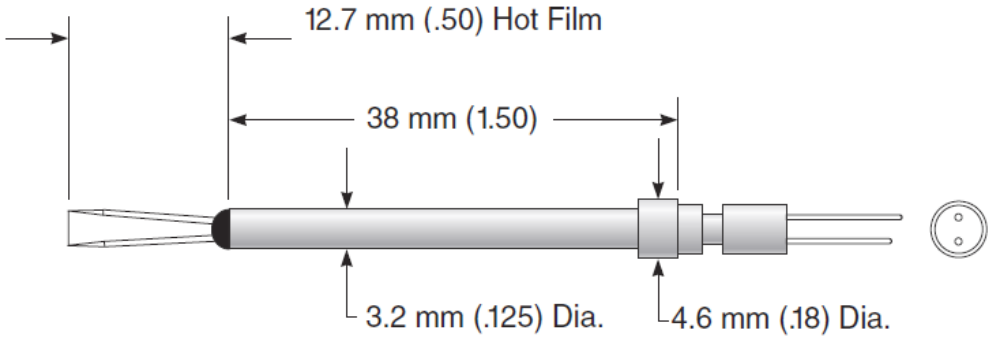

Figure 3.11 One-dimensional flow measurements probe.

In this study, 3 different velocity conditions were considered. The average velocities recorded using the HFA for these 3 conditions were 16 ± 1.4, 11 ± 1, and 9 ± 0.7 m/s during the 5 s camera recording time. In our study steady state velocities were reached within approximately 1 s.

(a)

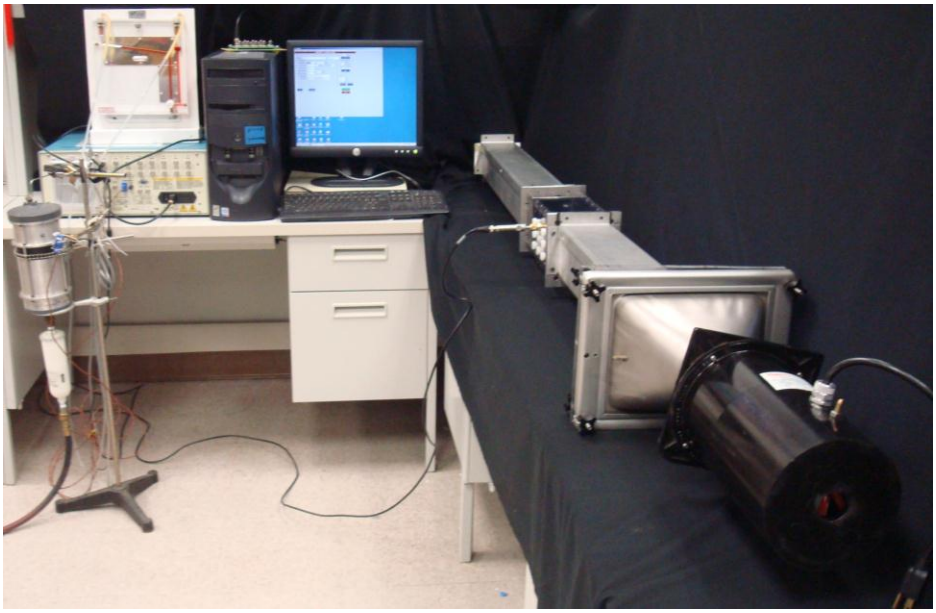

(b)

Figure 3.12 a) Hot film calibration unit, b) Experimental setup with the hotwire calibration unit.

4. EXPERIMENTAL MEASUREMENTS AND ASSOCIATED ERRORS

4.1 Particle Trajectory (Side-view Imaging)

4.1.1 Experimental Approach

For this set of experiments, the camera was mounted on the side of the clear polycarbonate test section to capture single particle behavior immediately before liftoff and its interaction with the different surfaces (Common flooring substrates discussed in section 3.1.2.1) using 4000 fps at a maximum flow speed of 16 m/s. A telecentric lens with 10x magnification was mounted on the camera to capture individual particle motion, typically 20-45 μm in size range. The resolution of the camera images was 512 x 1024 pixels. A calibration frame was taken before each experiment, yielded a spatial resolution of 0.9 μm/pixel. The side view experiments were repeated with the three different substrates for the different size ranges (typically 20-45μm) at 16 m/s (total of 60 experiments, 20 experiments/substrate). The particles were then tracked to investigate their behavior before liftoff using MATLAB code.

4.1.2 Measurements and Associated Errors

Image analysis was conducted to determine the paths followed by individual particles immediately before liftoff. The data recorded were analyzed using the MATLAB code developed by Estrada-Pérez and Hassan (2010). Particle trajectories were obtained by plotting their horizontal displacement in X direction (x), vertical

displacement in Z direction (z), particle velocity in x direction (u_p) and the particle size. The origin of coordinates obtained from the MATLAB code is the top left corner of the images recorded. However, the air flow was from the opposite direction (right to left). Accordingly, the following set of equations was assigned to avoid any negative trajectory values.

$$x_i\left(\mu m\right) = \left[x_0\left(pixels\right) - x_i\left(pixels\right) \right] \times cf\left(\mu m / pixels\right) \tag{4.1}$$

$$z_i\left(\mu m\right) = \left\{ \left[z_{\max}\left(pixels\right) - z_i\left(pixels\right) \right] \times cf\left(\mu m / pixels\right) \right\} + \frac{d_p}{2} \tag{4.2}$$

$$u_{p_i}\left(\mu m / s\right) = \left[u_{p_0}\left(pixels / time\right) - u_{p_i}\left(pixels / time\right) \right] \times cf\left(\mu m / pixels\right) \times \frac{1}{\Delta t\left(s\right)} \tag{4.3}$$

$$\Delta t = \frac{1}{fps} \tag{4.4}$$

where: x_i, x_0 are the horizontal displacement in the x direction at time t_i and t_0 respectively, t_0 is the time at particle initial movement, cf is the calibration factor discussed earlier, z_i is the vertical displacement in the z direction at time t_i measured from the particle centroid, z_{max} is the maximum vertical displacement during the entire particle movements, u_{p_i} is the particle velocity in the x direction at time t_i and x_i, d_p is the particle diameter estimated from the area of the pixels obtained by the code and fps is the camera frames per second (4000 fps for this set of experiments).

The error associated with such experiments is mainly caused by the code centroid estimations which are extensively discussed by Estrada-Pérez and Hassan (2010). In this study, the error in the vertical displacement was a maximum of 3 µm, that is the reason

we had to subtract the $z_i\,(pixels)$ from $z_{\max}\,(pixels)$ rather than $z_0\,(pixels)$ to be able to eliminate any negative value obtained from such error in the particle trajectory as will be shown in the result section. Additionally, a particle with an initially known size was used to estimate the calibration factor of about 0.9 µm /pixel for this experiment. Running the code with a well-known particle size and the same code parameters used in analyzing the experimental results reveals that the code can overestimate the actual particle size by around 3.5 µm in extreme conditions.

4.2 Particle Detachment and Resuspension Rate (Top-view Imaging)

4.2.1 Experimental Approach

In this set of experiments, the camera was positioned at the top of the clear polycarbonate test section to capture single layer particle detachment (not single particle as done in the first set of experiments) with respect to time, within a period of 0 to 5 s. The number of deposited microparticles was such that it was large enough to achieve acceptable statistical accuracy but not too large to cause an unacceptable number of collisions on the surface (Ibrahim et al. 2003). Based on initial experiments, 2000 frames per second was adequate to capture this component of particle motion. The resolution of the camera images was 512 x 512 pixels which correspond to 22 µm/pixel using the calibration frame.

4.2.1.1 Common Flooring

The substrates used in these experiments were hardwood, ceramic and glass slides (Fisherbrand 0.16 to 0.19 mm thick; Size: 22 mm), (section 3.1.2.1). The particle single layer initially deposited was about 431 ± 170 particles/cm^2 for the (10-30) μm glass bead particles, 360 ± 153 particles/cm^2 for the (30-50) μm glass bead particles and, 194 ± 64 particles/cm^2 for the 50-100 μm glass beads. A telecentric lens was mounted on the camera with 2x magnification and a halogen light source was used. The top view experiments were repeated 3 times for the 3 different surfaces, the 3 different particle size ranges and at 3 different speeds 16 ± 1.4 m/s, 11 ± 1 m/s, and 9 ± 0.7 m/s (81 experiments in total).

4.2.1.2 Paint Coating Effect on Metal Substrate

The substrates used in these experiments were Chemical Agent Resistant Coated metal (CARC) or non-coated metal used in military tanks. Two different types of micrometer particles were deposited on the top of each substrate by gravitational settling (Ibrahim, 2004), first, glass beads (Polysciences, Inc., Warrington, PA), spherical in shape with specific gravity of 2500 kg/m^3 in two different sizes. The mean diameters are 26.41 μm for the 10-30 μm particles range, and 45.31 μm for the 50-100 μm particles range. The second type of particles was stainless steel microspheres (Duke Scientific; diameter: 64.76 μm), with a much higher density of 8000 kg/m^3.

These set of experiments was specifically designed to capture the following:

1- Effect of applying a chemical agent resistant coating (CARC) on metal substrate (Can be included to the surface roughness effect).
2- Effect of different particle densities (Represented in different particle type, Glass beads 50-100 µm with 2500 kg/m^3 and Stainless steel 67-75 µm with 8000 kg/m^3) from metal and coated surfaces.
3- Effect of different particle size of Glass beads (10-30 µm and 50-100 µm) from metal and coated surfaces.

The experiments were repeated 4 times for the 2 different surfaces, the 3 different particle size ranges (2 different sizes glass beads in addition to the stainless steel particles) and at 3 different speeds 16 ± 1.4 m/s, 11 ± 1 m/s, and 9 ± 0.7 m/s (72 experiments in total).

4.2.1.3 Bacillus thuringiensis *var.* kurstaki *(Btk)*

This experiment was designed to investigate the resupension and detachment of single clusters *Bacillus thuringiensis* var. *kurstaki* (Btk), (6.4 µm aerodynamic diameter size) from glass substrates at 18 m/s using a 2000 frames/sec high speed camera for 5 sec total recording time. Due to the current camera maximum resolution of 22 µm/pixel it was impossible to detect the 6.4 µm bacteria clusters without increasing the magnification to 0.9 µm/pixel by using the 10x magnification lens. However, increasing the magnification usually decrease the focal length (Distance between the camera and the substrate) and the camera field of view. To overcome such limitation (very common with smaller particle size < 10 µm) the setup height had to be decreased to 2 inches

instead of 3 inches and the camera pixels was increased to 1024 x 1024. The experiment was conducted 5 times at different initial deposition concentrations for 3 different surface treatments, total of 15 times. First the glass was used untreated, and then it was treated by either RainX (Invisible windshield wiper) or Anti-foam B Silicone Emulsion (Sigma, MO).

4.2.2 Measurements and Associated Errors

The detachment percentage is defined as the number of particles detached from the surface at a certain time compared to the number initially deposited on the surface, Equation 4.5, (Ibrahim et al. 2003; Goldasteh et al. 2010).

$$\eta_{\det} = \left(\frac{N_0 - N}{N_0} \right) \times 100 \tag{4.5}$$

Where: $\eta_{det.}$ is the detachment percentage with respect to time, N_0 is the initial number of particles at time, t=0, N is the number of particles on the surface at time t.

The resuspension rate is defined as the fraction of deposited particles resuspended per unit time (Slinn 1978) or the normalized resuspension flux (Loosmore 2000), Equation (4.6).

$$\text{From definition, } \Lambda = -\left(\frac{dN / N_0}{dt} \right) \tag{4.6}$$

$$\text{Equation (4.6) can be estimated as, } \Lambda \Delta t = -\frac{\Delta N}{N_0} \tag{4.7}$$

Equation 4.7 will be used in our experiments to obtain the resuspension rate, where Λ is the resuspension rate, s^{-1}, Δt is a constant given by equation (4.4), $\Delta N=N_{i+1}-N_i$ where i is the number of frames taken by the camera, N_{i+1} and N_i were estimated by a curve fit to the experimental with R^2 valued around 0.95.

The error associated with this type of experiments is highly dependent on the measurement time and the number of particles recorded (N). Due to the triggering technique discussed earlier, the error associated with the time can be a maximum of 5 x 10^{-4} s for 2000 frame/s. The particle counting errors mainly depend on the accuracy of the code. According to Estrada-Pérez and Hassan (2010) for low initial particle density concentration (500 particles/500x500 pixels) the measured density should be the same as the actual particle density, meaning that the particles counted by the code should be almost the same as the actual particles initially deposited. However, our results showed a higher error of about (2 ± 2) % in the detachment percentage calculations. Very likely, the error arises from acceleration, whether due to a change in a particle's speed or its direction and/or random noise in the camera sensor and the finite size of pixels in the sensor as extensively discussed by Feng et al. (2011). While it is possible to design an experiment to reduce these particles position uncertainties, they can never be eliminated (Feng et al. 2011).

The analysis of variance (or ANOVA) is a powerful technique for analyzing experimental data based on quantitative measurements. It is particularly useful in factorial experiments where several independent sources of variation may be present (Lipson 1973). In our results 3 ways ANOVA statistical analysis was applied to verify

the level of statistical accuracy using a code earlier developed by Kassab (2009), based on 3 factors, the velocity, particle size and substrate (For more details see Appendix A). Unless otherwise indicated, the confidence level is taken as 95% (95 percent confidence indicates a significant difference between the parameters used in experiment).

4.3 3-D Measurement (Top and Side-view Imaging)

In this set of experiments, the effect of metal to metal contact was considered using a 3-D particle tracking technique. The metal particles were stainless steel microspheres (Duke Scientific; diameter: 64.76 μm, 8000 kg/m^3) and the metal surface was a stainless steel used in the military tanks. The camera located in the top was the Phantom with 800 x 250 pixels and the other camera located on the side was the Photron with 1024 x 200 pixels. Identical Telecentric lenses were mounted on both cameras at 4.5 x magnification with a special resolution of about 5 μm/ pixel.

5. MODELLING

5.1 Introduction

In general, resuspension models can be categorized into two main groups (Gillette et al. 2004). The first group includes theoretical models that explain the resuspension phenomena such as the force balance concept where particle resuspension is assumed to take place instantaneously when the aerodynamic forces exceed the surface adhesive force (Ziskind 2006, Kim et al 2010, and Zhang 2011). The second group consists of macroscopic, empirical models based on large-scale, and usually long-term, resuspension studies (Kim et al 2010). They are commonly presented in terms of a resuspension factor, K (Equation, 5.1), or a resuspension rate Λ (Equation 5.2).

$$K\left(m^{-1}\right) = \frac{Airborne\_concentartion\left(gm^{-3}\right)}{Initial\_surface\_concentration\left(gm^{-2}\right)} \tag{5.1}$$

$$\Lambda\left(s^{-1}\right) = \frac{\mathrm{Re}suspension\_flux\left(gm^{-2}s^{-1}\right)}{Initial\_surface\_concentration\left(gm^{-2}\right)} \tag{5.2}$$

In this section we will apply two of the current existing models to investigate the resuspension phenomena (one from each group) and verify the experimental results.

5.2 Resuspension Rate

Resuspension rates usually are derived from the theoretical analysis and can be compared with the experimental results. However, most of the empirical models were derived using resuspension data obtained months to years after deposition (Kim et al,

2010). Loosmore (2003) recognized the need for resuspension models applicable at shorter times and developed two empirical models for the resuspension rate (Equation 5.3 and 5.4).

$$\Lambda = 0.01\frac{u^{*1.43}}{t^{1.03}} \tag{5.3}$$

$$\Lambda = 0.42\frac{u^{*2.13}d_p^{0.17}}{t^{0.92}z_0^{0.32}\rho_p^{0.76}} \tag{5.4}$$

In 2010, Kim group modified the imperial correlations obtained by Loosmore. In this study, the analytical model earlier developed by Kim et al. (2010) will be used to verify the resuspension rate calculations obtained in our experiments, (Equation 5.5).

$$\frac{\Lambda d_p}{u^*} = 8.521\times10^{-3}\left(\frac{\rho_p}{\rho_f}\right)^{-0.3028}\left(\frac{u^*t}{d_p}\right)^{-1.0135}\left(\frac{z_0}{d_p}\right)^{-0.3269}\left(\frac{A_{132}}{d_p{}^3u^{*2}\rho_f}\right)^{-0.2961} \tag{5.5}$$

where: d_p is particle diameter (In our study taken as the mean diameter obtained using the coulter counter), ρ_p is the particle density, ρ_f is the air density at room temperature, z_0 is the surface roughness (In our study taken as the mean roughness (Ra)), t is time (the calculations will be evaluated at 5 s), A_{132} is the Hamaker constant and u^* is the friction velocity. The Hamaker constant, A_{132}, describes the dipole interactions between two materials (Particle 1 and Surface 2) in a medium (3, air) macroscopically (Kim et al. 2010) and is given by $A_{123} = A_{12} + A_{33} - A_{13} - A_{23}$, where, $A_{ij} \cong \sqrt{A_{ii}A_{jj}}$. For the glass substrate the A_{132} was directly taken from data earlier reported by Soltani and Ahmadi (1994) as 8.5 x 10^{-20} J. Regarding the ceramic and hardwood tiles, a surface finish was applied to improve the surface durability and add different aesthetic values to tiles. The

ceramic was glazed smooth finish with glassy material designed to melt on the surface of a ceramic body and to stay adhere upon cooling, hence the A_{132} for the ceramic was taken to be the same as glass (Mishulovich and Evanko 2003). The hardwood substrate was aluminum oxide finish, hence the A_{132} was calculated from the previous equation as 9.1×10^{-20} J, which can be calculated from the interaction between two materials, first material is assumed to be glass based on the fact that the glass beads particles contains 75% silica which was taken as 6.6×10^{-20} J (assumed to be vacuum fussed silica, Berqström 1997) and the second material is aluminum oxide which was taken as 14.5×10^{-20} J (Berqström 1997).

5.3 Detachment Modes

In 1990, Wang used the force and moment balance between the adhesion force and the external forces to determine the onset of movement. He assumed that the particle will leave the surface once the movement of particle is initiated and theorized three modes of inceptive motion on particle detachment (Wang 1990). These modes are

1. Lift-off: When the normal component of a force applied to an adhered particle exceeds the pull-off force, the particle will be lifted off the surface.
2. Sliding: When the tangential component of an applied force exceeds the total normal force multiplied by a coefficient of static friction, the particle will begin to slide and thus be resuspended.

3. Rolling: When the total torque about a point on the edge of the contact circle including the downward sticking force is equal to zero, the particle will begin to roll around that point and thus off the surface.

Using similar concepts different models where developed to investigated the particles initial motion (Zhang and Ahmadi 2000, Phares et al. 2000, Ibrahim 2004, Burdick et al. 2005, Guingo and Minier 2008, Ibrahim et al. 2008, Hu et al. 2010 and Tippayawong and Preechawuttipong 2011). Due to the similarity of our experimental method and Ibrahim study (2004). The force/moment balance approach will be applied based on previous analysis by Ibrahim (2004) to validate our experimental results. His model was used to estimating a single value of the free-stream velocity required to initial detachment. In Ibrahim model three different detachments modes where considered based on force/moment balance approach (Figure 5.1). These modes are

1. Direct lift-off, Equation (5.6)

$$F_L > F_{po} + F_g \tag{5.6}$$

2. Sliding, Equation (5.7)

$$F_D + \mu_f F_L > \mu_f (F_{po} + F_g), F_D > 0 \tag{5.7}$$

3. Rolling, Equation (5.8)

$$1.74RF_D + aF_L > a(F_{po} + F_g), {}^{a}\!/_{R} > 1 \tag{5.8}$$

where μ_f is the coefficient of friction taken to be 0.9 for glass particle on glass substrate and 0.6 for metal particles on metal substrates.

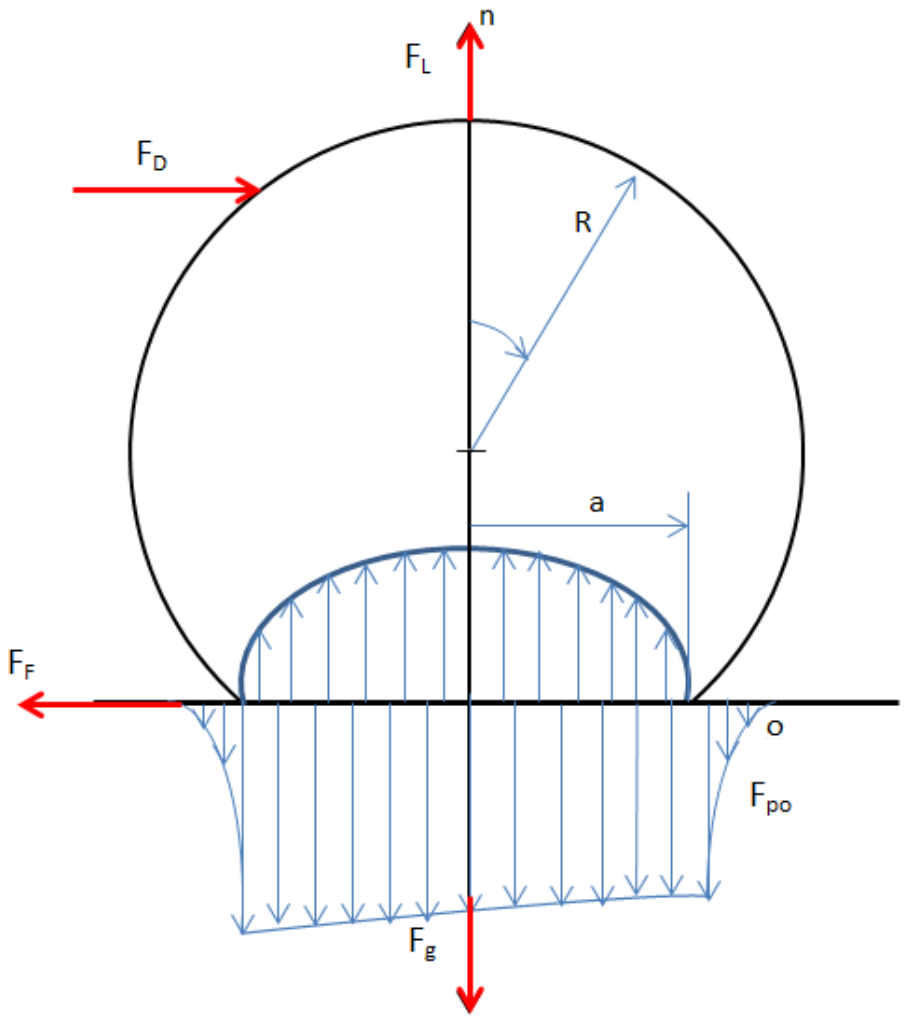

Figure 5.1 Schematic of the forces and moments acting in a microparticle on a surface.

As extensively discussed in Section 2.3, Equations (2.8 and 2.11) will be used to calculate the gravitational forces and lift forces respectively. Increasing surface roughness decrease the pull-off significantly. Cheng et al. (2002) showed that the rough-surface pull-off force is approximately 1% of its smooth-surface value for 17Å (~ 2 nm)

standard deviation heights on the substrate (Figure 5.2). Consequently the pull-off forces applied to a rough surface can be estimated by multiplying the smooth pull-off forces by the pull-off force reduction factor C, obtained from Figure 2.3 based on the Tabor's parameter and surface roughness. As mentioned earlier, the two most common adhesion models are the DMT and JKR. However, pull-off forces estimated from the DMT model (Equation 2.21) is 4/3 times the JKR force given by Equation 2.17. According to Tabor (1977), the DMT model is valid for $\mu_T < 0.1$ and the JKR model is valid for $\mu_T > 5$, where Tabor's parameter, μ_T can be calculated from Equation 2.23. However, Johnson and Greenwood (1997) proposed approach for the adhesion on the DMT-JKR transition that was adapted for the pull-off forces calculations by Ibrahim 2004. An equation (5.9) is estimation for the smooth-surface pull-off forces using Johnson and Greenwood (1997).

$$F_{po_s} = C_1 \pi \gamma R \tag{5.9}$$

where, C_1 is a constant obtained from Johnson and Greenwood (1997) as 1.61, and 1.51for stainless steel (SS) and Glass beads (GB) particles respectively (Ibrahim, 2004). As shown in Figure 5.2 the rough force pull-off calculations using Cheng et al. (2002) is only limited to a maximum of 2 nm which was valid in Ibrahim (2004) modeling since he only used smooth glass surfaces. However, in our study surface roughness measurements were much higher. Consequently, the rough pull off forces for our case expected to be even lower than estimated in equation (2.25).

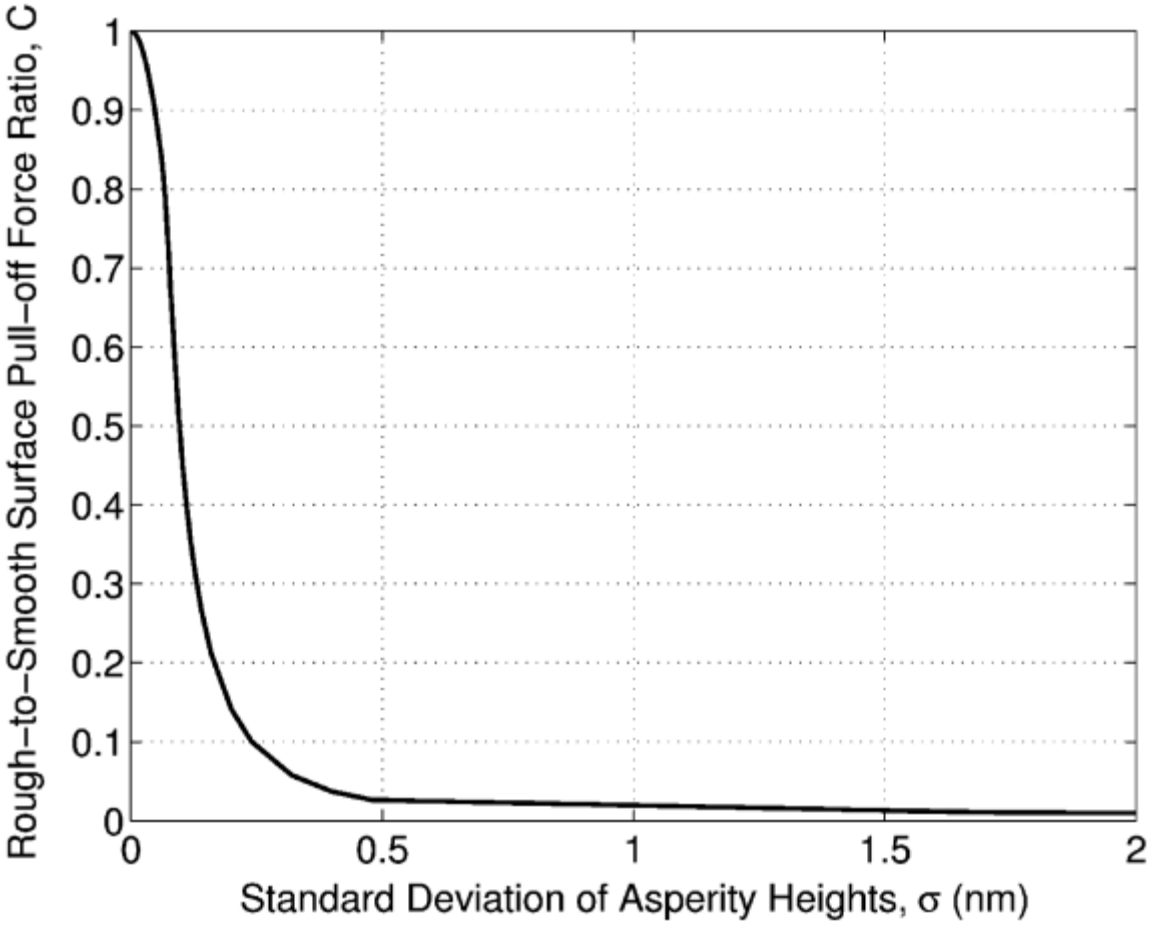

Figure 5.2 Reduction factor of particle pull-off force, *C*, with increasing surface roughness as characterized by the standard deviation of surface asperity heights σ (Cheng et al. 2002).

In 2007, Szarek and Dunn modified the Corn empirical expression for the adhesion force (Equation (5.10), Hinds 1999) by taking into consideration the empirical pull-off force reduction dimensionless factor C and a theoretical coefficient C_2 (Equation (5.11)). The theoretical coefficient, C_2 is specified by Maugis (1991) to be between 0.75

which account for the DMT-JKR transition, as dictated by Tabor's parameter. Tabor's parameter can be interpreted as the ratio of the elastic displacement of the particle's surface at the point of separation from the substrate surface to the equilibrium atomic spacing. Low values of Tabor's parameter represent small, hard (non-compliant) particles, whereas large values represent large, soft (compliant) particles.

$$F_{po} = \pi \gamma d \left[1 + 0.009\left(\%RH\right)\right] \tag{5.10}$$

$$F_{po} = C\pi \gamma d \left[1 + 0.009\left(\%RH\right)\right] C_2 \tag{5.11}$$

It should be noted that Equation (5.11) is the total forces of adhesion of electrically neutral particles resting on electrically neutral surface. The electrostatic interaction may prevail over the van der Waals one in adhesion of rough bodies (Ziskind et al. (1995). According to Bowling (1988) small particles of less than 50 µm, van der Waals forces predominate over electrostatic charges. Tests made by John (1995) to investigate the possibility that the electrostatic charges could build up on the surface and affect the resuspension results found no effect was caused by the accumulation of electrostatic charges on the surface. The role of the electrostatic forces or its magnitude in adhesion phenomena is debatable (Ziskind 2006). The electrostatic forces acting on a particle is much lower than the gravity effect by at least two orders of magnitude (Yao et al. 2006). Consequently, uncharged materials can be assumed to have relatively small electrostatic charges compared to van der Waals forces. Thus, in this study the contribution from the electrostatic forces was not considered (John 1995, Ibrahim 2004, Kim et al. 2010, and Yao and Fairweather 2010).

On the other hand, the mean aerodynamic drag force will be modeled based on the formula given by Ibrahim (2004), (Equation 5.12). Provided that the buoyancy, virtual mass and Basset forces are negligible with respect to the drag force because the densities of the microspheres in the present experiments (8000 kg/m^3 and 2500 kg/m^3 for SS and GB, respectively) are much larger than that of air (Armenio and Fiorotto 2001, Ibrahim 2004, Yao and Fairweather 2010, and Tippayawong and Preechawuttipong 2011).

$$F_D = 3 f_o \pi \mu_f d u_c \left[1 + 3\tilde{\mathrm{Re}}_p \Big/ 8 + 9\tilde{\mathrm{Re}}^2{}_p \log_e \left(\tilde{\mathrm{Re}}^2{}_p \right) \Big/ 40 + 0.1879\tilde{\mathrm{Re}}^2{}_p \right] \quad (5.12)$$

where, the factor f_o = 1.7009 accounts for wall effect (O'Neill 1968). $\tilde{\mathrm{Re}}^2{}_p$ is the microparticle Reynolds number, $\tilde{\mathrm{Re}}^2{}_p = u_c R / \nu$ and u_c is the flow velocity at a height from the wall equals to the microparticle radius and can be estimated from Soltani and Ahmadi (1995) as $u^+ = 1.84 y^+$.

6. RESULTS

6.1 Experiments

6.1.1 Common Flooring

6.1.1.1 Particle Trajectory

Results obtained from tracking 80 particle trajectories (20 particles for each surface) indicated that the glass beads (ranging from 20-45 μm) experienced three different types of motion (Tables 6.1, 6.2, 6.3 and Figure 6.1). Rolling/bouncing, liftoff motion and complex motion where particles travel with rolling/bouncing motion on the surface for a certain distance before liftoff.

Table 6.1 Particle motion on glass substrates

GLASS SUBSTRATE (20 particles)			
Rolling/Bouncing *(#particles/Total particles, r Conditions)*		**Liftoff** *(#particles/Total particles, r Conditions)*	
5/20=<u>25%</u> , $r > 0.6$		**15/20=<u>75%</u>, $0.03 < r < 0.4$**	
Pure rolling/bouncing	Potential liftoff	Immediate liftoff	Complex liftoff
5/5=100%	0/5=0%	4/15=27%, t>1	11/15=73%, t<1

Table 6.2 Particle motion on hardwood substrates

HARDWOOD SUBSTRATE (20 particles)			
Rolling/Bouncing *(#particles/Total particles, r Conditions)*		**Liftoff** *(#particles/Total particles, r Conditions)*	
6/20=<u>30%</u> , *r* >0.6		**14/20=<u>70%</u>, 0.02< *r* <0.2**	
Pure rolling/bouncing	Potential liftoff	Immediate liftoff	Complex liftoff
2/6=33%	3/6=66%	10/14=71%, t>1s	5/14=36%, t<1s

Table 6.3 Particle motion on ceramic substrates

CERAMIC SUBSTRATE (20 particles)			
Rolling/Bouncing *(#particles/Total particles, r Conditions)*		**Liftoff** *(#particles/Total particles, r Conditions)*	
16/20=<u>80%</u> , *r* >0.2		**4/20=<u>20%</u>, 0.03< *r* <0.2**	
Pure rolling/bouncing	Potential liftoff	Immediate liftoff	Complex liftoff
10/16=63%, t<0.43s	3/6=37%, t>0.43s	1/4=25%	3/4=75%

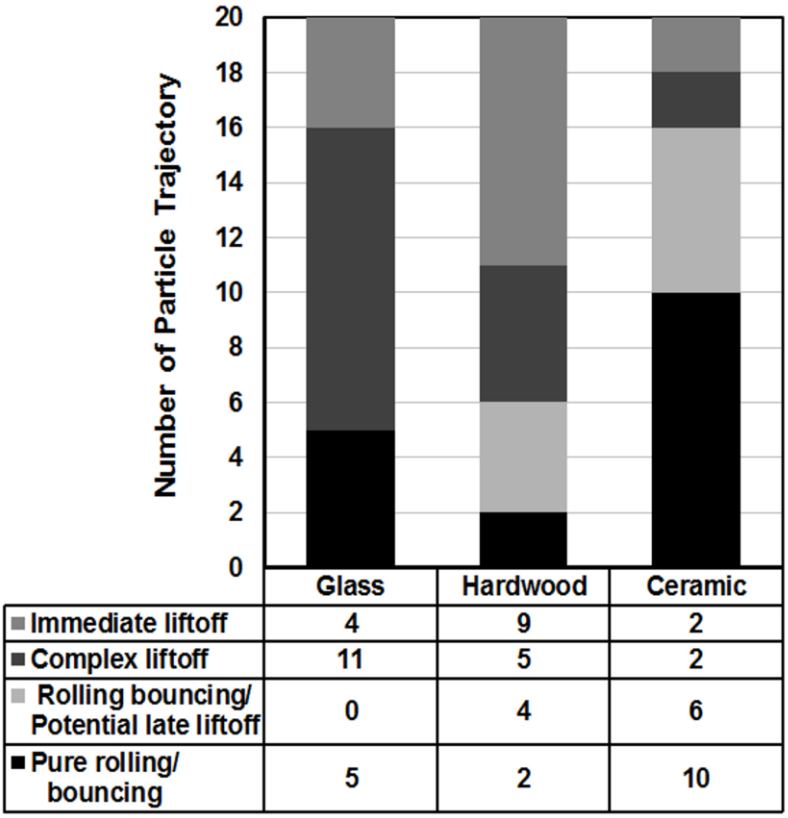

	Glass	Hardwood	Ceramic
Immediate liftoff	4	9	2
Complex liftoff	11	5	2
Rolling bouncing/ Potential late liftoff	0	4	6
Pure rolling/ bouncing	5	2	10

Figure 6.1 Type of motion on glass, ceramic, and hardwood substrates for glass beads 20-45 μm in size range for air velocities 0-16 m/s.

Analysis showed that the particle velocity in the x direction, u_p was dominant compared to the velocity in the z direction, w_p (Figure 6.2). To investigate the significance of the particle vertical velocity fluctuation a parameter was developed. The parameter was used to compare the energy associated with the vertical velocity fluctuations caused by the up/down motion of the particles in the vertical direction, z, and the particle total kinetic energy (dominated by the velocity magnitudes). The vertical

velocity fluctuation energy was calculated from the area under the power spectrum curves of the particle vertical velocity data. To obtain the kinetic energy, the average values of the KE_p data (Figure 6.3) were considered for each particle. The ratio of the vertical velocity fluctuation energy, E_{w_p} (Equation 6.1) and the average particle total kinetic energy was scaled to obtain a quantity of order 1 that will be referred to as *r (*Equation 6.2).

$$E_{w_p} = E_{w_{p(n-1)}} + \left\{ \frac{1}{2} \times \left[\left(FFT_{mag} \right)_{n-1} + \left(FFT_{mag} \right)_n \right] \times 2\pi \left[\left(FFT_{freq} \right)_n - \left(FFT_{freq} \right)_{n-1} \right] \right\} \tag{6.1}$$

$$r = \left(E_{w_p} \Big/ KE_P \right) \times 10^{-17} \tag{6.2}$$

where, KE_p (J) is the particle kinetic energy = 0.5 * m* v^2, v^2 (m^2/s^2) = u_p^2 + w_p^2, m (kg) = ρ_p * V_p, V_p (m^3) = 1/6 * π *d^3 and $t_{ref} = t_i - t_0$, t_0 is the time corresponding to particle initial movement, t_i is the variable time corresponding to each frame. It should be noted that the particle potential energy estimated to be at least 100x less than the particle kinetic energy and considered to be neglected in the particle energy calculations.

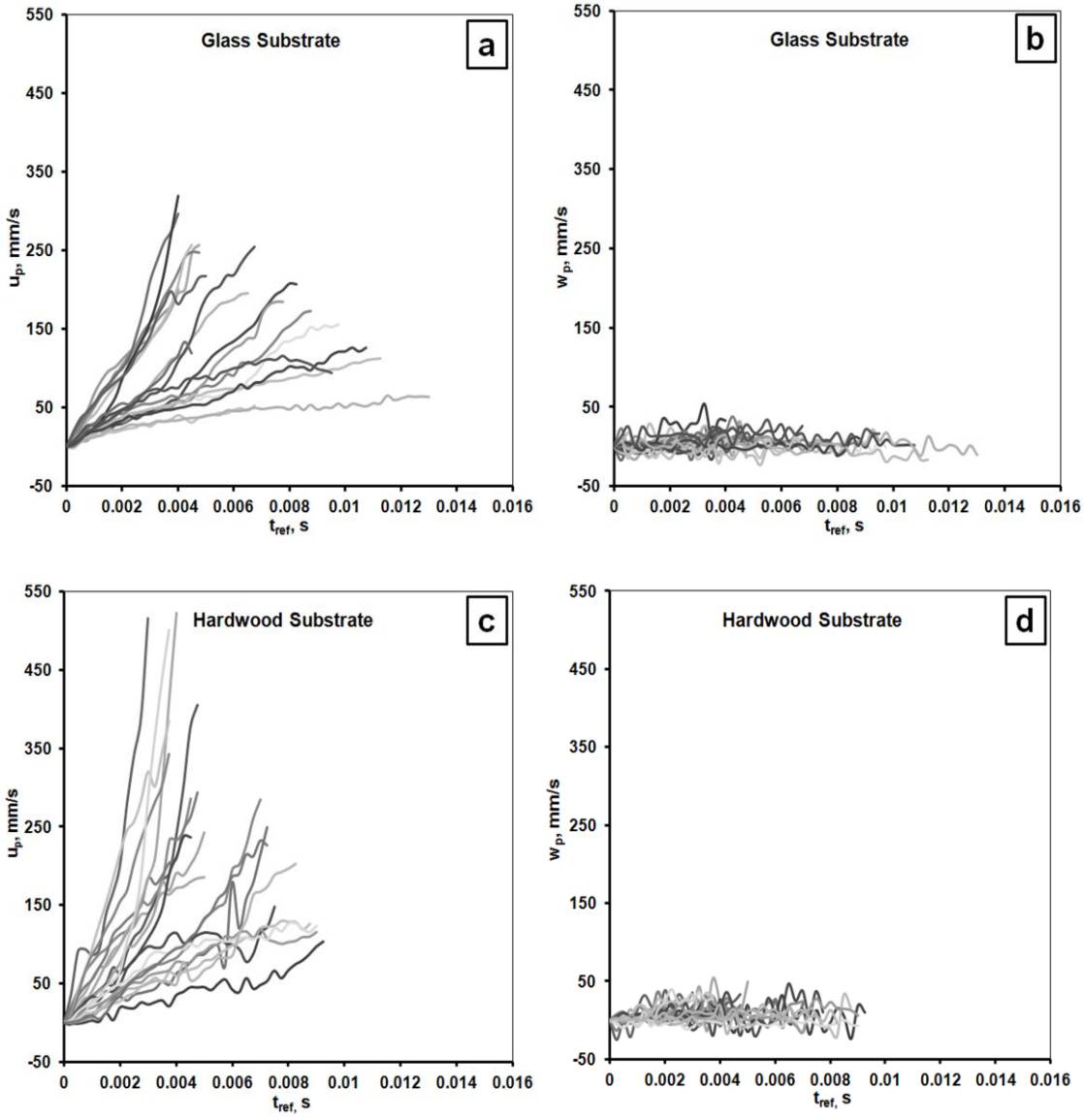

Figure 6.2 Change in particle vertical and horizontal velocity component with respect to time.

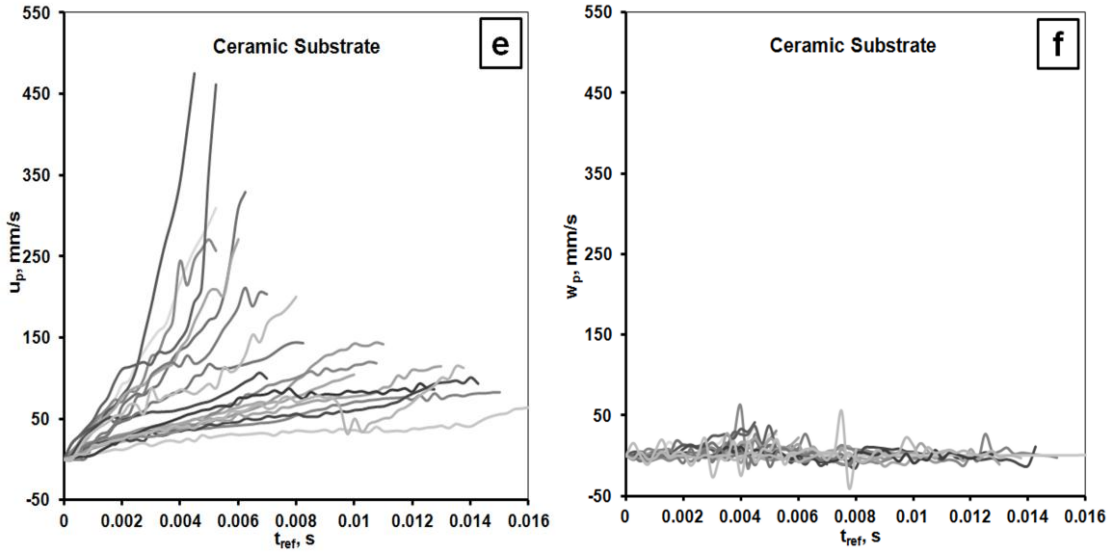

Cont. Figure 6.2.

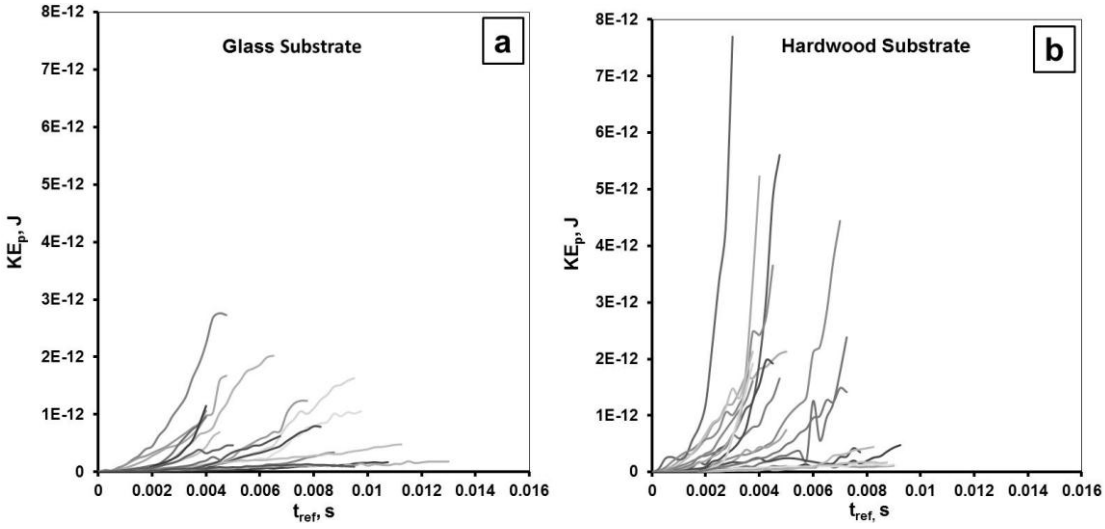

Figure 6.3 Change in particle kinetic energy with respect to time.

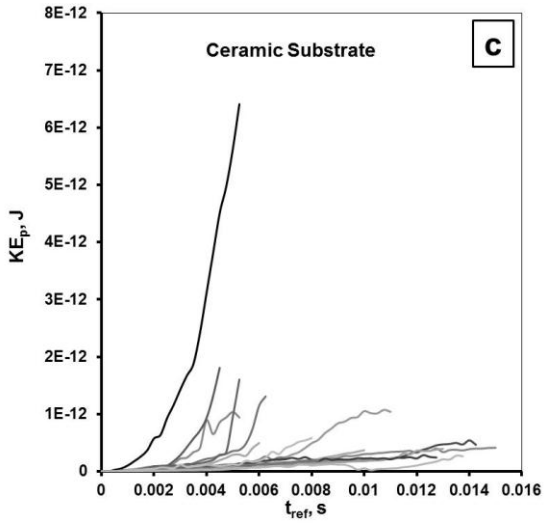

Cont. Figure 6.3.

Particle liftoff seems to be associated with minimum *r* parameter, representing a higher kinetic energy. The longer it takes the particle to start its initial movement the more rapid is the liftoff where the time, t, is the time it will take the particle to begin its initial movement since starting the camera and the blower by synchronized triggering. Additionally, the higher the vertical velocity fluctuation energy compared to the particle average kinetic energy, reflected in relatively larger *r*, the more likely the particle will remain on the surface with rolling/bouncing motion (Figure 6.4a, 6.4c, and 6.4e) as the kinetic energy is not sufficient to overcome the bouncing effect caused by the velocity fluctuation in the z direction.

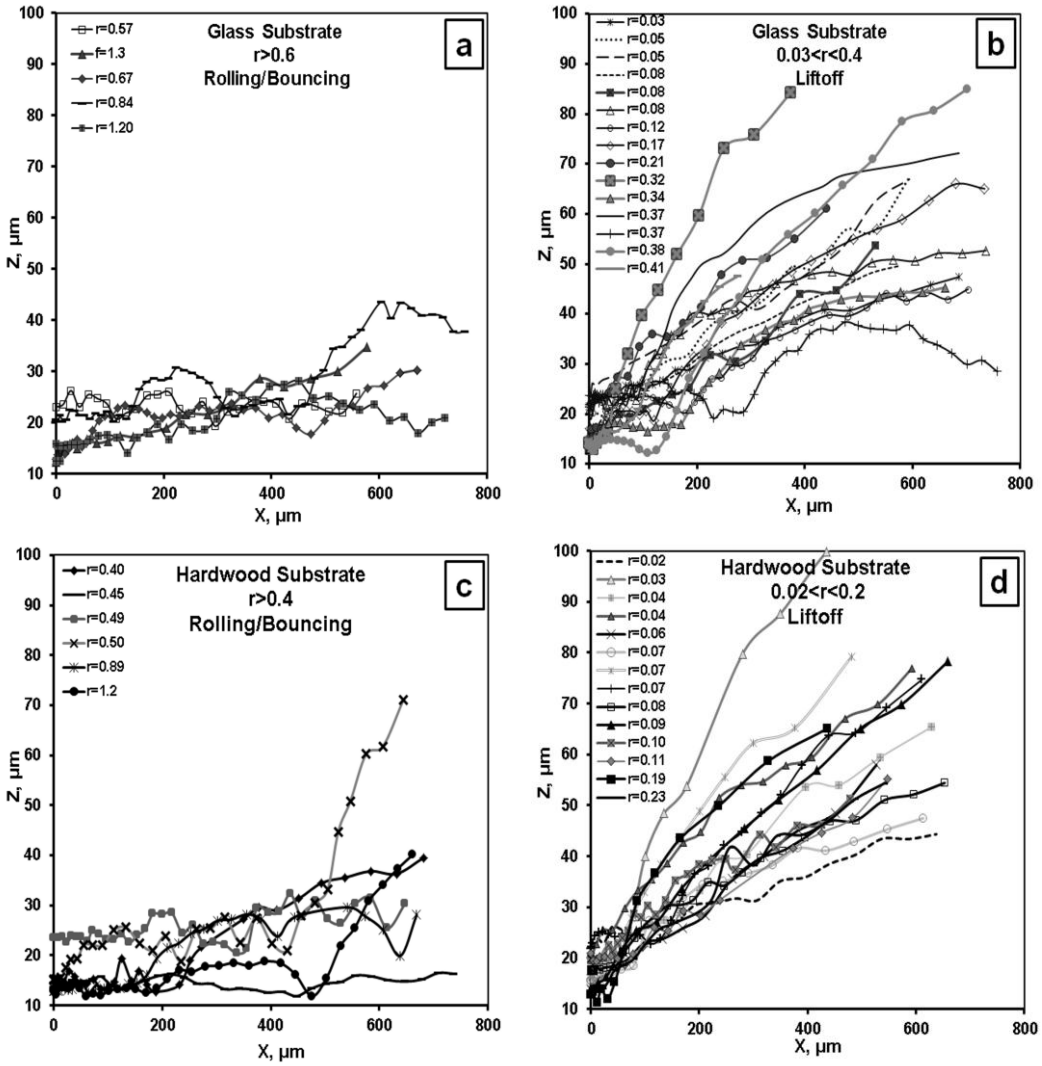

Figure 6.4. Particle trajectory for the glass beads particles (20-45µm in size range) on glass, hardwood and ceramic substrate as a function of *r*.

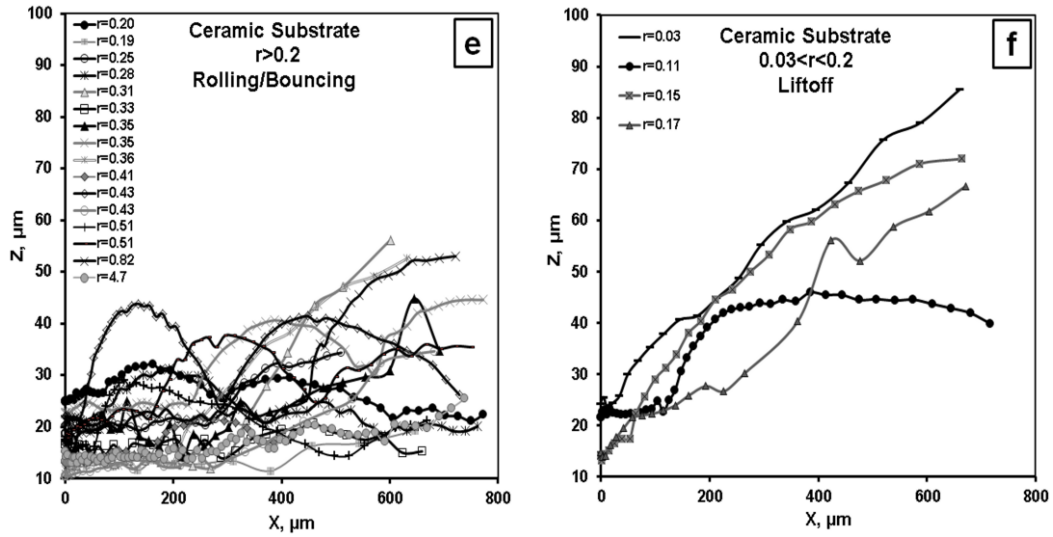

Cont. Figure 6.4

Surface roughness seems to significantly affect the particle initial motion prior to liftoff. Particles deposited on glass substrates, the smoothest roughness with 100x less roughness, needed about 50% less kinetic energy for liftoff motion to occur (Figure 6.4b, 6.4d, and 6.4f). Additionally, about 70-75% of the particles from glass and hardwood substrates will eventually liftoff, compared to 20% liftoff from the ceramic substrate (Immediate and complex liftoff Figure 6.1). Although the majority of the particle trajectories from glass and hardwood substrates seem to eventually liftoff (Figure 6.4b and 6.4d), a closer look reveals that the bigger the surface roughness (typically hardwood in this case), the longer it will take for the particle initial motion ($t > 1$ s) to cause a more rapid liftoff with minimum or no initial rolling/bouncing motion (Figure 6.5).

In contrast, particle trajectories from the glass substrates seem to display a complex motion, as particles travel about 25% with a rolling/bouncing motion before completely leaving the surface. In this case, the majority of particle trajectories from the glass substrate tend to travel in the horizontal direction parallel to the surface after liftoff rather than the rapid increase liftoff as seen on the hardwood substrates. In other words, over the same recording time, the glass substrate is expected to have the highest resuspension percentage, as confirmed by the detachment percentage results presented in the next section. Particles on the ceramic substrate, however, seem to struggle to achieve liftoff as 80% of the particles recorded showed a rolling/bouncing motion (Figure 6.4e). A closer examination of the ceramic rolling/bouncing particles (80% of the total particles), shown in Figure 6.4e, reveals that about 40% of these particle trajectories show a potential of late liftoff after initial rolling/bouncing at travelling distances of about 40% of the recorded distance (Figure 6.1).

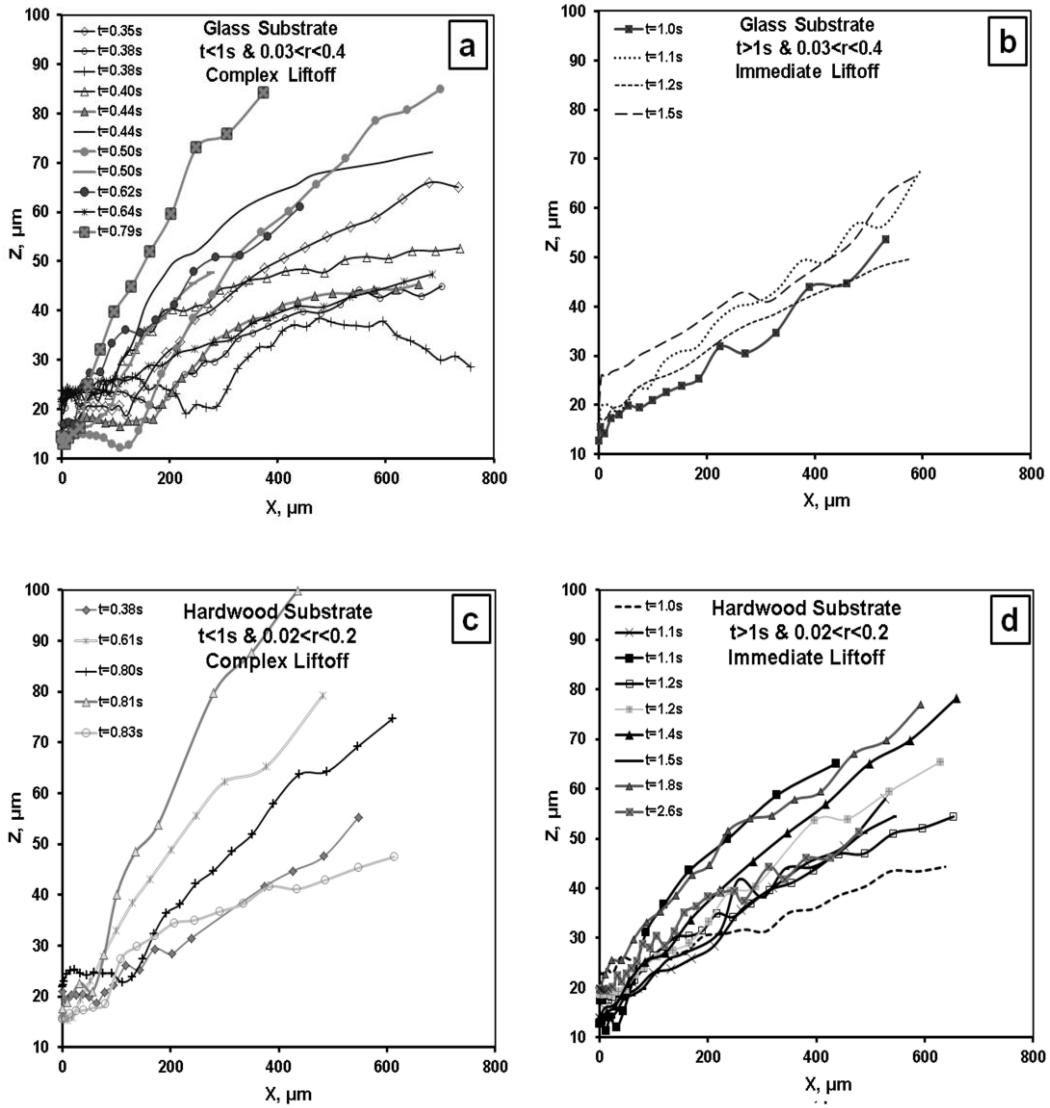

Figure 6.5 Time effect on particle trajectory for the glass beads particles on glass, hardwood and ceramic substrate, where the time, t, is the time it will take the particle to begin its initial movement since starting the camera and the blower simultaneous triggering.

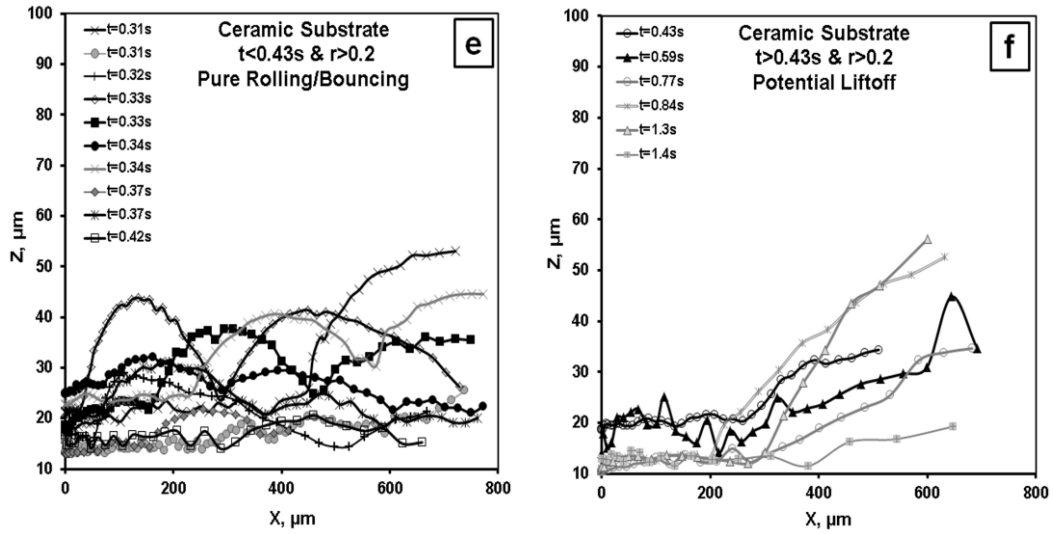

Figure 6.5 Cont.

According to Wu et al. (1992), when the particle relaxation time, Equation 6.3, is much greater than the turbulent time scale, Equation 6.4, the particle should eventually return to the surface under the influence of gravity.

$$\tau_p = \frac{\rho_p d_p^{\,2} C_c}{18\mu} \tag{6.3}$$

where τ_p is the particle relaxation time, s, which is used to characterize the time required for a particle to adjust or relax its velocity to a new condition of forces, C_c is the Cunningham correlation factor, $C_c = 1 + \frac{2.52}{d}\lambda$ and λ is the free stream path = 0.066 µm (Hinds, 1999).

$$t_L = \frac{L}{U} \tag{6.4}$$

Where, t_L is the turbulent time scale, s, which represents the size of the largest eddies in the flow; and L is the integral length scale, for fully developed pipe flow $L = 0.07 d_h$ (Versteeg and Malalasekera 1995).

In our particle size range and flow conditions the particle relaxation time, τ_p = (0.004-0.018) s, is at least 10x more than the turbulent time scale, t_L = 0.0004 s, hence, the particle trajectories will follow a parabolic path, having a constant horizontal velocity as it moves downstream but reaching a maximum height before returning to the surface under the influence of gravity.

6.1.1.2 Particle Detachment

The detachment percentage data initially follow an exponentially increasing trend for a period of ~ 1 s, followed by a plateau phase during the remainder of the 5 s recording time, with higher detachment percentage observed on glass (Figures 6.6, 6.7,and 6.8). Changing the velocity, substrate and particle size for the glass beads will significantly affect particle resuspension with at least 97.5% statistical accuracy using ANOVA statistical analysis at t=5 s (Table 6.4 and Figure 6.9). In general, less particle resuspension was observed on hardwood flooring compared to the ceramic and glass substrates, especially for the larger particle size; the highest resuspension was obtained by using glass substrate. Increasing the particle size will result in increased resuspension, as very likely larger particles penetrate higher into the boundary layer and thus experience higher removal forces. As the particle size increases, removal forces increase

more rapidly than adhesion forces. Larger surface roughness (such as hardwood in our case) provides more shielding, acting against resuspension.

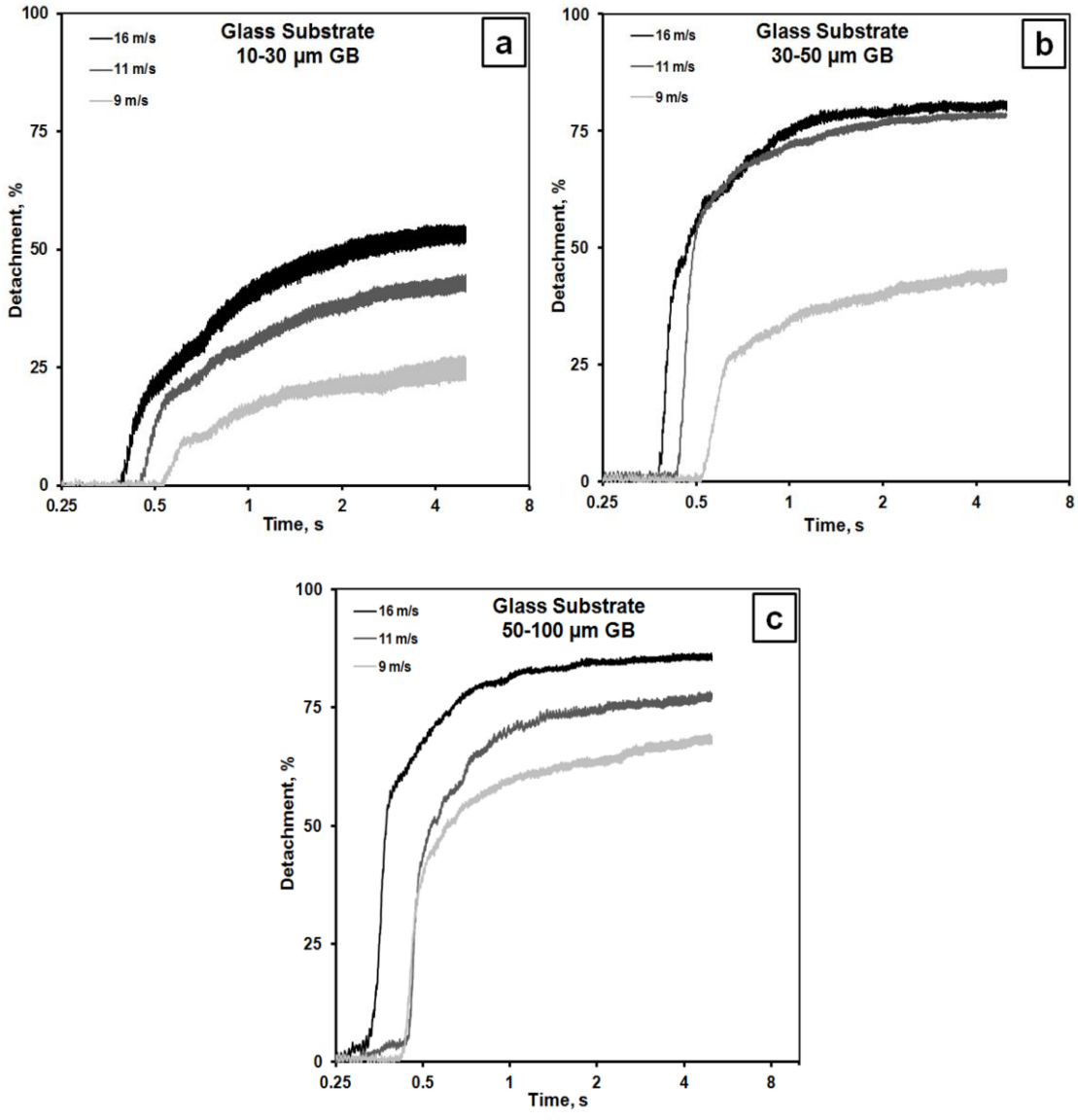

Figure 6.6 Time dependence of detachment percentage of different sizes glass beads particles on a glass substrate.

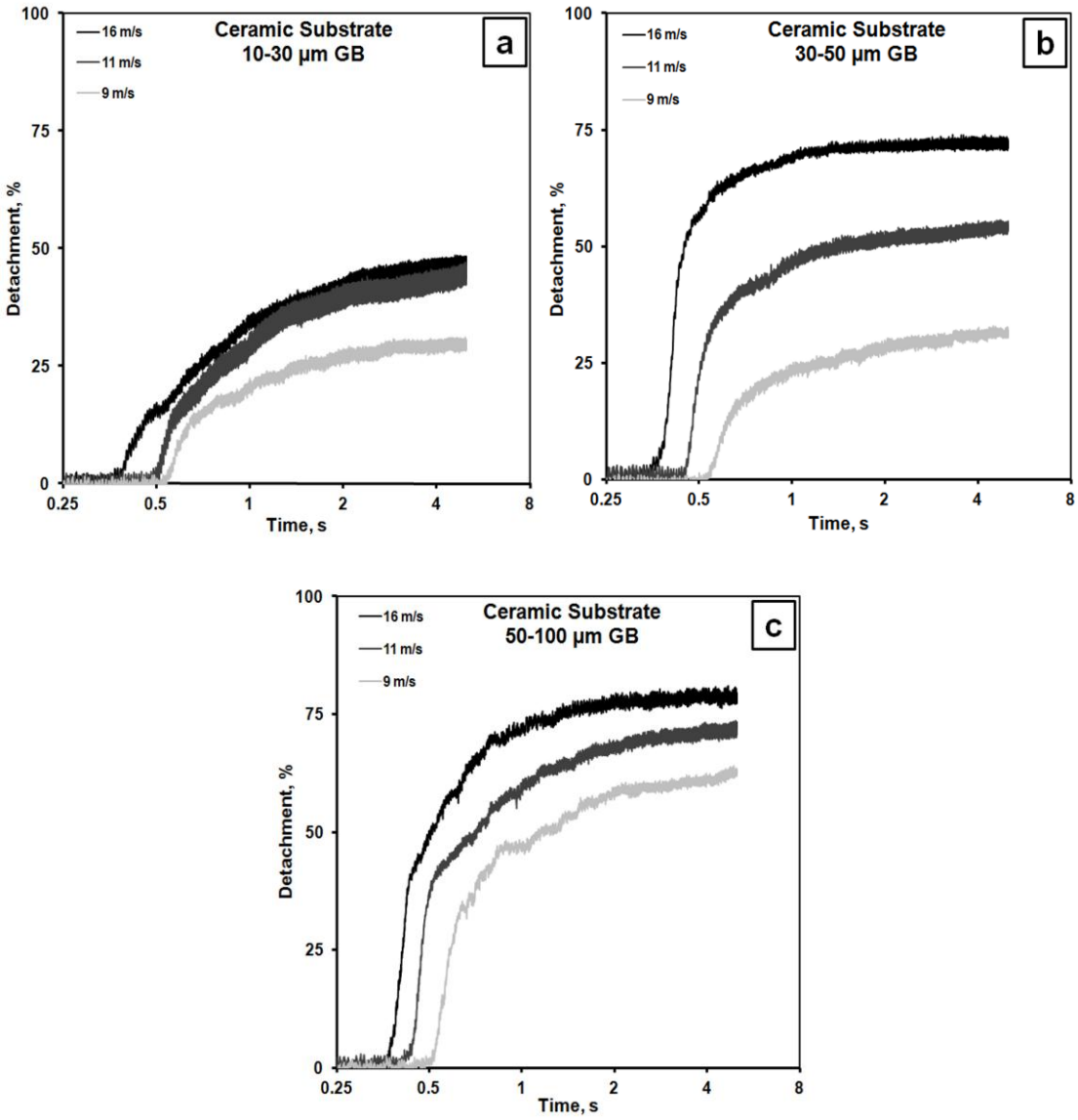

Figure 6.7 Time dependence of detachment percentage of different sizes glass beads particles on a ceramic substrate.

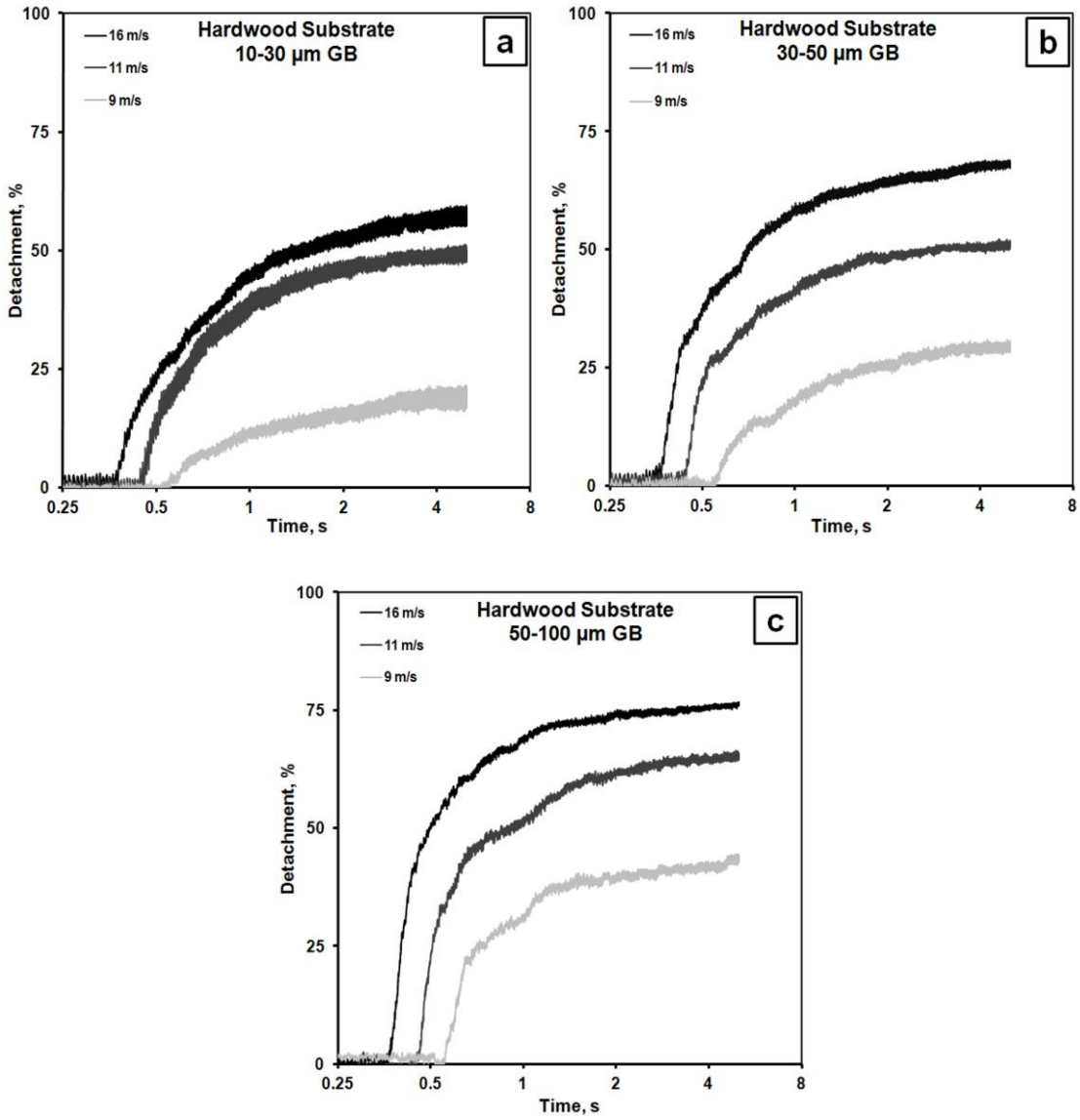

Figure 6.8 Time dependence of detachment percentage of different sizes glass beads on a hardwood substrate.

Table 6.4 Analysis of variance, ANOVA, statistical results for detachment percentage shown in Figure 6.9.

Source of variation	**SS[1]**	**DF[2]**	**MS[3]**	**MSR[4]**	**Confidence level, %**				
					95	**97.5**	**99**	**99.5**	**99.9**
Velocity, c	1.25E+04	2	6.23E+03	**43.14**	3.49	4.48	5.85	6.99	**9.95***
Substrate, r	1.62E+03	2	8.12E+02	**5.63**	3.49	**4.48***	5.85	6.99	9.95
Size range, g	1.18E+04	2	5.89E+03	**40.78**	3.49	4.48	5.85	6.99	**9.95***
c-r interaction	4.96E+02	4	1.24E+02	**0.86**	2.87	3.51	4.43	5.17	7.1
c-g interaction	6.96E+02	4	1.74E+02	**1.21**	2.87	3.51	4.43	5.17	7.1
r-g interaction	1.12E+03	4	2.81E+02	**1.95**	2.87	3.51	4.43	5.17	7.1
c-r-g	5.70E+02	8	7.13E+01	**0.49**	2.45	2.91	3.56	4.09	5.44
Residual	2.89E+03	20	1.44E+02	**1.00**					

[1]SS = sum of squares

[2]DF = degree of freedom

[3]MS = mean square

[4]MSR = mean square ratio

* Higher experimental mean square ratio (MSR) than the F ratio found in F distribution tables for a certain confidence level.

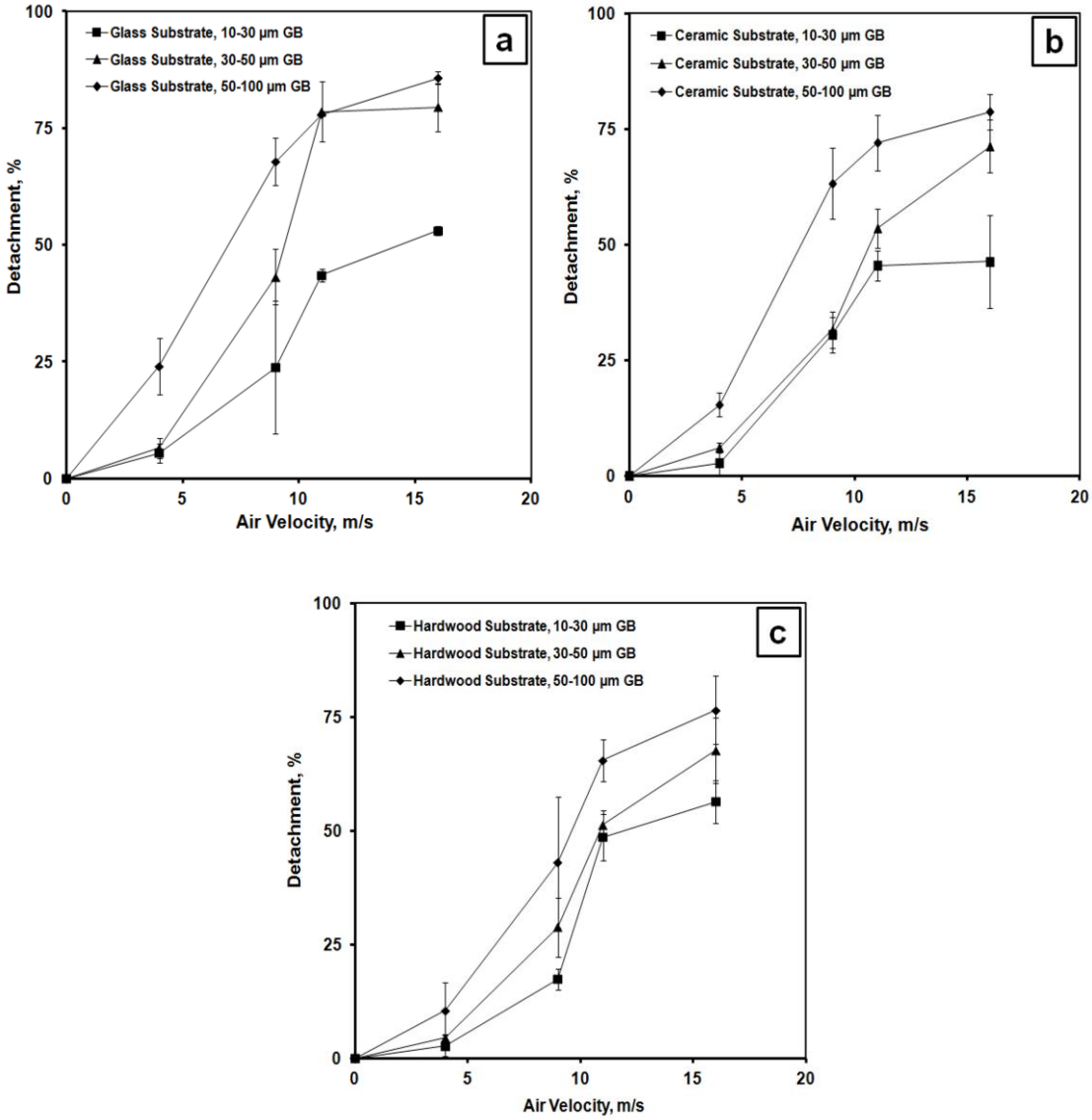

Figure 6.9. The dependence of detachment percentage of the different sizes glass bead particles on glass, ceramic and hardwood substrates in a velocity range of 0-16 m/s after 5 s.

6.1.1.3 Resuspension Rate

In general, resuspension rates of particles from the surfaces change over time and ranging from 0 to 7 s^{-1} with three regimes to be considered. The first regime lasts for less than 0.5 s with zero values for the resuspension rate in all different cases; the second regime is characterized by rapid exponential increase. However, the third regime exhibits opposite behavior of slower exponential decay that lasts until the end of the 5 s recording (Figures 6.10, 6.11, 6.12). For resuspension to occur, the aerodynamic drag force must be greater than the adhesion force (Wu et al. 1992). Very likely, the adhesion forces were initially higher than the drag forces causing the particles to stick to the surface with zero resuspension rates in the first 0.5 s. However, the increase in air speed with time from the stationary state to the desired speed caused the rapid increase in the resuspension rate in the second regime due to the corresponding increase in drag force. Beyond this time, the particles most easily resuspended have been removed, resulting in a nonlinear decrease in resuspension rate (Loosmore 2003). In addition, resuspension occurs when particles acquire enough energy to escape from the adhesive potential well and deeper wells result in lower resuspension rates. Allowing for variations in the strength of adhesive force among the particles, resuspension rate is found to decrease approximately inversely with time. This is typically what we observed in the third regime of our experiments.

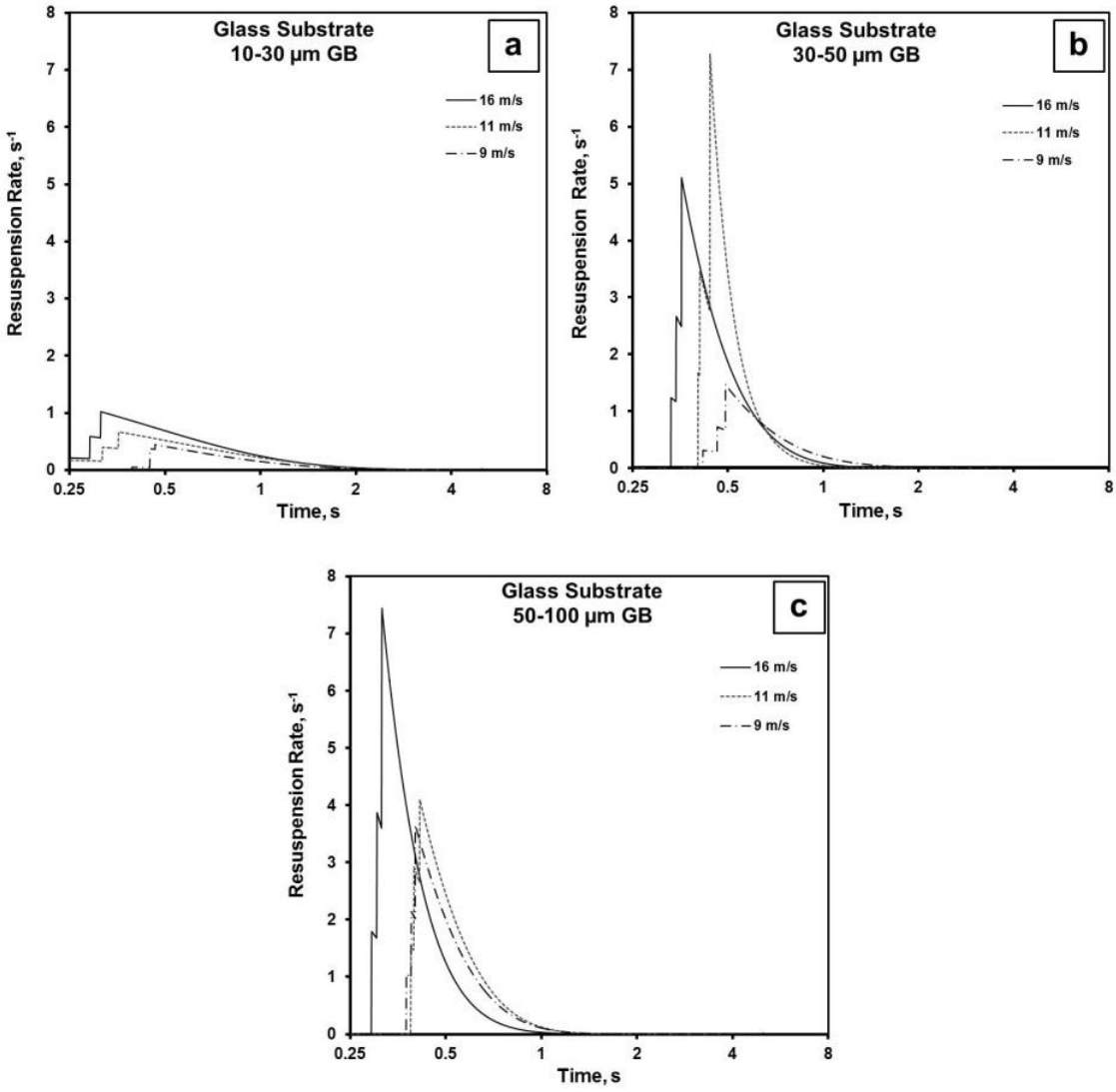

Figure 6.10 Time dependence of resuspension rate of different sizes glass bead particles on a glass substrate.

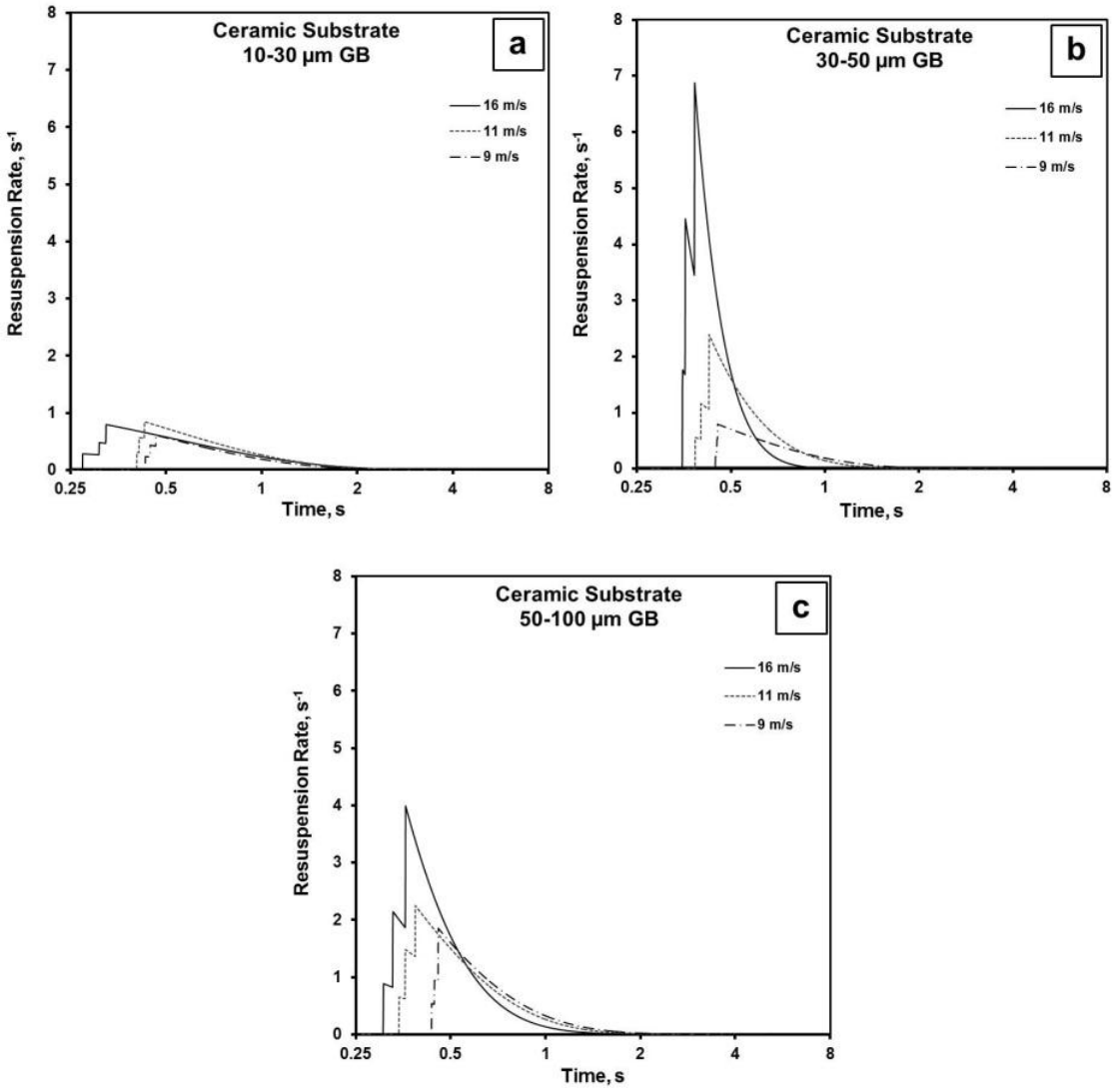

Figure 6.11 Time dependence of resuspension rate of different sizes glass bead particles on a ceramic substrate.

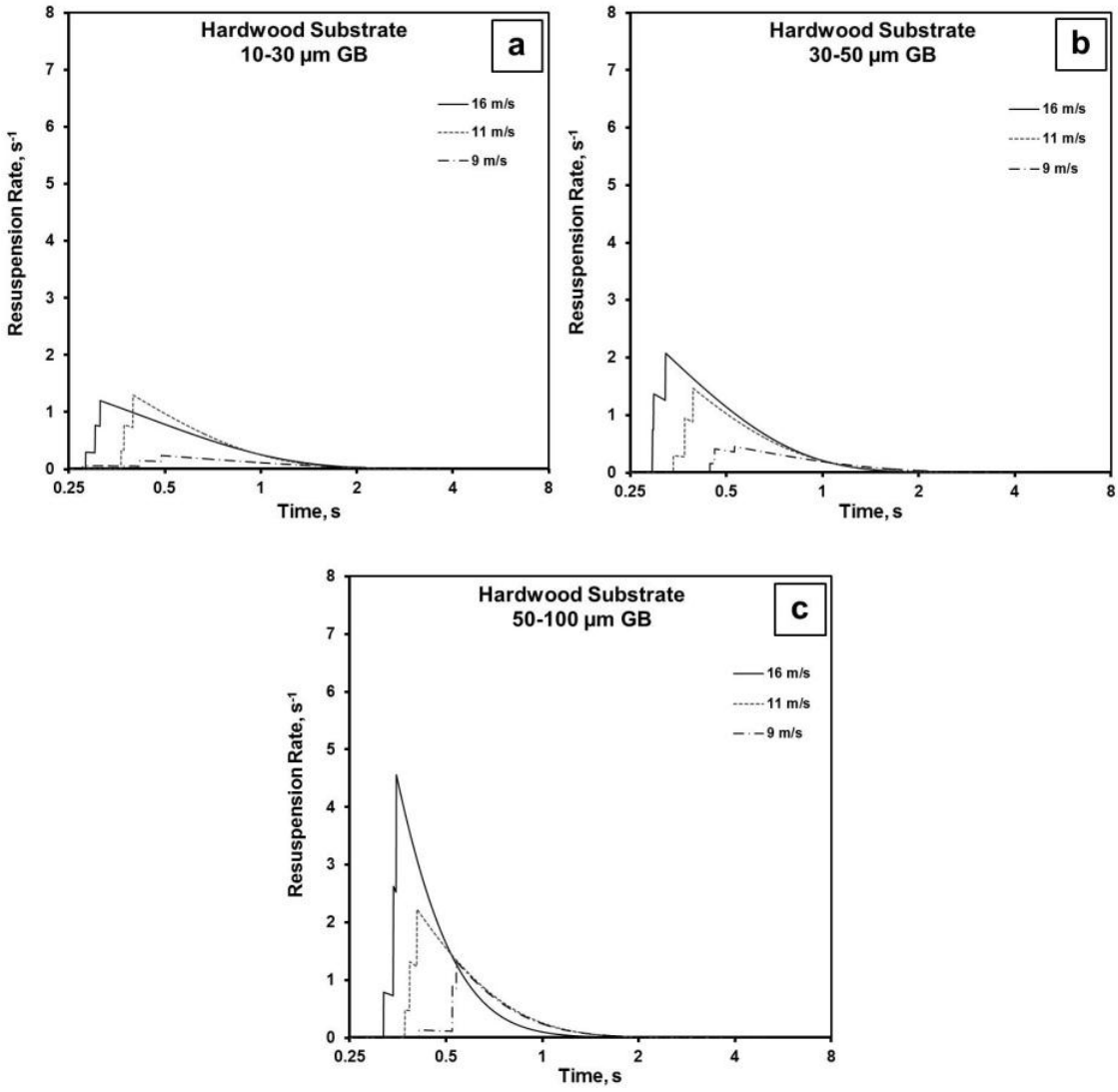

Figure 6.12 Time dependence of resuspension rate of different sizes glass bead particles on a hardwood substrate.

6.1.1.4 Summary

Resuspension may involve rolling or sliding (Jordan 1954; Hinds 1999). However, the rolling detachment is the dominant mechanism for particle removal in turbulent flows (Zhang and Ahmadi 2000, and Ibrahim et al. 2003). Despite the extensive studies of resuspension phenomena, there is still a significant lack of information about the path of particles very close to the surface (Harris and Davidson, 2008). Further data are needed to provide insight in the micro-mechanics of the particle removal process (Zhang and Ahmadi 2000). In this study, particle trajectories immediately before liftoff were investigated experimentally, using 3 different substrates representing different roughness characteristics. We found that glass beads (sizing ranging from 20-45 μm) experienced three different types of motion,

1. Rolling motion without any liftoff as earlier reported in literature; however, our high-speed imaging studies reveal that the particles also experience vertical bouncing while rolling on the surface.
2. Complex motion, where the particles simultaneously roll while bouncing up and down for a certain time before liftoff.
3. Immediate liftoff with no initial rolling or bouncing.

Particles experiencing rolling/bouncing motion seem to have stronger vertical velocity fluctuation energies compared to the total average kinetic energy. Conversely, rapid liftoff seems to be associated with higher kinetic energy. The longer it will take the particle to start its initial movement the more rapid is the liftoff once motion is initiated. Particle surface interactions were varied by changing the surface roughness, significantly

affecting initial motion prior to liftoff. Particles deposited on the smoothest substrate (100x less roughness for glass compared to hardwood and ceramic), required about 50% less particle kinetic energy/vertical velocity fluctuation to eventually liftoff. The greater the surface roughness (typically hardwood in our case), the longer it took the particle for initial motion to start ($t > 1$ s) causing a more rapid liftoff with a minimum or no initial rolling/ bouncing motion. In contrast, particle trajectories from the glass substrates seemed to have a complex motion, and the particle needs to travel about 25% with a rolling/bouncing motion before completely leaving the surface and lifting off. In this case, the majority of particle trajectories from the glass substrate tended to be directed parallel to the surface after liftoff. The ceramic substrate showed the most rolling/bouncing motion, for 80% of the particles recorded.

Changing the velocity, substrate and particle size for the glass bead particles significantly affects the detachment percentage with at least 97.5% statistical accuracy using ANOVA statistical analysis. The surface with the smallest roughness, glass, displayed the highest detachment over the entire particle size range tested. Very likely, larger particles penetrate higher into the boundary layer and thus experience higher removal forces. Larger surface roughness (such as hard wood in our case) provides more shielding, acting against resuspension. Moreover, the detachment percentage data initially follow an exponentially increasing trend for a period of ~1 s, followed by a plateau phase during the remainder of the 5 s imaging time.

Our experimental results point out the importance of identifying the different types of particle motion that occur prior to liftoff, and how their relative contributions

change with different particle and substrate materials. Incorporating these insights into the representation of particle-surface interactions in existing models will help improve their ability to accurately predict resuspension phenomena.

6.1.2 Paint Coating Effect on Metal Substrate

6.1.2.1 Particle Detachment and Resuspension Rate

Changing air velocity and particle size for the glass beads (GB) will significantly affect particle resuspension especially in the coated metal substrate (Figure 6.13a). However, for similar particle size (50-100 GB and 67-75 SS) particle density didn't show a significant effect (2500 kg/m^3 in glass beads particles, and 8000 kg/m^3 in the stainless steel particles), Figure 6.13a, and 6.13b. Very likely larger particles penetrate higher into the boundary layer and thus experience higher removal forces. As the particle size increases, removal forces increase more rapidly than adhesion forces. Removal forces depend on the Reynolds number and are generally proportional to Re^2 - Re^4, and, thus, to d_p^2 - d_p^4, while the adhesion forces are proportional to d_p.

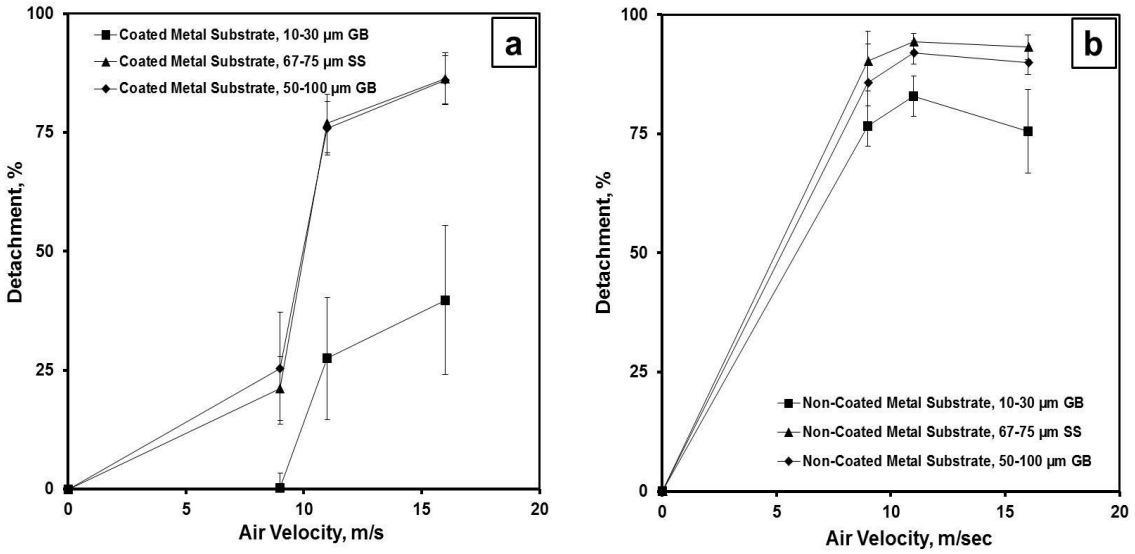

Figure 6.13 The dependence of detachment percentage of the different particles and sizes in a velocity range of 0-16 m/s after 5 s, a) Coated metal substrate (CARC), and b) Non-coated metal substrate.

In general, detachment from the non-coated metal substrate was consistently higher than the CARC coated metal substrates regardless of air speed used (Figure 6.13b) and in all different particle sizes and types, Figure 6.14. Larger surface roughness (1.19 µm in the CARC substrate compared to 0.09 µm in the non-coated metal substrate) provides more shielding, acting against resuspension. Detachment from the SS 67-75 µm (Figure 6.13b) and GB 50-100 µm (Figure 6.13c) look identical under the same flow conditions.

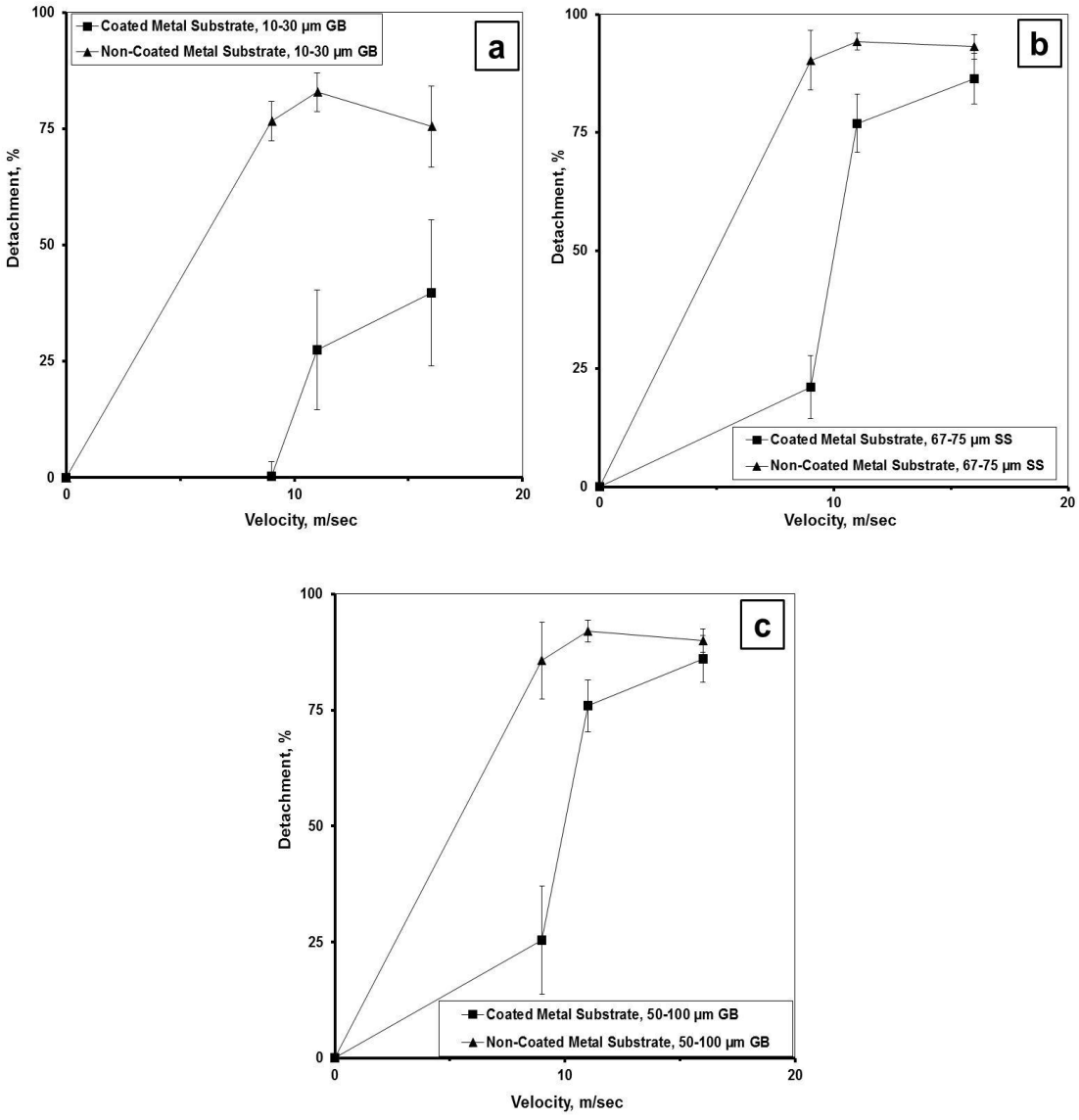

Figure 6.14 The dependence of detachment percentage of the different particles and sizes in a velocity range of 0-16 m/s after 5 s, a) Coated metal substrate (CARC),and b) Non-coated metal substrate.

Moreover, detachment percentage data initially follow an exponentially increasing trend for a certain period, followed by a plateau phase during the remainder of the 5 s recording time, with much higher detachment percentage observed on non-coated metal substrate (Figure 6.15). And the resuspension rate results shown in Figure 6.15 is similar to the results obtained in Figures (6.10, 6.11, and 6.12). However, the resuspension rates from the non-coated metal substrates were 6 times more than the resuspension rate from the coated metal substrate (CARC), (Figure 6.16). This phenomenon is also clear in the detachment data results.

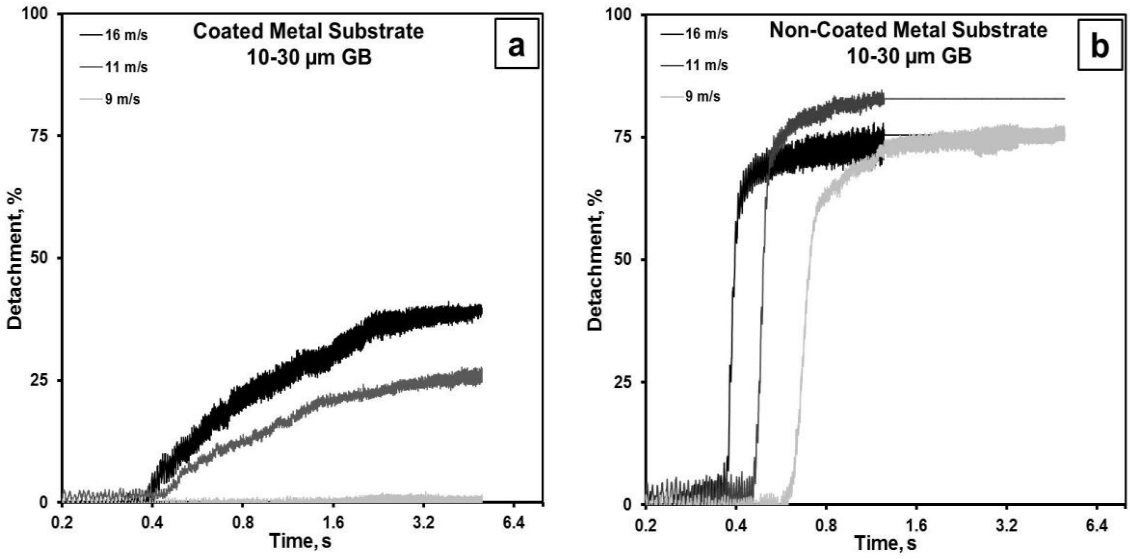

Figure 6.15 Time dependence of detachment percentage under different conditions (particle type, particle size, air speed, surface roughness).

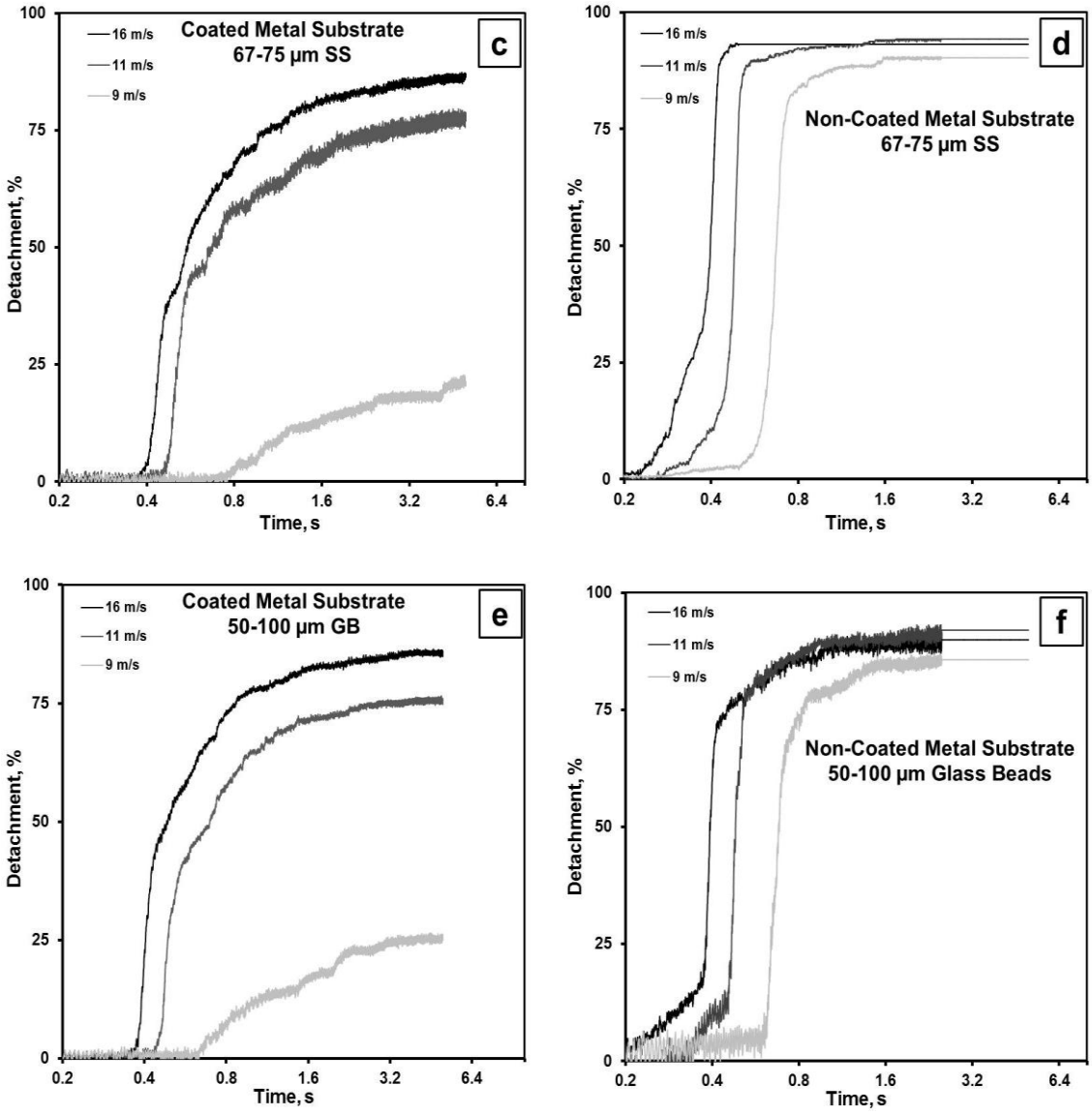

Cont. Figure 6.15

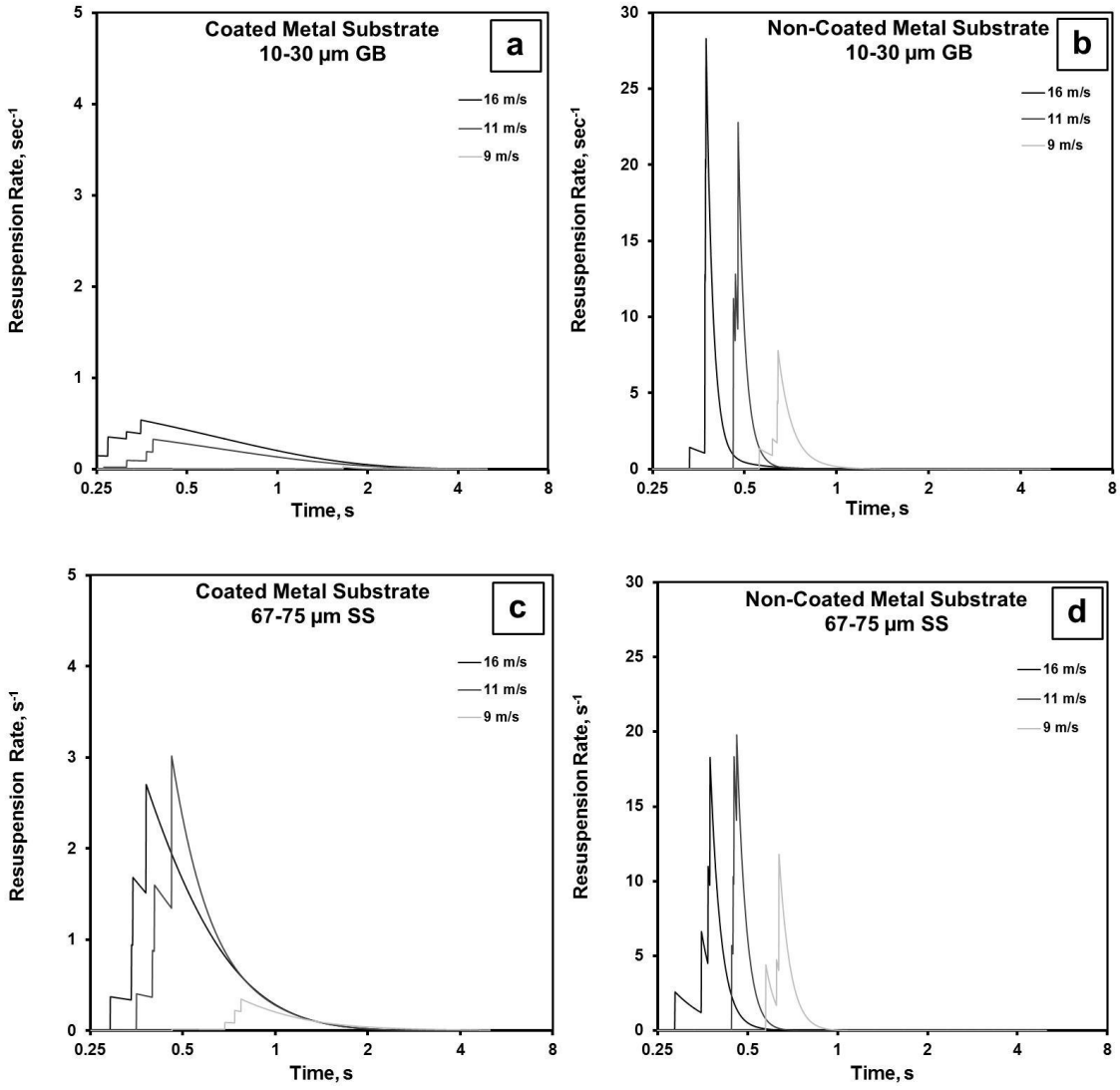

Figure 6.16 Time dependence of resuspension rate under different conditions (particle type, particle size, air speed, surface roughness).

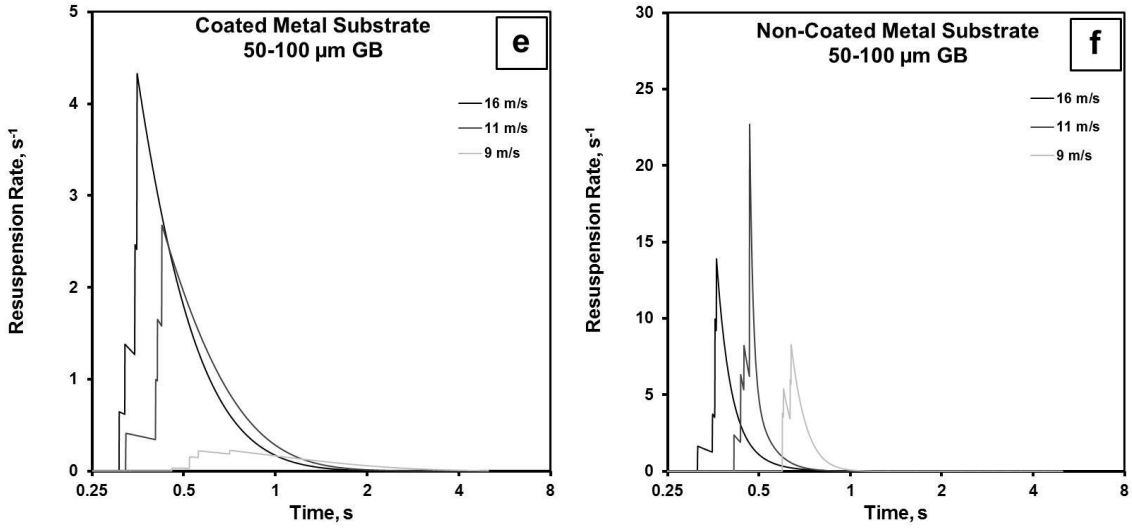

Cont. Figure 6.16

6.1.2.2 Summary

Resuspension from the non-coated metal substrate was consistently higher than the CARC coated metal substrates in all different particle sizes and type. Additionally, the surface with the smallest roughness, non-coated metal substrate, displayed the highest detachment over the entire particle size range tested. Larger surface roughness provides more shielding, acting against resuspension. Moreover, Particle size effect on the resuspension seems to be dominant regardless of particle type or surface roughness. Very likely, larger particles penetrate higher into the boundary layer and thus experience higher removal forces. However, particle density does not have a significant difference in the bigger particle size studied.

6.1.3 Relative Humidity and Residence Time

Increasing relative humidity from 48% to 90% reduced the detachment percentage by at least 6 times at 16 m/s and 24 hour residence time, Figure 6.17a and 6.17b. Very likely the water adsorbed within the interface asperities increases the effective contact area and, consequently, increases the pull-off force (Quon 2000 and Ando et al. 2000). However, particle residence time on the surface has been found to affect the detachment percentage, especially when the relative humidity is high (Ibrahim et al. 2004). To investigate the contribution of the residence time on the detachment percentage reduction, the glass beads particles were deposited at the glass substrates (10 samples total) then 5 samples were tested immediately after deposition (zero residence time) and the other 5 samples where left sealed overnight (24 hours residence time). Results confirmed previous observations for Ibrahim et al. (2004). Increasing residence time from 0 to 24 hours at the same relative humidity (48%) decreased the detachment percentage from 73 ± 15 to 28 ± 13 respectively Figure 6.17b, 6.17c and 6.18. On the other hand, increasing the relative humidity by 10% only, from 38% to 48% at zero residence time didn't affect the detachment percentage Figure 6.19.

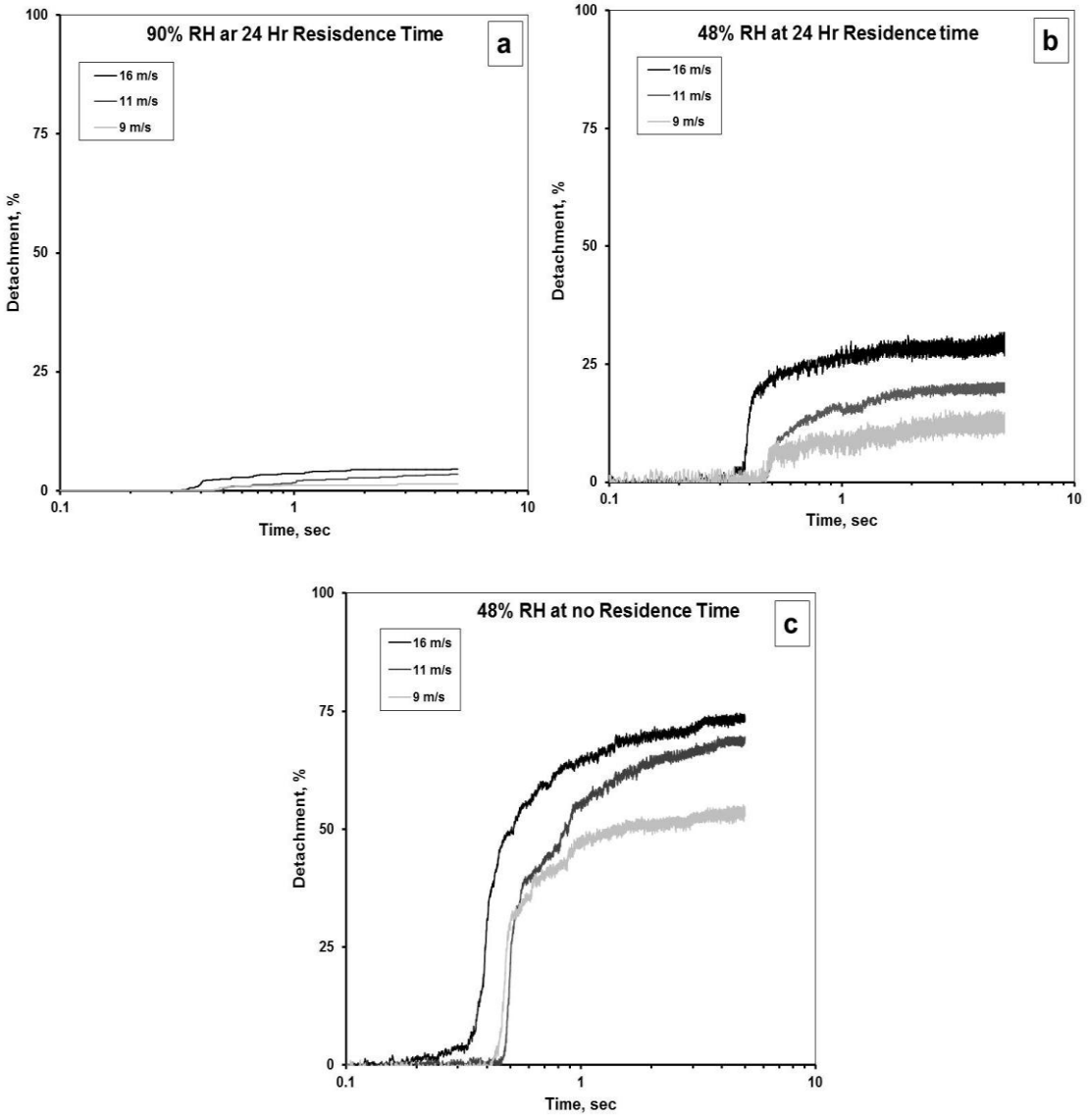

Figure 6.17 Effect of relative humidity and residence time on the detachment percentage of 30-50 μm glass bead particles on a glass substrate at different velocities.

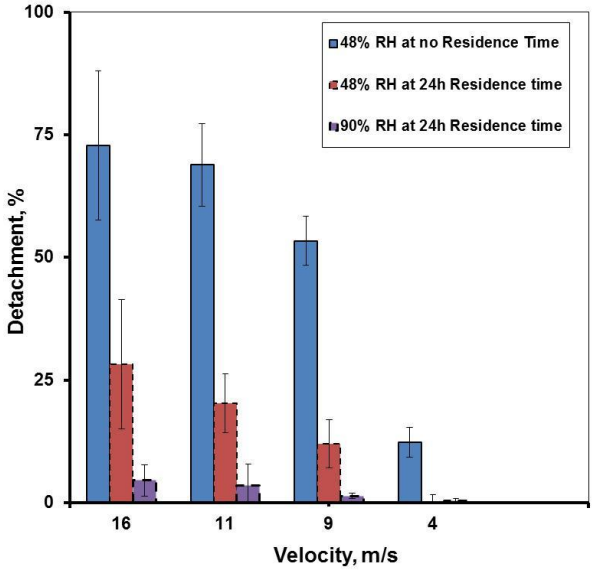

Figure 6.18 Effect of relative humidity and residence time on the detachment percentage of 30-50 µm glass bead particles on a glass substrate at 16 m/s and 5 s.

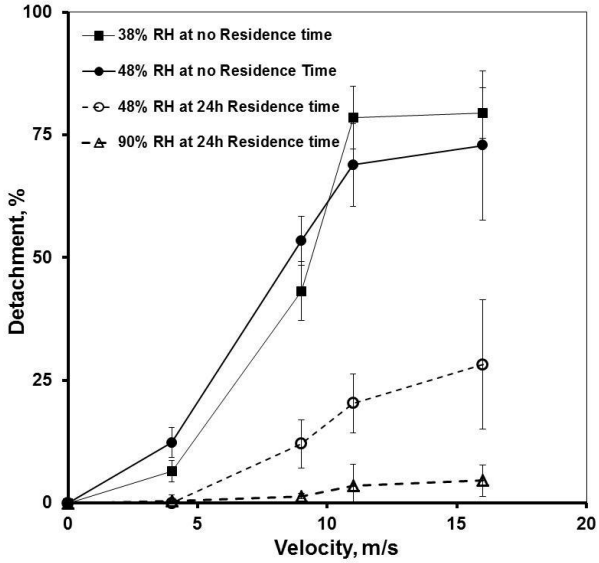

Figure 6.19 The dependence of detachment percentage on relative humidity and residence time in a velocity range of 0-16 m/s after 5 s.

6.1.4 Viable Particle Resuspension (Bacteria)

Results show zero resuspension and detachment for the single layer clusters of Btk spores on the glass substrate during the entire 5 s recording time at an increasing air speed from 0- 18 m/s in all particle concentrations and surface treatments. Very likely, the adhesive nature of bacteria is due to various outer membrane features such as pili, flagella, proteins, and lipopolysaccharides (LPSs). Once in contact with a material, the bacterium is able to engage in interactions dependent on the surface characteristics of both the bacterium and the material surface. In our flow conditions the shear flow was not sufficient for the removal of bacteria.

6.1.5 3-D Measurements

In this section, the experience we gained from the side-view and top-view imaging measurements and data analysis experiments were combined to initiate a methodology for 3-D particle tracking technique (section 4.3). The experimental setup was the exact same setup used in our previous experiments with the exception of using 2 cameras one from the top and the other from the side Figure (3.8). To minimize any error in data analysis, identical Telecentric lenses were mounted on both cameras at 4.5 x magnifications with a special resolution of about 5 μm/ pixel.

In 2000, Zhang and Ahmadi used an ensemble of 8192 particles for particle resuspension and the subsequent trajectory analyses. They found that large-size particles move away roughly perpendicular to the wall due to the action of the lift force. However, there was no experimental data that could provide insight in the micro-

mechanics of the particle removal process and validate their numerical results. Herein, we introduced detailed experiments for particle trajectories in section 6.1.1.1 that we successfully used to investigate the particle path before liftoff from different surfaces and obtained the mode associated with each surface. In this section, we tracked the SS particles on SS surfaces using two cameras simultaneously to obtain 3-D particle taking for the microparticles. Figure 6.20 shows the details particle path for 5 different SS micro-particles. Results obtained from the x-z trajectory (Figure 6.21a) are similar to the results obtained earlier from the side view trajectory experiments. In general, the particles seems travel in a constant angle to the left rather than going straight with the air stream line in the flow direction (x-y direction, Figure 6.21). The benefit of the 3-D particle tracking that the z-y trajectory can also be obtained (Figure 6.22). This technique has never been used in literature to investigate the resuspension phenomena which may introduce other aspects to investigate the problem.

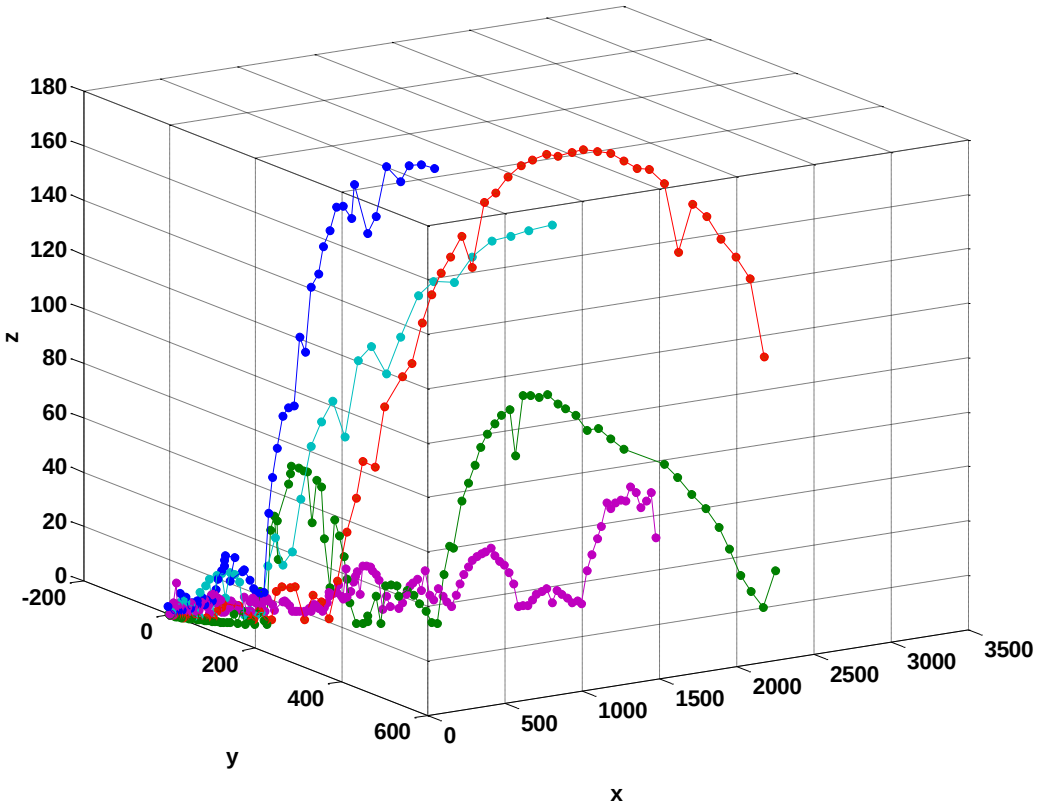

Figure 6.20 3-D particle path trajectory for the SS particle on the SS surface (x, y, and z dimensions are in µm).

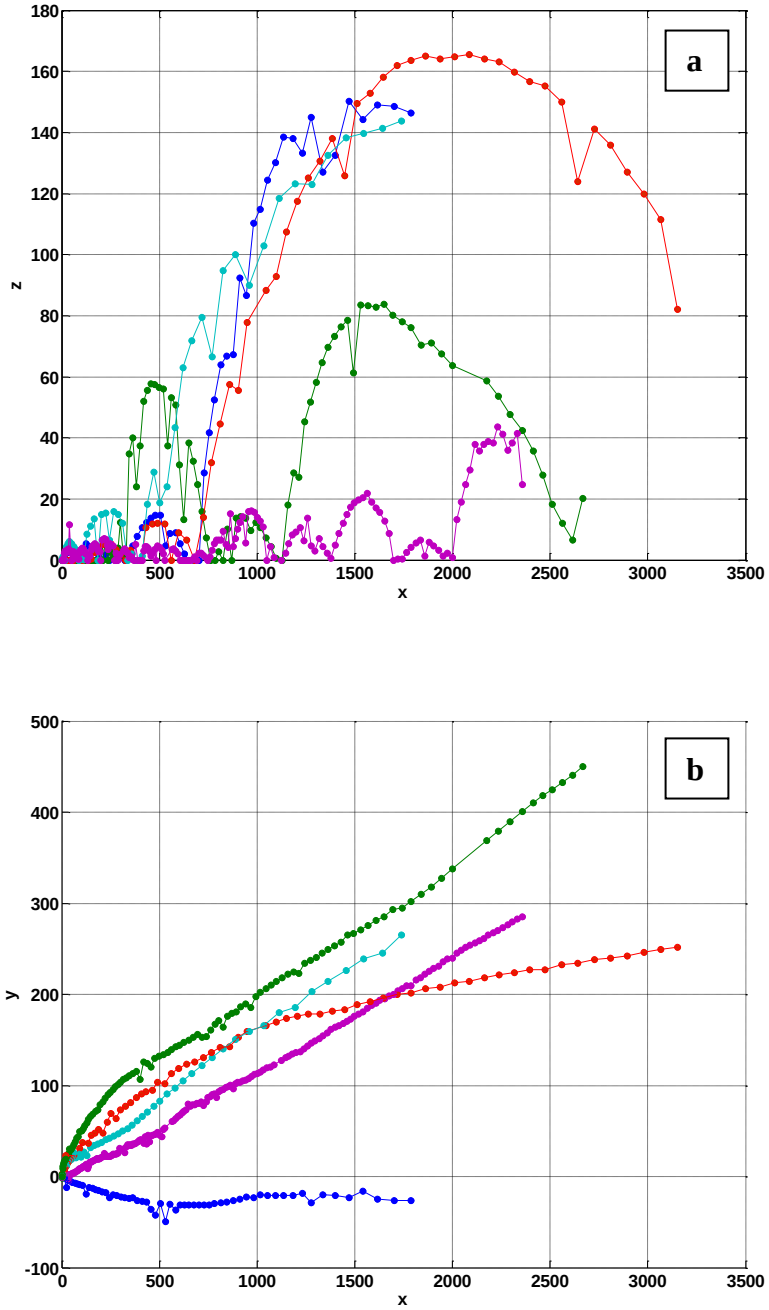

Figure 6.21 Particle trajectory for the SS particles on SS surface, a) x-z trajectories, b) x-y trajectories, and c) z-y trajectories (x, y, and z dimensions are in µm).

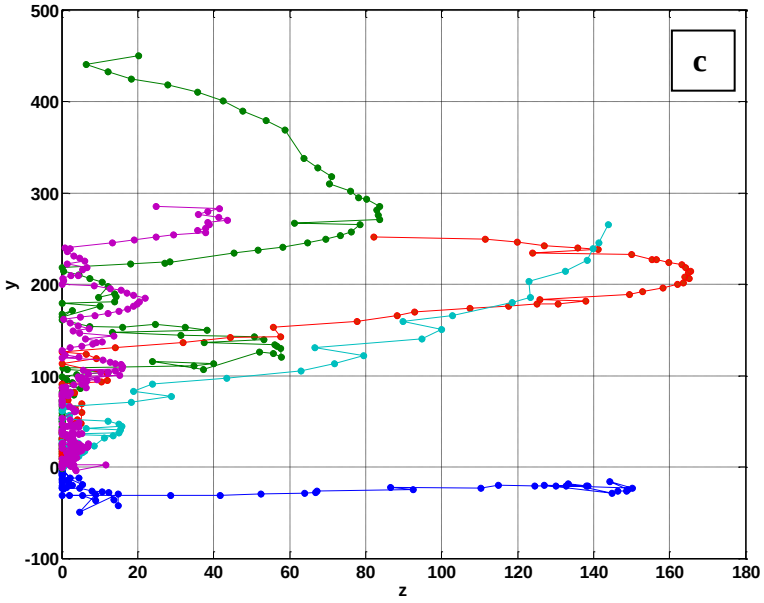

Cont. Figure 6.21

6.2 Modeling

6.2.1 Resuspension Rate

The resuspension rate experimental results were compared to those predicted by Kim's analytical model (Figure 6.22). In general, a ratio around one obtained when the resuspension rates were compared for the glass substrate at the smaller particle size range, < 50 μm (Figure 6.23). Very likely, such agreement is a reflection of the similarity of our experimental approach under these conditions with that of Ibrahim (2003) that was used to establish the correlations in the Kim model. Since Ibrahim's experiments were performed using smooth glass substrates. In contrast, the analytical

model tends to underestimate resuspension rates by a 10x factor in the ceramic and hardwood substrates. This seems to be consistent with previous observations that the roughest surfaces were the most under predicted by Kim's model (Kim et al. 2010).

In our experiments, we observe that the Kim analytical model most accurately predicts resuspension phenomena in the smooth glass substrates, whose roughness is 100x less than the other surfaces we examined at smaller particle sizes. According to Fuller and Tabor (1977) a roughness of only 1 μm is sufficient to reduce the adhesion to a small fraction of its value on a smooth surface. Since the glass substrate is much smoother, the adhesion mechanism may be expected to be better represented by the Hamaker constant that is incorporated in the model. This mechanism may not fully capture what is happening in the other rougher substrates. These differences are supported by Figure 6.1 where the "rolling/bouncing late liftoff" mechanism is seen only on the ceramic and hardwood surfaces. Therefore, in order to make more accurate predictions, our results suggest that resuspension models should be refined to incorporate the different types of particle motion prior to liftoff in order to better represent the particle surface interactions associated with different substrates.

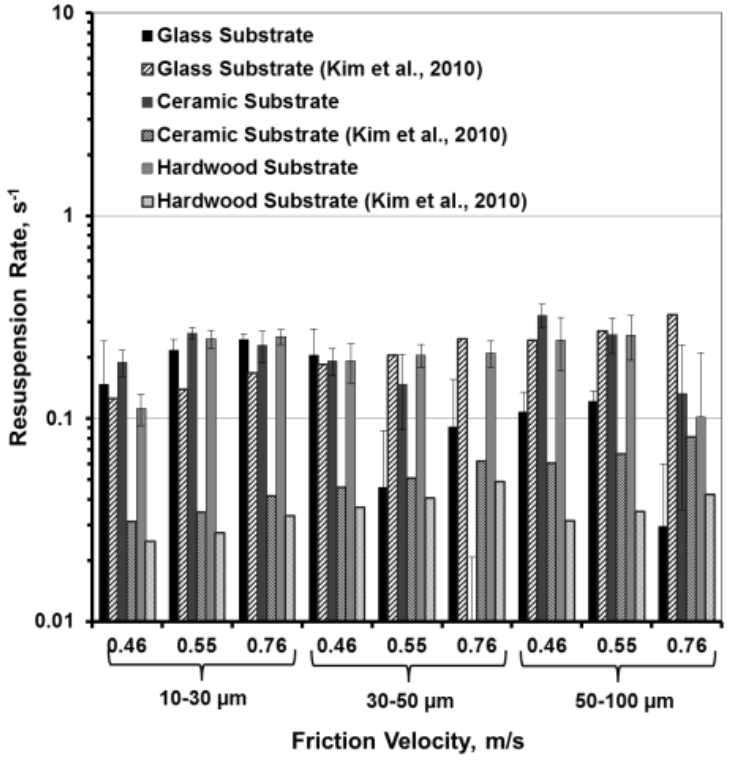

Figure 6.22 Comparison between our resuspension rate experimental results and Kim et al. (2010) analytical model at t=5 s.

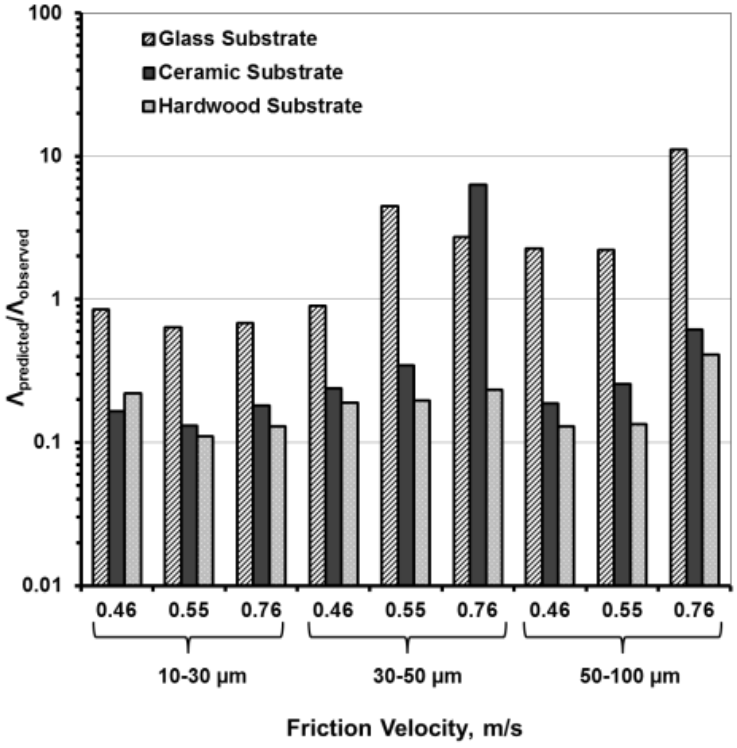

Figure 6.23 Performance of the Kim et al. (2010) analytical model against our experimental data at t=5 s.

6.2.2 Detachment Modes

Figure (6.24) demonstrate the minimum detachment velocities required for the different detachment modes to occur. As extensively discussed in section 5.3, the model was based on Ibrahim et al. (2003) force/moment balance approach (Figure 6.25), while taking into consideration the surface roughness effect in the adhesion forces from Cheng et al. (2002) and Szarek and Dunn (2007).

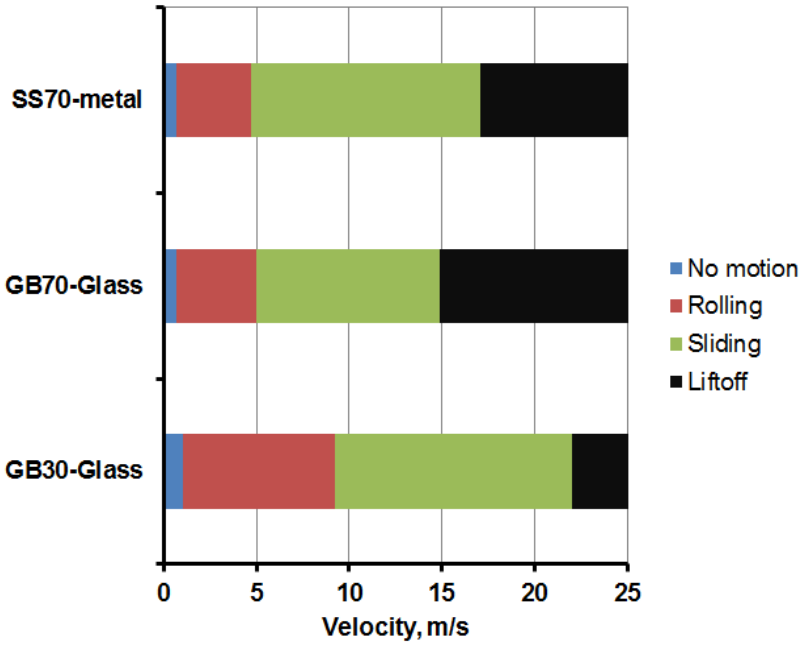

Figure 6.24 Velocity required for various detachment modes.

Results showed that the particle will start rolling then sliding and finally lift-off. Detachment by direct lift-off required a minimum of 14 m/s for both GB70 particles on glass surface and SS70 particles on metal surface, and the velocity increased to 21 m/s for the smaller particles (GB30 on glass surface). However, these results were 6 times smaller than earlier reported by Ibrahim et al (2003) for the same particles, Figure (6.26), especially for the lift-off to occur provided that the rolling was the dominant mode for their experiments. Very likely, such difference is due to the fact that in Ibrahim study it took much longer to reach the steady state free-stream velocity, 7-11 s compared to 1 s in our experiments. In our case we reached the steady state velocity much faster and consequently the direct liftoff. Additionally, the model suggested a sliding mechanism

although none of our experimental data showed any sliding. The experimental results emphasized the previous conclusions of Ibrahim that the particles will start its motion by rolling and not sliding. Furthermore, the rolling mechanism should help the particle liftoff and such interruption is not presented in the model.

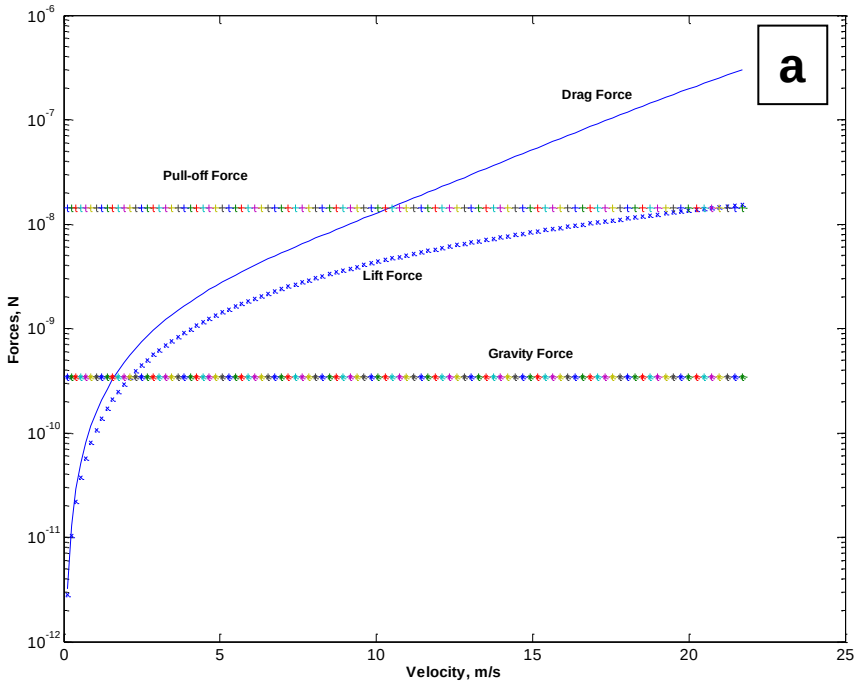

Figure 6.25 The progress of the different forces the free-stream velocity, a) GB30 on glass surface, b) GB70 on glass surface, and c) SS70 on metal surface.

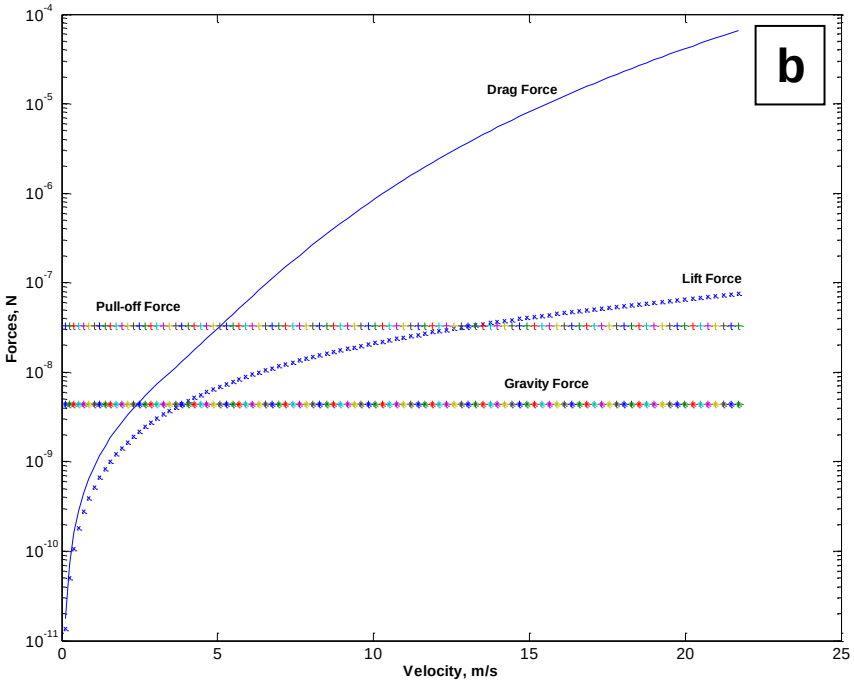

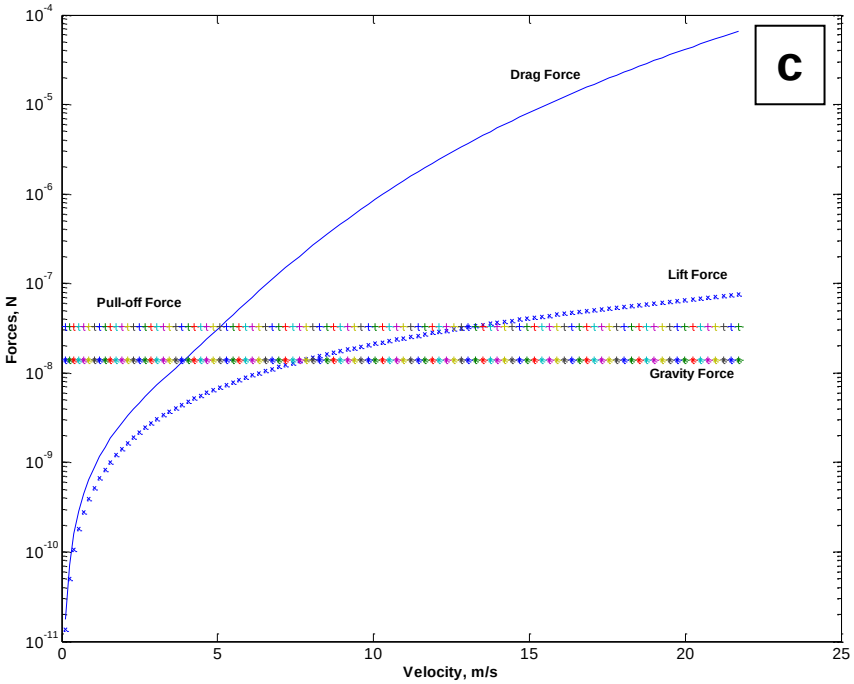

Figure 6.25 Cont.

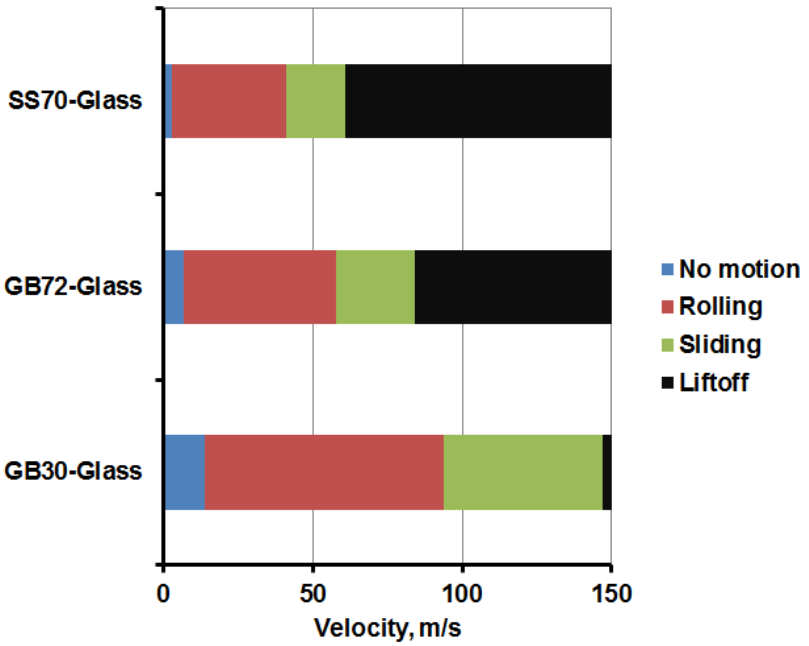

Figure 6.26 Velocity required for various detachment modes (Ibrahim et al. 2003).

7. CONCLUSIONS AND RECOMMENDATIONS FOR FUTURE WORKS

7.1 Conclusions

Resuspension may involve rolling or sliding (Jordan 1954; Hinds 1999). However, previous numerical results proved that the rolling detachment is the dominant mechanism for particle removal in turbulent flows with no emphasize on the experimental part (Zhang and Ahmadi 2000, and Ibrahim et al. 2003). Additionally, despite the extensive studies of resuspension phenomena, there is still a significant lack of information about the path of particles very close to the surface (Harris and Davidson 2008). Further data are needed to provide insight in the micro-mechanics of the particle removal process (Zhang and Ahmadi 2000). In this study, global particle detachment, resuspension rate, detachment modes and particle trajectories immediately before liftoff were investigated. Different experimental parameters where taken into consideration such as, air velocity, detachment time, residence time, particle size, particle type, surface roughness and relative humidity. In general, particle detachment increases with increasing friction velocity, particle size, detachment time and decreases with increasing surface roughness, relative humidity and residence time with no significant impact on the particle type.

We found that micro-particles (sizing ranging from 20-45 μm) experienced three different types of motion,

1. Rolling motion without any liftoff as earlier reported in literature; however, our high-speed imaging studies reveal that the particles also experience vertical bouncing while rolling on the surface.
2. Complex motion, where the particles simultaneously roll while bouncing up and down for a certain time before liftoff.
3. Immediate liftoff with no initial rolling or bouncing.

Particles experiencing rolling/bouncing motion seem to have stronger vertical velocity fluctuation energies compared to the total average kinetic energy. Conversely, rapid liftoff seems to be associated with higher kinetic energy. The longer it will take the particle to start its initial movement the more rapid is the liftoff once motion is initiated. Particle surface interactions were varied by changing the surface roughness, significantly affecting initial motion prior to liftoff. Particles deposited on the smoothest substrate (100x less roughness for glass compared to other surfaces), required about 50% less particle kinetic energy/vertical velocity fluctuation to eventually liftoff. The greater the surface roughness (hardwood in this experiment), the longer it took the particle for initial motion to start ($t > 1$ s) causing a more rapid liftoff with a minimum or no initial rolling/ bouncing motion. In contrast, particle trajectories from the glass substrates seemed to have a complex motion, and the particle needs to travel about 25% with a rolling/bouncing motion before completely leaving the surface and lifting off. In this case, the majority of particle trajectories from the glass substrate tended to be directed parallel to the surface after liftoff. The ceramic substrate showed the most rolling/bouncing motion, for 80% of the particles recorded. These results were also

confirmed by an initial 3-D particle tracking for the SS particles on SS surfaces. 3-D particle tracking showed that the particles seem to travel in a constant angle to the left rather than going straight with the air stream line in the flow direction. This technique has never been used in literature to investigate the resuspension phenomena which may introduce other aspects to investigate the problem. The detachment mode model confirmed the experimental results.

Changing the velocity, substrate and particle size for the glass bead particles significantly affects the detachment percentage with at least 97.5% statistical accuracy using ANOVA statistical analysis. The surface with the smallest roughness, glass, displayed the highest detachment over the entire particle size range tested. Very likely, larger particles penetrate higher into the boundary layer and thus experience higher removal forces. Larger surface roughness (such as hard wood in our case) provides more shielding, acting against resuspension. Moreover, the detachment percentage data initially follow an exponentially increasing trend for a period of ~1 s, followed by a plateau phase during the remainder of the 5 s imaging time.

On the other hand, resuspension from the non-coated metal substrate was consistently higher than the CARC coated metal substrates in all different particle sizes and types. Additionally, the surface with the smallest roughness, non-coated metal substrate, displayed the highest detachment over the entire particle size range tested. Larger surface roughness provides more shielding, acting against resuspension. Moreover, particle size effect on the resuspension seems to be dominant regardless of

particle type or surface roughness. However, particle density is not a significant difference in the bigger particle size studied.

Our experimental results point out the importance of identifying the different types of particle motion that occur prior to liftoff, and how their relative contributions change with different particle and substrate materials. Incorporating these insights into the representation of particle-surface interactions in existing models will help improve their ability to accurately predict resuspension phenomena.

7.2 Recommendations for Future Work

It is recommended to extend this work using a smaller particle size ~ 5 μm and more varieties of surface roughness. Additionally, more attention should be given to extend the 3-D particle tracking technique introduced in this study. This technique has never been used in literature to investigate the resuspension phenomena which may introduce other aspects to investigate the problem.

On the other hand, a better adhesion model is essential to accurately incorporate the experimental results regarding the effect of surface roughness on the different detachment modes. Furthermore, it is recommended to enhance Ibrahim 2004 model to include the possibilities of complex motion when the particles start rolling then finally liftoff. The model was designed for one mode to occur and as proposed by our experiments several modes are expected.

REFERENCES

Ando, Y. (2000). The Effect of Relative Humidity on Friction and Pull-off Forces Measured on Submicron-Size Asperity Arrays. *Wear*. 238:12-19.

Andrews, R. E., Faust Jr., R. M., Wabiko, H., Raymond, K. C., and Bulla, L. B. (1987). The Biotechnology of *Bacillus Thuringiensis*. *CRC Cri. Rev. Biotechnol*. 6:163-232.

Andrews, R. E., Bibilops, M. M., and Bulla, L. A. (1985). Protease Activation of the Entomocidal Protoxin of *Bacillus thuringiensis* subsp. *kurstaki*. *Appl. Environ. Microbiol.* 50:737-742.

Ardey, N., and Mayinger, F. (1998). Aerosol Resuspension by Highly Transient Containment Flow: Insights by Means of Laser Optical Methods. *Kerntechnik*. 63:68-75.

Armenio, V., and Fiorotto, V. (2001). The Importance of the Forces Acting on Particles in Turbulent Flows. *Phys. Fluids.* 13:2437-2440.

Boor, B. E. (2010). Monolayer & Multilayer Particle Resuspension from Indoor Surfaces: Literature Review and Experimental Methodology. M.S. Thesis, The University of Texas at Austin.

Boor, B. E., Siegel, J. A., and Novoselac, A. (2011). Development of an Experimental Methodology to Determine Monolayer and Multilayer Particle Resuspension from Indoor Surfaces, *ASHRAE Transactions*, 117:434-441.

Bottiger, J. R., Deluca, P. J., Stuebing, E.W., and Vanreenen, D. R. (1998). An Ink Jet Aerosol Generator. *J. Aerosol Sci.* 29:S965-S966.

Bottiger, J. R., and Deluca, P. J. (1999). Low Concentration Aerosol Generator. US Patent 5,918,254. Issued June 29, 1999. US Patent Office, Washington, DC.

Bowling, R. A. (1988). A Theoretical Review of Particle Adhesion, in, *Particles on Surfaces 1: Detection, Adhesion and Removal*, K. L. Mittal, ed. Plenum Press, New York.

Braaten, D. A. (1994). Wind Tunnel Experiments of Large Particle Reentrainment-Deposition and Development of Large Particle Scaling Parameters. *Aerosol Sci. Technol.* 21:157-169.

Braaten, D. A., Paw, K. T., and Shaw, R. H. (1990). Particle Resuspension in a Turbulent Boundary Layer-Observed and Modeled. *J. Aerosol Sci.* 21:613-628.

Bulla, L. A., Faust Jr., R. M., Andrews, R., and Goodman, N. (1985). Insecticidal Bacilli., in *The Moleculer Biology of the Bacilli*, Academic Press. Inc., New York.

Burdick, G. M., Berman, N. S., and Beaudoin, S. P. (2005). Hydrodynamic Particle Removal from Surfaces. *Thin Solid Film.* 488:116-123.

Cheng, W., Brach, R. M., and Dunn, P. F. (2002). Surface Roughness Effects on Microparticle Adhesion. *J. Adhesion.* 78:929-965.

Cleaver, J. W., and Yates, B. (1973). Mechanism of Detachment of Colloidal Particles from a Flat Substrate in a Turbulent Flow. *J. Colloid Interface Sci*. 44:464-474.

Cohen, B.L. (1977). Hazards from plutonium toxicity. *Hlth. Phys.* 32:359-379.

Corn, M., and Stein, F. (1965). Re-entrainment of Particles from a Plane Surface. *Amer. Ind. Hyg. Assoc. J.* 26:325-336.

Corn, M., and Stein, F. (1966). Adhesion of Atmospheric Dustfall Particles to a Glass Slide. *Nature.* 211:60-61.

Estrada-Pérez, C. E. (2009). Experimental Two-Phase Flow Characterization of Subcooled Boiling in a Rectangular Channel, M.S. Thesis, Texas A&M University.

Estrada-Pérez, C. E., and Hassan, Y. A. (2010). PTV Experiments of Subcooled Boiling Flow Through a Vertical Rectangular Channel. *Int. J. Multiphase Flow.* 36:691-706.

Feng, Y., Goree, J., and Liu, B. (2011). Errors in Particle Tracking Velocimetry with High Speed Cameras. *Rev. Sci. Instrum.* 82(053707):1-7.

Fox, R. W., McDonald, A. J., Pritchard, P. J. (2004). *Introduction to Fluid Mechanics*. (6^{th} ed.). John Wiley & Sons, Inc. New York.

Gillette, D. A., Lawson Jr., R. E., and Thompson, R. S. (2004). A "Test of Concept" Comparison of Aerodynamic and Mechanical Resuspension Mechanisms for Particles Deposited on Field Rye Grass *(Secale cercele).* Part1. Relative particle flux rates. *Atmos. Environ.* 38:4789-97.

Goldasteh, I., Ahmadi, G., and Ferro, A. (2010). Effect of Air Flow on Dust Particles Resuspension from Common Floorings. Proceedings of ASME 2010 3^{rd} Joint US-European Fluids Engineering Summer Meeting and 8^{th} International

Conference on Nanochannels, Microchannels, and Minichannels, August 1-5, 2010, Montreal, Canada.

Grzybowski, K., and Gradoń, L. (2007). Re-entrainment of Particles from Powder Structures: Experimental Investigations. *J. Soc. Powder Technol.*. 18:427-439.

Guingo, M. and Minier, J. P. (2008). A New Model for the Simulation of Particle Resuspension by Turbulent Flows Based on a Stochastic Description of Wall Roughness and Adhesion Forces. *J. Aerosol Sci*. 39:957-973.

Hall, D. (1988). Measurements of the Mean Force on a Particle Near a Boundary in Turbulent Flow. *J. Fluid Mech.* 187:451-466.

Happel, J., and Brenner, H. (1973). *Low Reynolds Number Hydrodynamics*. Noordhoff Intl. Pub., Leiden.

Harris, A. R., and Davidson, C. I. (2008). Particle Resuspension in Turbulent Flow: A Stochastic Model for Individual Soil Grains. *Aerosol Sci. and Technol.* 42:613-628.

Hertz, H. (1896). *Miscellaneous Papers.* MacMillan and Co., London.

Hinds, W. C. (1999). *Aerosol Technology: Properties, Behavior, and Measurement of Airborne Particles* (2nd ed). John Willy & Sons, New York.

Hu, S., Kim, T. H., Park, J. G., and Busnaina, A. A. (2010). Effect of Different Deposition Medium on the Adhesion and Removal of Particles. *J. of Electrochemical Soc.* 157:H662-H665.

Ibrahim, A. H. (2004). Microparticle Detachment from Surfaces by Fluid Flow. Ph.D. Dissertation, University of Notre Dame.

Ibrahim, A. H., and Dunn, P. F. (2006). Effects of Temporal Flow Acceleration on the Detachment of Microparticles from Surfaces. *J. Aerosol Sci*. 37:1258-1266.

Ibrahim, A. H., Dunn, P. F., and Brach, R. M. (2003). Microparticle Detachment from Surfaces Exposed to Turbulent Air Flow: Controlled Experiments and Modeling. *J. Aerosol Sci.* 34:765-782.

Ibrahim, A. H., Dunn, P. F., and Brach, R. M. (2004a). Microparticle Detachment from Surfaces Exposed to Turbulent Air Flow: Microparticle Motion after Detachment. *J. Aerosol Sci.* 35:1189-1204.

Ibrahim, A. H., Dunn, P. F., and Brach, R. M. (2004b). Microparticle Detachment from Surfaces Exposed to Turbulent Air Flow: Effects of Flow and Particle Deposition Characteristics. *J. Aerosol Sci.* 35:805-821.

Ibrahim, A. H., Dunn, and Qazi, M. F. (2008). Experiments and Validation of a Model for Microparticle Detachment from a Surface by Turbulent Air Flow. *J. Aerosol Sci.* 39:645-656.

Incropera, F. P., and DeWitt, D. P. (2002*). Fundamentals of Heat and Mass Transfer* (5^{th} ed.). John Wiley & Sons. New York.

John, W. (1995). Particle Surface Interaction: Charge Transfer, Energy Loss, Resuspension, and Deagglomeration, *Aerosol Sci. and Technol*. 23:2-24.

Johnson, K. L., and Greenwood, J. A. (1997). An Adhesion Map for the Contact of Elastic Spheres. *J. Colloid Interface Sci*. 192:326-333.

Johnson, K. L., Kendall, K., and Roberts, A. D. (1971). Surface Energy and the Contact of Elastic Solids. *Proceedings of the Royal Society of London,* Series A. 324:301-313.

Jordan, D. W. (1954). The Adhesion of Dust Particles, *Brit. J. Appl. Phys.* 3:S194-S197.

Kassab, A. S. (2009). Effect of Collection Method and Archiving Conditions on the Survivability of Vegetative and Spore Forming Bacteria. M.S. Thesis, Texas A&M University.

Katainen, J., Paajanen, M., Ahtola, E., Pore, V. and Lahtinen, J. (2006). Adhesion as an Interplay between Particle Size and Surface Roughness. *J. Colloid Interface Sci*. 304:524-529.

Kay, J . M. and Neddermardn, M. (1974). *Fluid Mechanics and Heat Transfer* (3^{rd} ed.) Cambridge University Press, Cambridge.

Kays, W., Crawford, M. and Weigand, B. (2005). *Convection Heat and mass Transfer* (4^{th} ed.). McGraw-Gill, New York.

Kim, Y., Gidwani, A., Wyslouzil, B. E., and Sohn, C. W. (2010). Source Term Models for Fine Particle Resuspension from Indoor Surfaces. *Building and Environment.* 45:1854-1865.

Krauter, P., and Biermann, A. (2007). Reaerosolization of Fluidized Spores in Ventilation Systems. *Appl. Environ. Microbiol.* 73:2165-2172.

Krupp, H. (1967). Particle Adhesion Theory and Experiment. *Advan. Colloid Interface Sci.* 1:111-239.

Lassey, K. R. (1980). The possible importance of short-term exposure to resuspended radionuclides. *Hlth. Phys.* 38:749-761.

Leighton, D., and Acrivos, A. (1985). The Lift on a Small Sphere Touching a Plane in the Presence of a Simple Shear Flow. *J. Appl. Math. and Phys*. 36:174-178.

Lipson, C., and Sheth, N. J. (1973). *Statistical Design and Analysis of Engineering Experiments.* McGraw-Hill, New York.

Lohaus, J. H., Novoselac, A., and Siegel, J. A. (2008). Particle Resuspension from Indoor Flooring Materials. *Proceedings of the 11th International Conference on Indoor Air and Climate*, paper ID 342, 1.

Loosmore, G. A. (2000). Dust Resuspension and the Implications for Contaminant Transport. Ph.D. Dissertation, University of California, Berkeley.

Loosmore, G. A. (2003). Evaluation and Development of Models for Resuspension of Aerosols at Short Times after Deposition. *Atmospheric Environment*. 37:639-647.

Madigan, M. T., Martinco, J. M., and Parker, J. (2000). Endospore-Forming, Low GC, Gram-Positive Bacteria, in *Brock Biology of Microorganisms*, Prentice-Hall, Inc., Upper Saddle River, New Jersey.

Masironi, L. A. and Fish, B. R. (1964). Direct Observation of Particle Reentrainment from Surfaces, in *Surface Contamination*, B. R. Fish, ed. Tennessee, June 1964.

Maugis, D. (1991). Adhesion of Sphere: The JKR-DMT Transition Using a Dugdale Model. *J. Colloid Interface Sci.* 150:243-269.

Miller, R. W. (1996). *Flow Measurement Engineering Handbook* (3rd ed.). McGraw Hill, New York.

Mishulovich, A., and Evanko, J. L. (2003). Ceramic Tiles from High-Carbon Fly ash. *International Ash Utilization Symposium*, Center for Applied Energy Research, University of Kentucky.

Mollinger, A. M., and Nieuwstadt, F. T. M. (1996). Measurements of the Lift Force on a Particle Fixed to the Wall in the Viscous Sublayer of a Fully Developed Turbulent Boundary Layer. *J. Fluid Mech.* 316:285-306.

Moody, L. F., Princeton, N., J. (1944). Friction Factor for Pipe Flow. *Transactions of the ASME*. Pittsburge, Pa. 66: 671-684.

Mukai, C., Siegel, J. A. and Novoselac, A. (2009). Impact of Airflow Characteristics on Particle Resuspension from Indoor Surfaces. *Aerosol Sci. and Technol.* 43:1022-1032.

Nicholson, K. W. (1993). Wind Tunnel Experiments on the Resuspension of Particulate Material. *Atmospheric Environment.* 27A:181-188.

O'Neill, M. E. (1968). A Sphere in Contact With a Plane Wall in a Slow Linear Shear Flow. *Chem. Eng. Sci*. 23:1293-1298.

Phares, D. J., Smedley, G. T., and Flagan, R. C. (2000). Effect of Particle Size and Material Properties on Aerodynamic Resuspension from Surfaces. *J. Aerosol Sci.* 31:1335-1354.

Prandtl, L. and Tietjens, O. G. (1934). *Applied Hydro and Aerodynamics*, Eng. Soc. Monographs, New York.

Qian, J., and Ferro, A. R. (2008). Resuspension of Dust Particles in a Chamber and Associated Environmental Factors. *Aerosol Sci. and Technol.* 42:566-578.

Quon, R. A., Ulman, A., and Vanderlick, T. K. (2000). Impact of Humidity on Adhesion Between Rough Surfaces. *Langmuir.*16:8912-8916.

Rubinow, S. I., and Keller, J. B. (1961). The Transverse Force on Spinning Sphere Moving in a Viscous Fluid. *J. Fluid Mech*. 11:447-459.

Saffman, P. G. (1965). The Lift on a Small Sphere in a Slow Shear Flow. *J. Fluid Mech.* 22:385-400.

Slinn, W. G. N. (1978). Parameterisations for Resuspension and for Wet and Dry Deposition of Particles and Gases for Use in Radiation Dose Calculations. *Nuclear Safety*. 19:205-219.

Soltani, M, and Ahmadi, G. (1994). On Particle Adhesion and Removal Mechanisms in Turbulent Flows. *J. Adhes. Sci. and Technol*. 8:763-785.

Soltani, M., and Ahmadi, G. (1995). Direct Numerical Simulation of Particle Entrainment in Turbulent Channel flow. *Phys. Fluids*. 7:647-657.

Stahly, D. P., Andrews, R. E., and Yousten, A. A. (1991). The Genus *Bacillus*- Insect Pathogens., in *The Prokaryotes* (2^{nd} ed.), A. Ballows, ed. Springer Verlag, New York.

Szarek, T. R., and Dunn, P. F. (2007). An Apparatus to Determine the Pull-Off Force of a Conducting Microparticle from a Charged Surface. *Aerosol sci. and Technol.* 41:43-50.

Tabor, D. (1977). Surface Forces and Surface Interaction. *J. Colloid Interface Sci.* 58:2-13.

Tippayawong, N., and Preechawuttipong, I. (2011). Analysis of Microparticles Resuspension in Turbulent Flows with Horizontally Vibration Surface. *Aust. J. of Basic and appl. Sci.* 5:356-363.

Versteeg, H. K. and W. Malalasekera (1995). *An Introduction to Computational Fluid Dynamics*. Longman Scientific & Technical, Essex.

Wang, H. C. (1990). Effects of Inceptive Motion on Particle Detachment from Surfaces. *Aerosol Sci. Technol.* 13:386-393.

Wu, Y., Davidson, C. I., and Russell, A. G. (1992). Controlled Wind Tunnel Experiments for Particle Bounceoff and Resuspension. *Aerosol Sci. and Technol*. 17:245-262.

Yao, J., Zhang, Y., Wang, C. H., and Liang, Y. C. (2006). On The Electrostatic Equilibrium of Granular Flow in Pneumatic Conveying System. *ALCHE J.* 52: 3775-3793.

Yao, J., and Fairweather, M. (2010). Inertial particle Resuspension in a Turbulent, Square Duct Flow. *Phys. Fluids.* 22(3):033303.

Zenz, F. A, (1964). Conveyability of Materials of Mixed Particle Size. *Ind. Eng. Chem. Fundamentals.* 3:65.

Zhang, F. (2011) The Modelling of Particle Resuspension in a Turbulent Boundary Layer. PhD. Dissertation, School of Mechanical and Systems Engineering, Newcastle University.

Zhang, H., and Ahmadi, G. (2000). Aerosol Particle Transport and Deposition in Vertical and Horizontal Turbulent Duct Flows. *J. Fluid Mech*. 406:55-80.

Ziskind, G. (2006). Particle Resuspension from Surfaces: Revisited and Re-evaluated, *Rev. Chem. Eng*. 22:1-123.

Ziskind, G., Fichman, M., and Gutfinger, C. (1995). Resuspension of Particulates from Surfaces to Turbulent Flows-Review and Analysis. *J. Aerosol Sci.* 26:613-677.

APPENDIX A

ANALISIS OF VARIANCE

The Analysis of Variance (or ANOVA) is a powerful and common statistical procedure in the social sciences. It can handle a variety of situations. Additionally, it is a powerful technique for analyzing experimental data involving quantitative measurements which is particularly useful in factorial experiments where several independent sources of variation may be present (Lipson, 1973). In this study, unless otherwise indicated, the confidence level is taken to be 95%.

The Analysis of Variance (or ANOVA) can be applied using the following equations:

Among columns, the sum of squares along columns, SS_c is defined as:

$$SS_c = \frac{\sum T_c^2}{nrg} - \frac{T^2}{N}$$

Among rows, the sum of squares along rows, SS_r is defined as:

$$SS_r = \frac{\sum T_r^2}{nrg} - \frac{T^2}{N}$$

Among groups, the sum of squares along groups, SS_g is defined as:

$$SS_g = \frac{\sum T_g^2}{nrg} - \frac{T^2}{N}$$

Column-row interaction implies that the sum of squares, SS_{cr} is defined as:

$$SS_{cr} = \frac{\sum T_{cr}^2}{ng} - \frac{T^2}{N} - SS_c - SS_r$$

Column-group interaction implies that the sum of squares, SS_{cg} is defined as:

$$SS_{cg} = \frac{\sum T_{cg}^2}{nr} - \frac{T^2}{N} - SS_c - SS_g$$

Row-group interaction implies that the sum of squares, SS_{rg} is defined as:

$$SS_{rg} = \frac{\sum T_{rg}^2}{nc} - \frac{T^2}{N} - SS_r - SS_g$$

Column-row-group interaction implies that the sum of squares, SS_{crg} is defined as:

$$SS_{crg} = \frac{\sum T_{crg}}{n} - \frac{T^2}{N} - SS_c - SS_r - SS_g - SS_{cr} - SS_{cg} - SS_{rg}$$

Total sum of squares, SS_{total} is defined as:

$$SS_{total} = \sum x^2 - \frac{T^2}{N}$$

The residual or error, $SS_{residual}$ is defined as:

$$SS_{residual} = SS_{total} - SS_c - SS_r - SS_g - SS_{cr} - SS_{cg} - SS_{rg} - SS_{crg}$$

The mean square, MS is defined as:

$$MS = \frac{SS}{DF}$$

The mean square ratio, MSR is defined as:

$$MSR = \frac{MS}{MS_{residual}}$$

Where:

r = number of rows = number of substrates (Glass, Ceramic and Hard wood) = 3

g = number of groups = number of particle size range ((10-30) µm and (30-50) µm glass beads) = 2

c = number of columns = number of velocities = 5

n = number of replications = 3

N = number of observations or sample size

x = sample response = Detachment Percentage value

T = summation of all sample responses

T_r = summation of sample responses by row

T_c = summation of sample responses by column

T_g = summation of sample responses by group

T_{rg} = summation of sample responses by row and column

T_{cg} = summation of sample responses by column and group

T_{cr} = summation of sample responses by column and row

T_{crg} = summation of sample responses by column, row and group

SS = sum of squares

DF = degree of freedom

MS = mean square

MSR = mean square ratio

Higher experimental mean square ratio (MSR) than the F ratio found in F distribution tables for a certain confidence level i.e. 95 percent confidence indicates a significant difference between the parameters used in experiment.